The Accretion Process for SgrA*

Andreas Eckart

I.Physikalisches Institut der Universität zu Köln
Max-Planck-Institut für Radioastronomie, Bonn

STRONGGRAVITY
EU FP7-SPACE research project 312789 2013 - 2017

8th FERO meeting, 2016, Sept. 11 – 15,

VINICE HNANICE, Czech Republic

Finding Extreme Relativistic Objects

F. Peissker, M. Valencia-S., M. Parsa, M. Zajacek, B. Shahzamanian A. Borkar, G.Karssen, C. Straubmeier, M. Subroweit, V. Karas, M. Dovciak, D. Kunneriath, et al. ,

EU FP7-SPACE project: Strong Gravity http://www.stronggravity.eu/

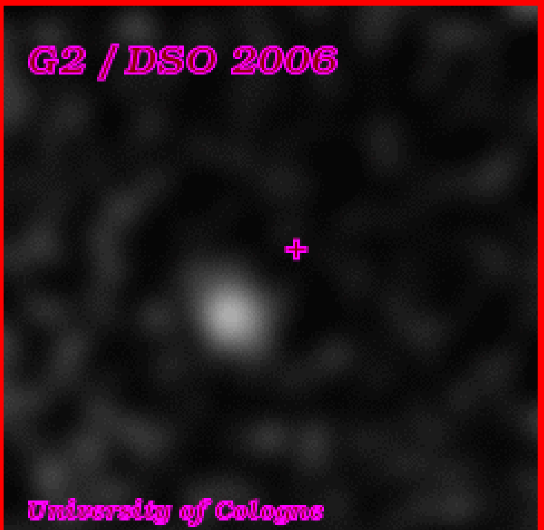

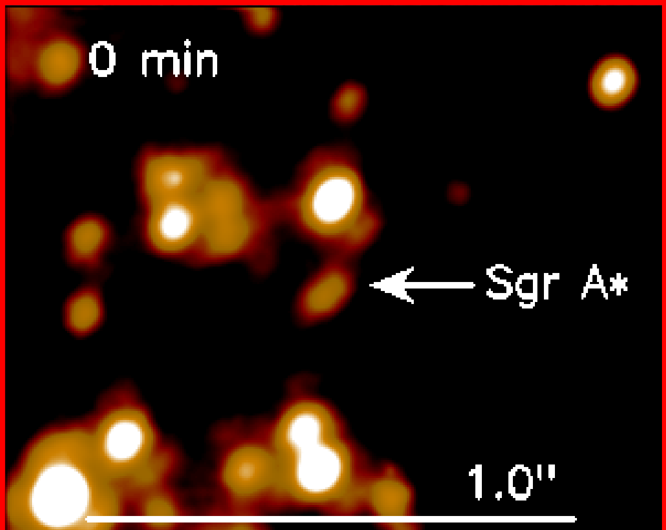

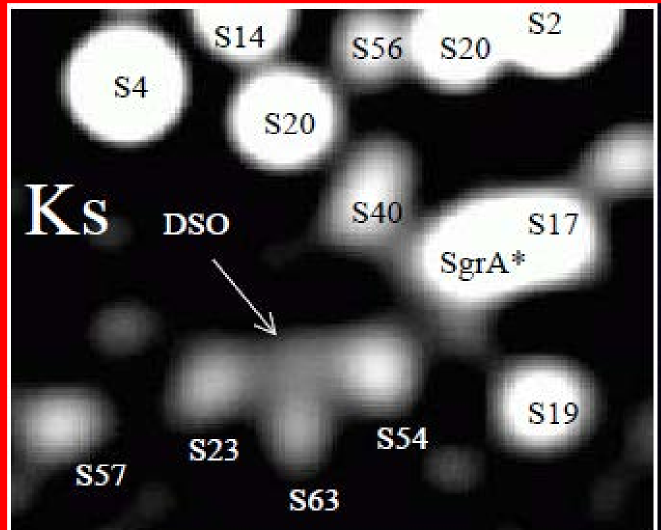

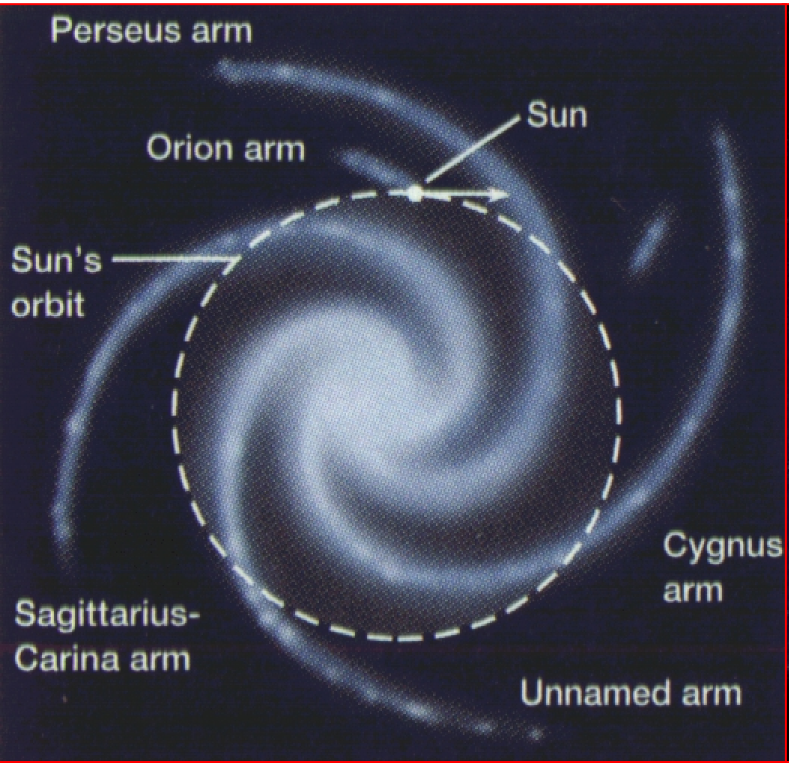

Perseus arm
Sun
Orion arm
Sun's orbit
Cygnus arm
Sagittarius-Carina arm
Unnamed arm

SgrA* and its Environment

Orbits of High Velocity Stars
in the Central Arcsecond

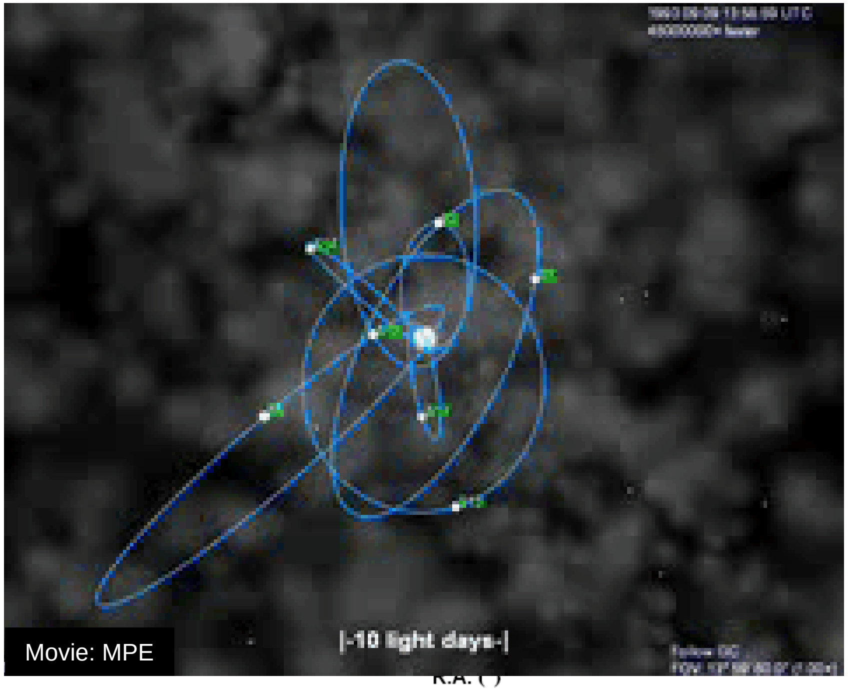

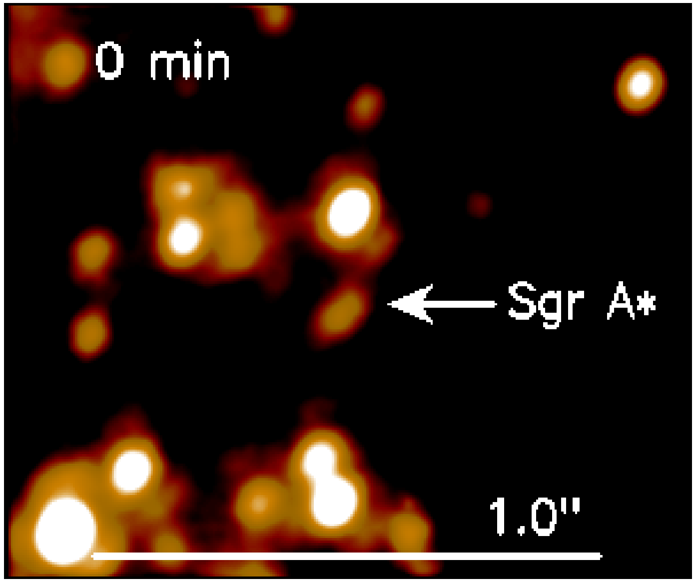

Eckart & Genzel 1996/1997 (first proper motions)
Eckart+2002 (S2 is bound; first elements)
Schödel+ 2002, 2003 (first detailed elements)
Ghez+ 2003 (detailed elements)
Eisenhauer+ 2005, Gillessen+ 2009
(improving orbital elements)
Rubilar & Eckart 2001, Sabha+ 2012, Zucker+2006
(exploring the relativistic character of orbits)

~4 million solar masses
at a distance of
~8+-0.3 kpc

Accretion of winds onto SgrA*

Starvation?

NIR and X-ray observations as well as simulations suggest stellar winds contribute up to 10^-4 MSun/yr at Bondi radius (10^5 rS) (Krabbe+ 1995, Baganoff+ 2003)

At this accretrion rate SgrA* is 10^7 times under luminous (e.g. Shcherbakov & Baganoff 2010)

Accretion of gaseous clumps from the Galactic Centre Mini-spiral onto Milky Way's supermassive black hole ? (Karas, Vladimir; Kunneriath, Devaky; Czerny, Bozena; Rozanska, Agata; Adhikari, Tek P. ; 2016grg..conf...98K)

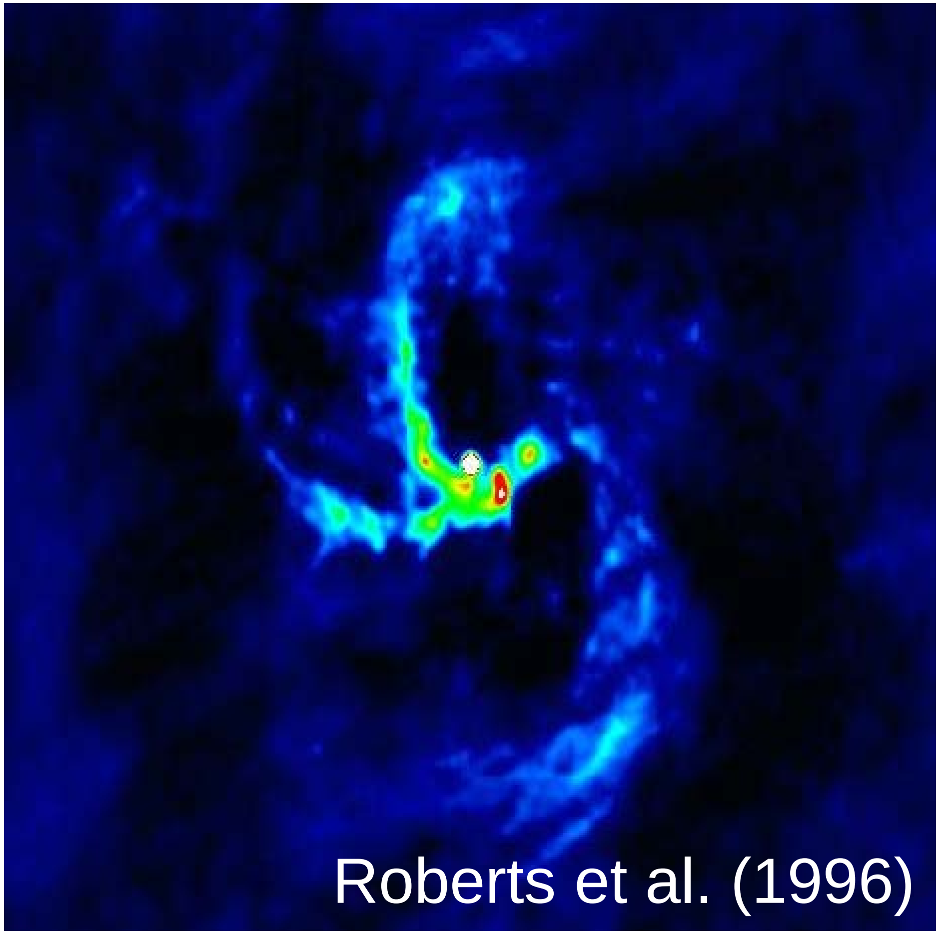

Structure of the accretion disk

CASE 1: low accretion rate
high opacity

$$\dot{M}/\dot{M}_E \lesssim 0.1$$

thin accretion disk
compared to diameter
efficiency: $\eta \approx 0.1$

CASE 0
plus advection
dominated accretion
for LLAGN

$$\dot{M}/\dot{M}_E << 1$$

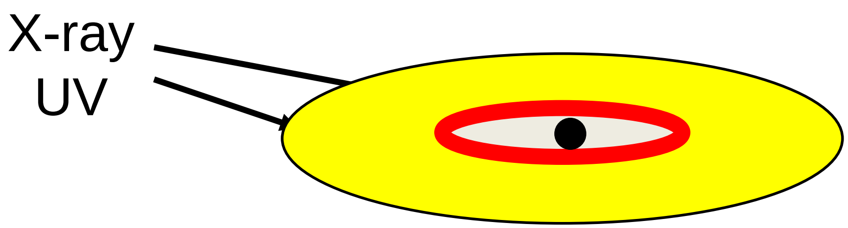

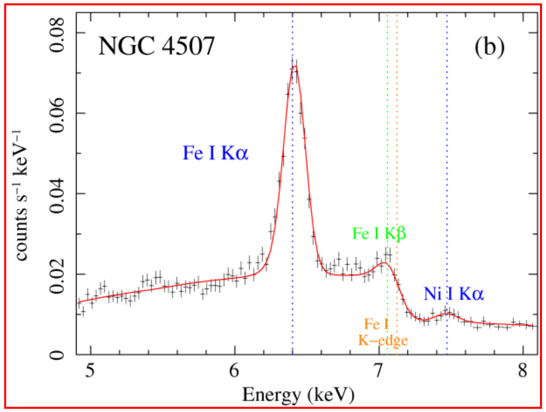

Suzaku data

CASE 2: high accretion rate
radiation heats disk
disk inflates and cools
at larger radii, i.e.
radiation becomes
inefficient.

$$\dot{M}/\dot{M}_E \gtrsim 1$$

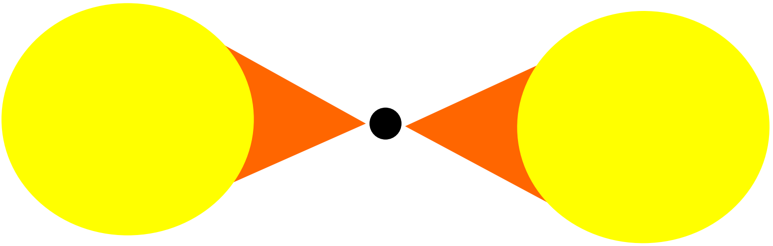

looks like a
10**4 K
young star

SgrA* as an extreme LLAGN Nucleus

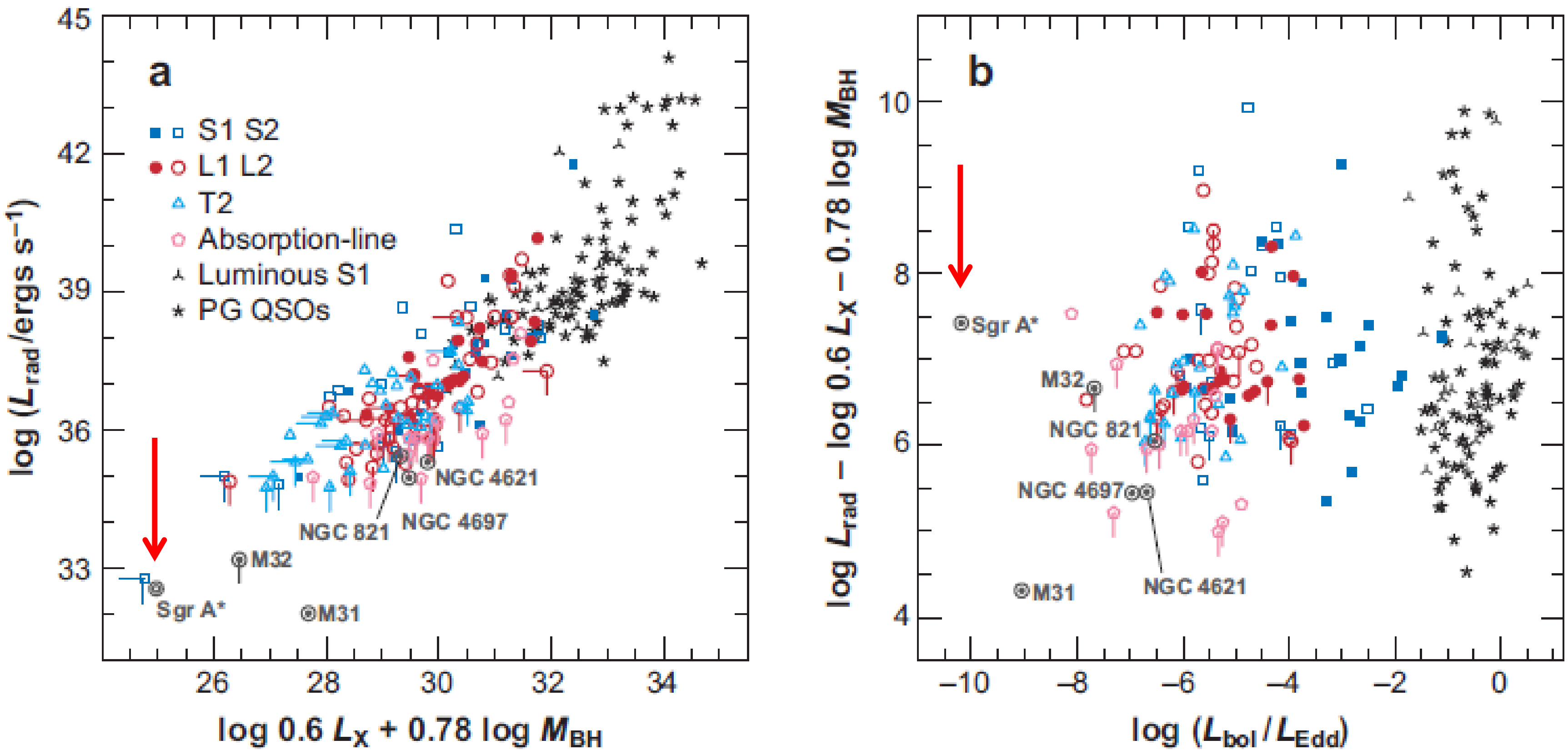

Ho 2008: Fundamental plane correlation among core radio luminosity, X-ray (a) luminosity, and BH mass. (*b*) Deviations from the fundamental plane as a function of Eddington ratio.

SgrA* is accreting in an advection dominated mode, else ist luminosity would be than 10^7 times higher

- Radio/sub-mm single dish and VLBA monitoring
- NIR polarization of SgrA* over the past ~10 years
- Stability of the SgrA* system
- Synchtotron Self Compton modelling

- Monitoring the Dusty S-cluster Object (DSO alias G2) orbiting SgrA*
- In NIR line emission as well as
- In NIR continuum polarization

Flare Activity of SgrA*

Seeing the effect of ongoing accretion

Observations

SgrA* on 3 June 2008: VLT L-band and APEX sub-mm measurements

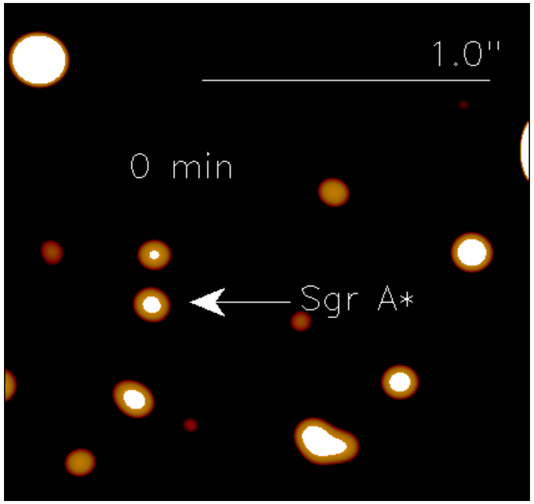

VLT 3.8um L-band

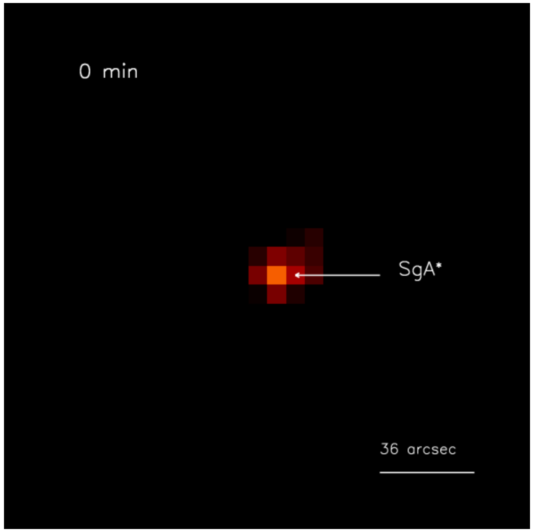

APEX 1.3 mm

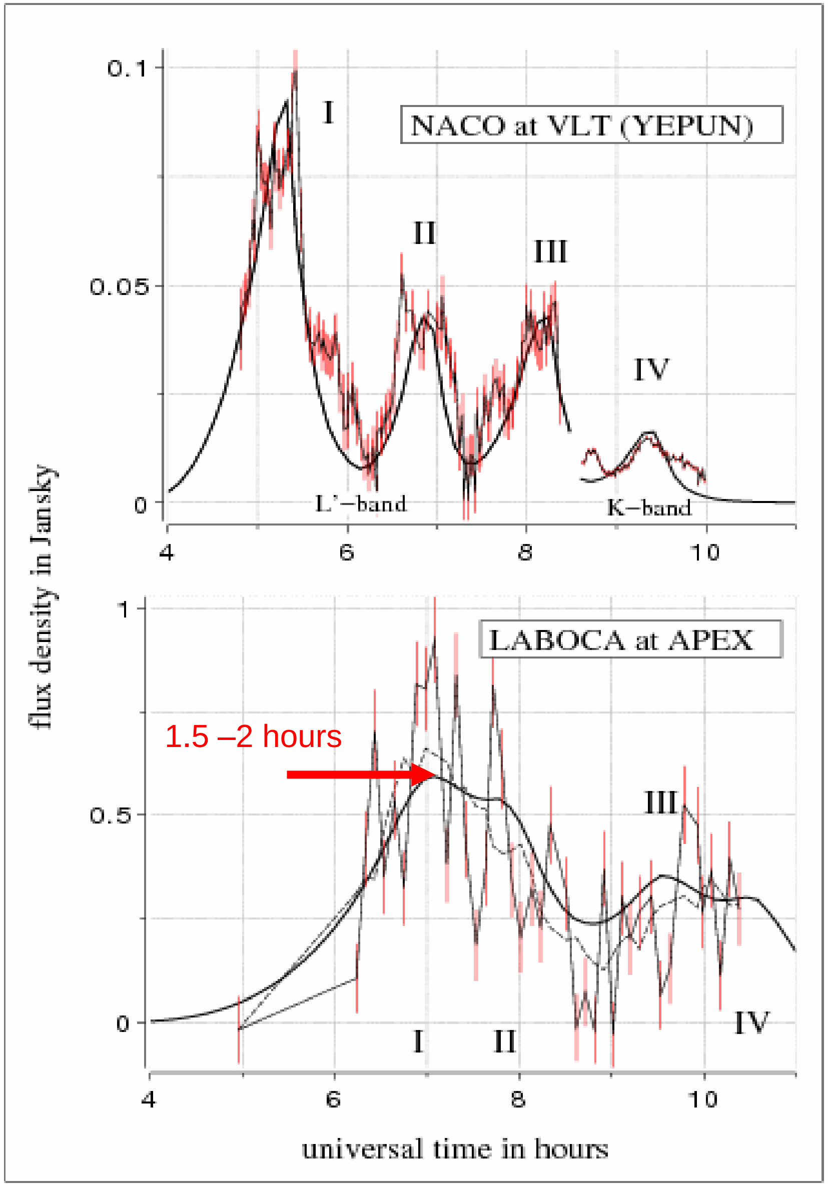

Eckart et al. 2008; A&A 492, 337

Garcia-Marin et al.2009

Simultaueous NIR/X-ray Flare emission 2004

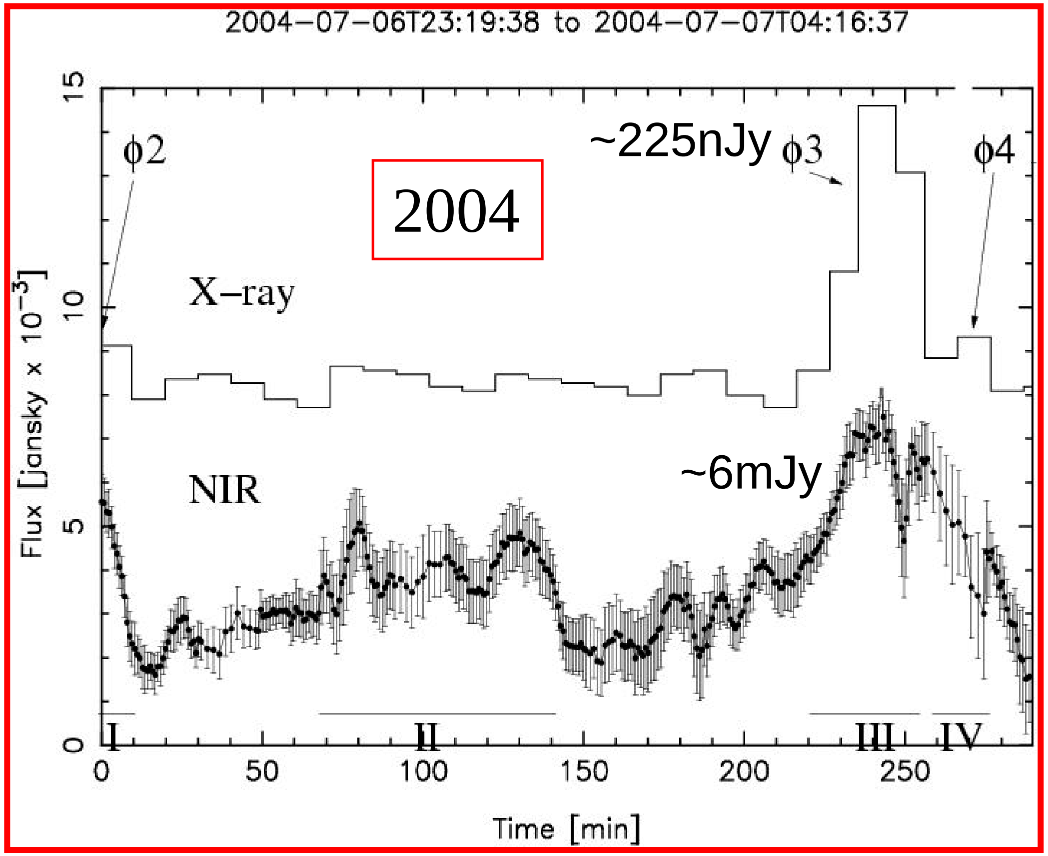

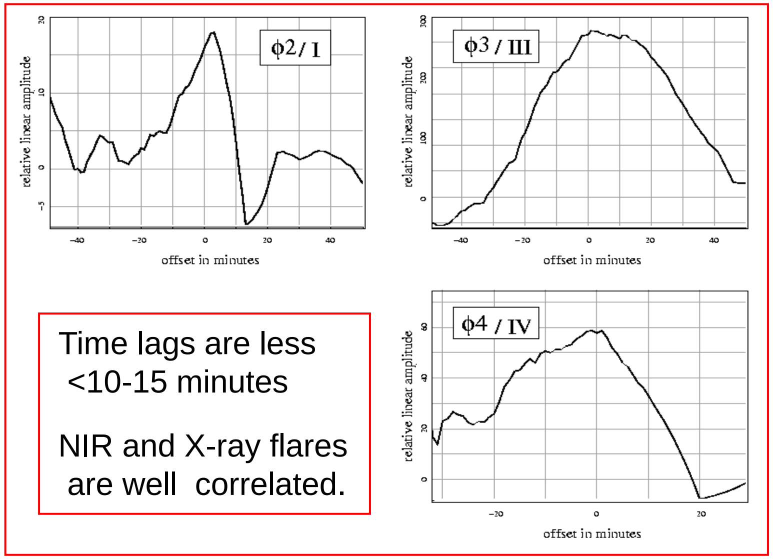

Flare emission originates from within <10mas form the position of SgrA*

First simultaneous NIR/X-ray detection

2003 data: Eckart, Baganoff, Morris, Bautz, Brandt, et al. 2004 A&A 427, 1

2004 data: Eckart, Morris, Baganoff, Bower, Marrone et al. 2006 A&A 450, 535

see also Yusef-Zadeh, et al. 2008, Marrone et al. 2008

Bright He-stars provide mass for accretion

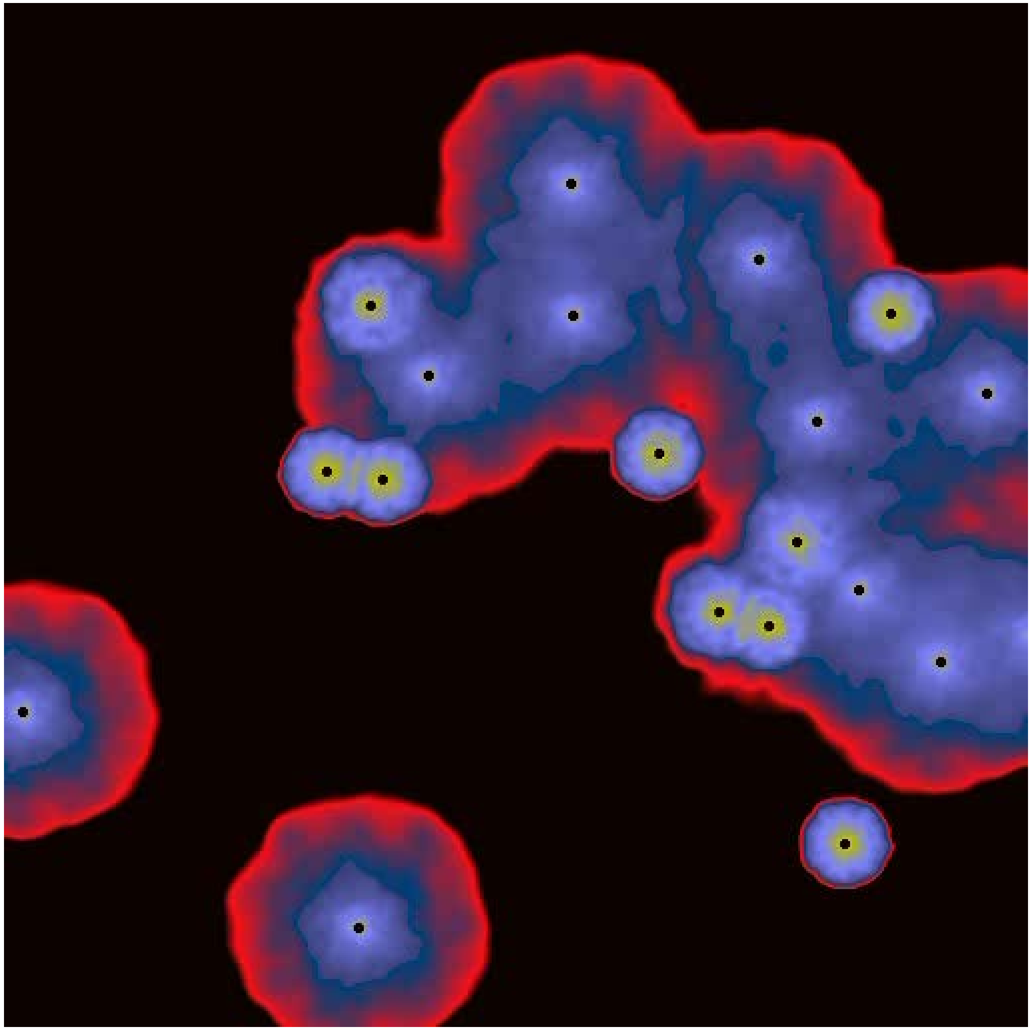

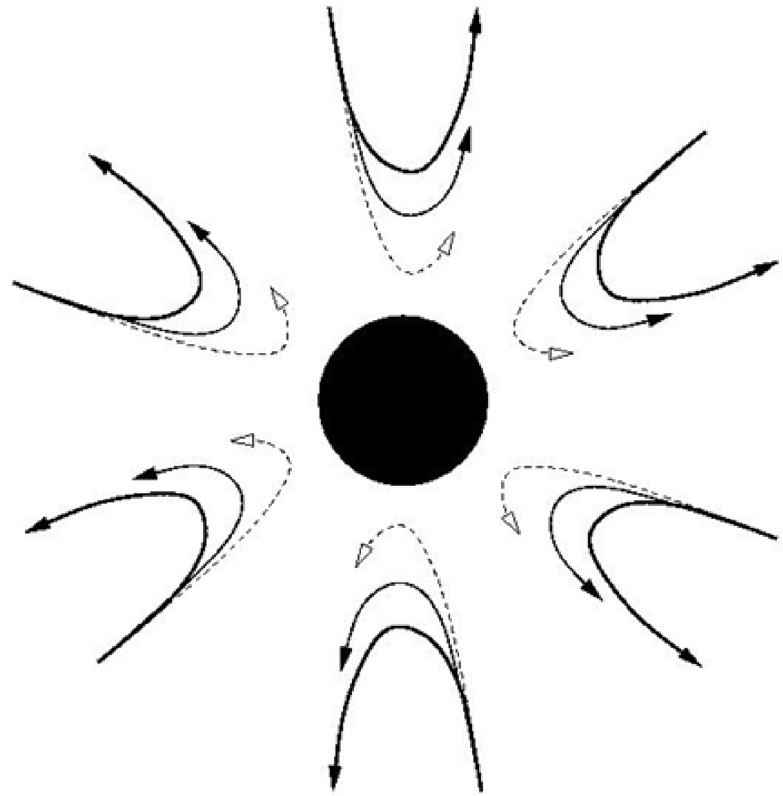

radius dependent
accretion

Cuadra, Nayakshin, Springel, and Di Matteo 2005/6

Shcherbakov & Baganoff ApJ, 2010

Sub(mm) Flare Activity of SgrA*

Seeing the effect of ongoing accretion

SgrA* 345GHz/100GHz varibility

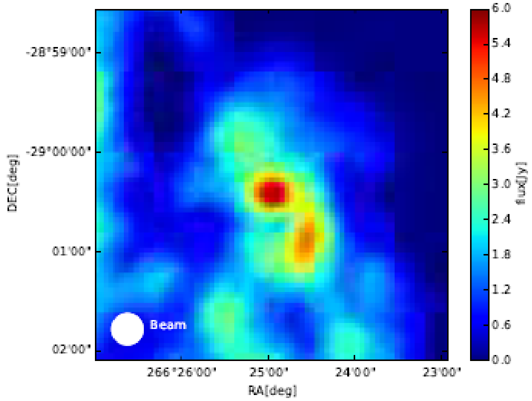

Fig. 1. A single measurement map of the GC from 2009-05-17T04:19:58, the extended submm emission from the surroundings of Sgr A* (CNR and Minispiral) dominate the data.

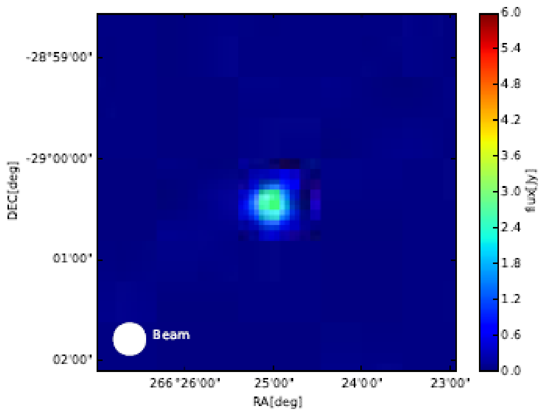

Fig. 2. A single measurement map of the GC from 2009-05-17T04:19:58 with subtracted background. The remaining point-like source represents the submm emission from Sgr A* itself.

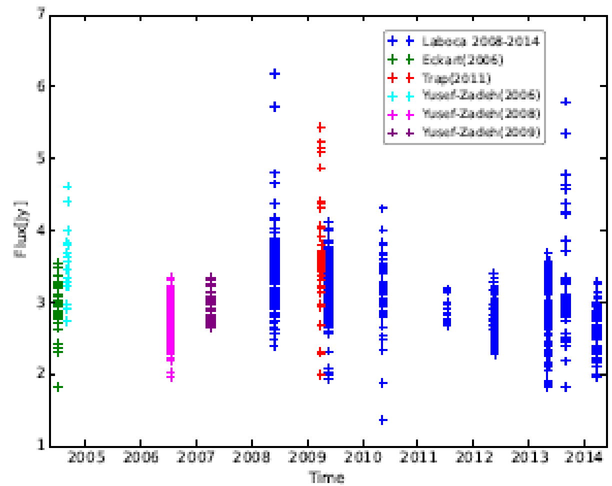

Fig. 3. All light curves obtained between 2004 and 2014. This plot contains both the LABOCA data (blue markers) and the literature data (other colors).

Borkar et al. MNRAS 2016
Subroweit et al. 2016

SgrA* 345GHz/100GHz varibility

Borkar et al. MNRAS 2016
Subroweit et al. 2016

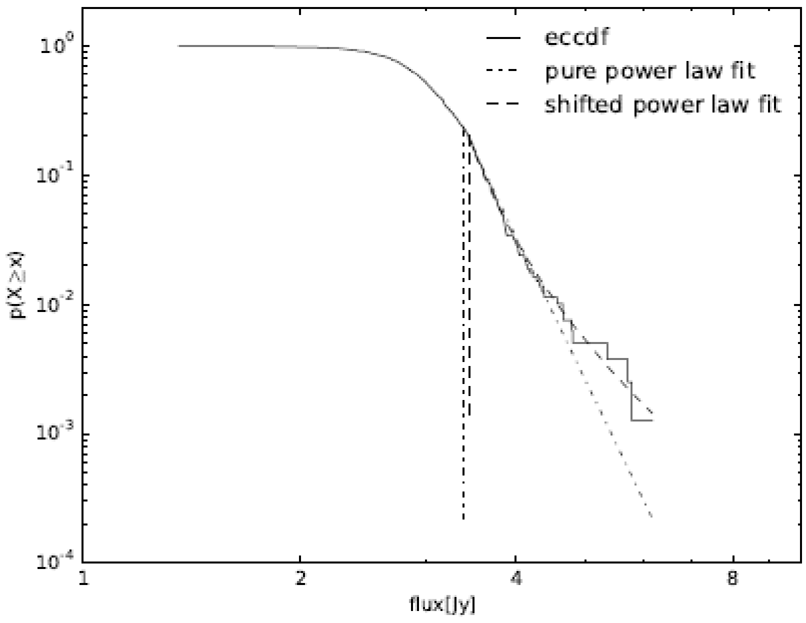

345 GHz LABOCA

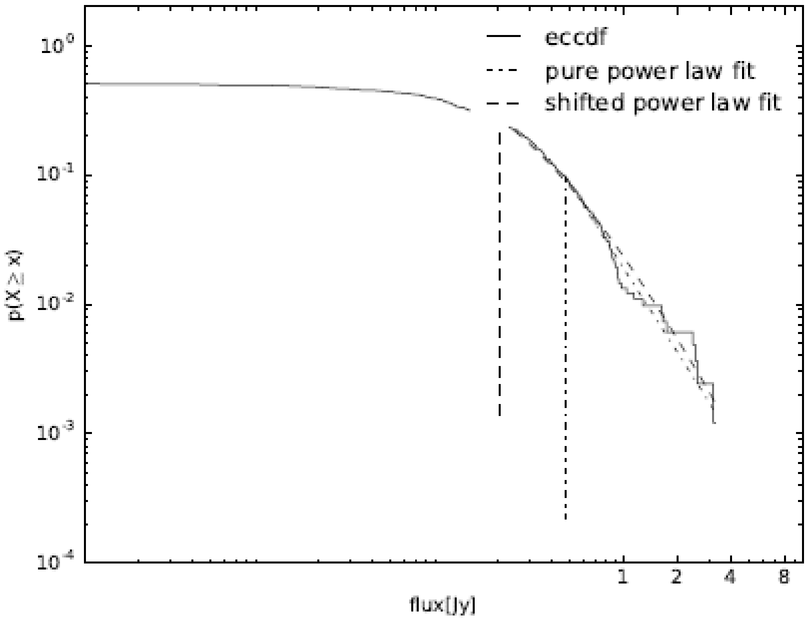

100 GHz ATCA

$$S(100\ \mathrm{GHz}, t) \sim S(\nu_0 = 100\ \mathrm{GHz}, t) + S_{\mathrm{adiab}}(\nu_0 > 100\ \mathrm{GHz}, t)$$

SgrA* 345GHz/100GHz varibility

Borkar et al. MNRAS 2016
Subroweit et al. 2016

SgrA* peaks around 350 GHz

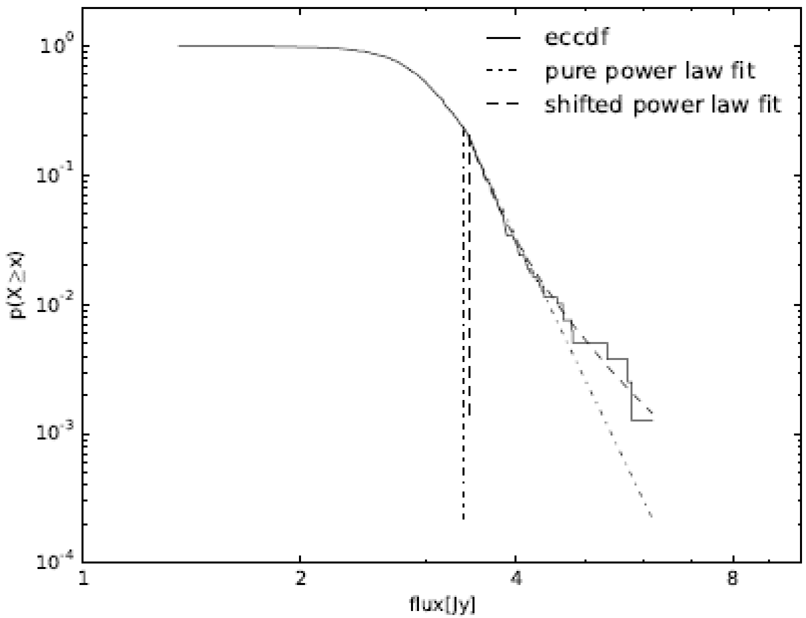

345 GHz LABOCA

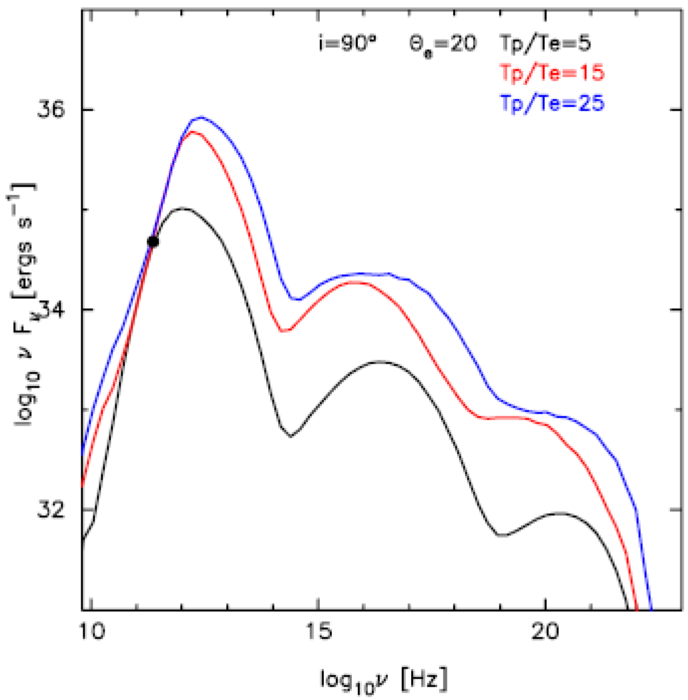

$$S(100\ \mathrm{GHz}, t) \sim S(\nu_0 = 100\ \mathrm{GHz}, t) + S_{\mathrm{adiab}}(\nu_0 > 100\ \mathrm{GHz}, t)$$

Adiabatic Expansion in SgrA*

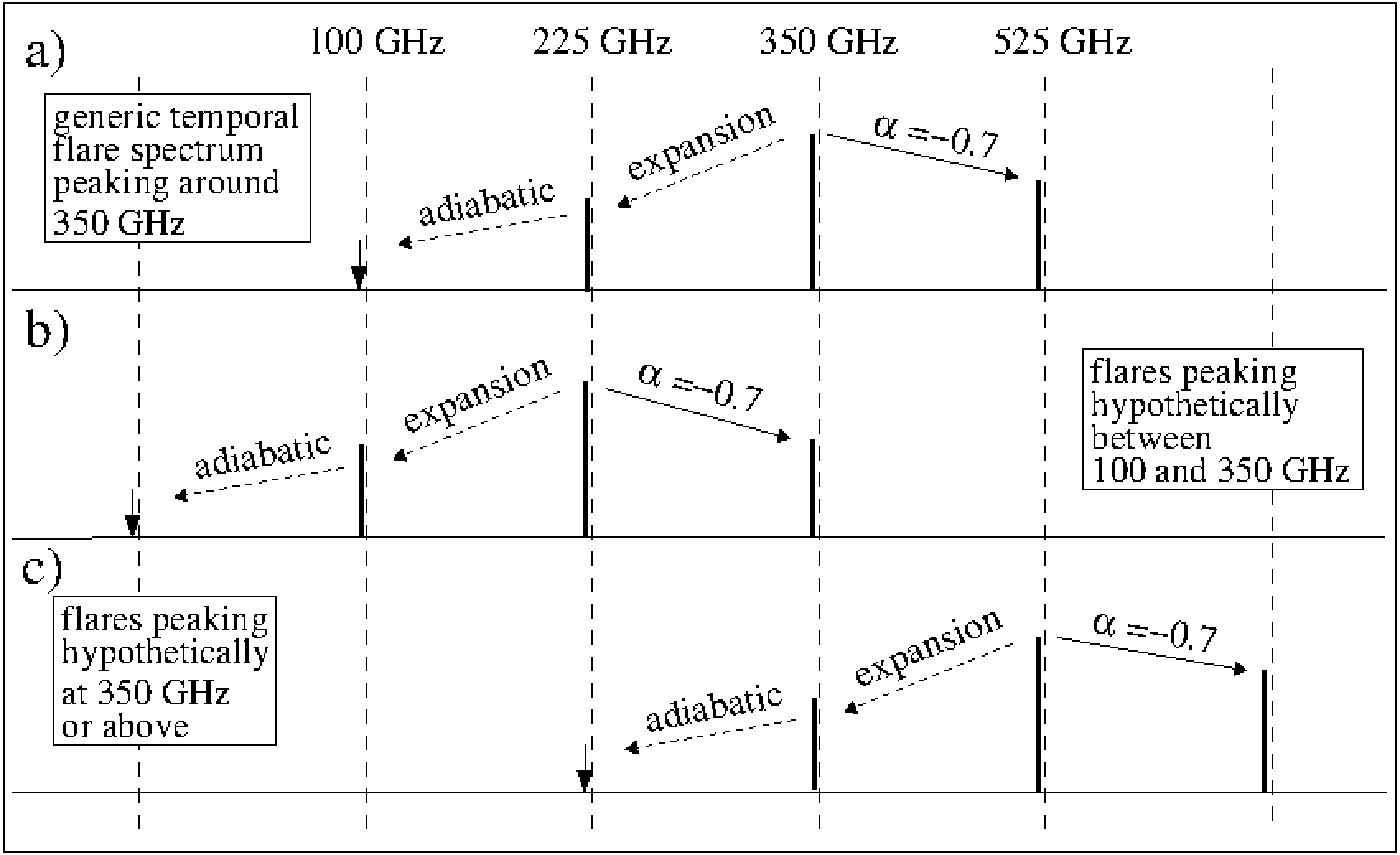

Subroweit et al. 2016 submitted

Adiabatic Expansion in SgrA*

$$\nu_m = \nu_{m0}\left(\frac{R(t)}{R_0}\right)^{-(4p+6)/(p+4)}$$

van der Laan (1966)

$$p = 1 - 2\alpha_{sync} \sim 2.4,$$

$$\frac{R(t)}{R_0} \sim \left(\frac{\nu_m}{\nu_{m0}}\right)^{-1/2.44} \sim \left(\frac{100\,\mathrm{GHz}}{350\,\mathrm{GHz}}\right)^{-1/2.44} \approx 1.67$$

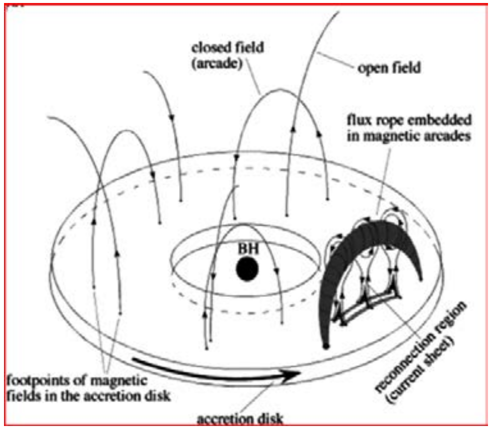

Yuan et al. 2009

$$R(t) = v_{exp}t + R_0$$

starting at ~1 Rs

$$v_{exp} \times 0.5\,\mathrm{h} \sim 0.67\,R_S.$$

$$v_{exp} \sim 0.01\,\mathrm{c}$$

Subroweit et al. 2016 submitted

VLBI Imaging and Polarization SgrA*

Imaging the effect of ongoing accretion

The Event Horizon Telescope

- 25 uas at 1.3 mm
- 22 uas scatter

broadened point source

- Observed :

37 uas deconvolved

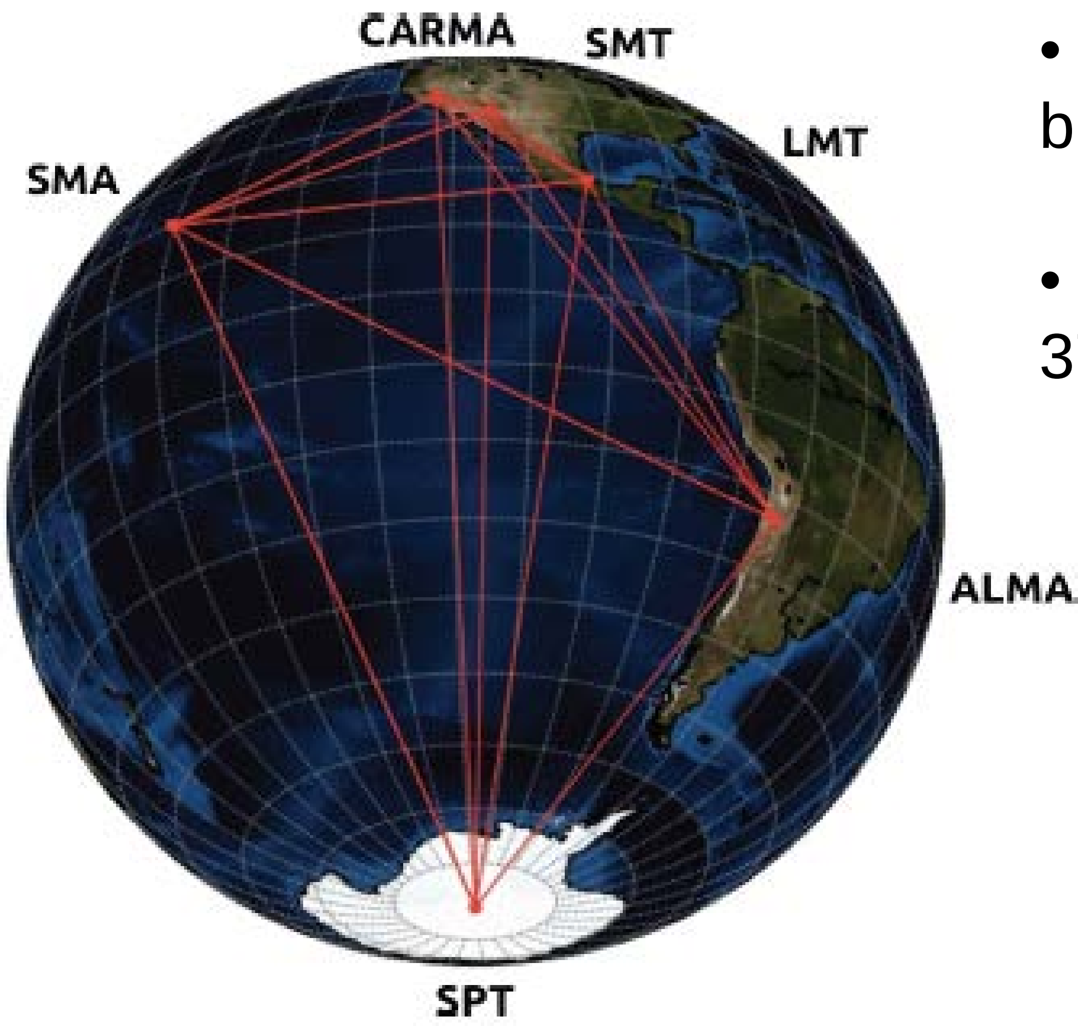

The Event Horizon Telescope including projected site additions in 2015, as seen by Sgr A*. The SMA critically anchors the E-W baselines. (Credit: L. Vertatschitsch)

VLBI at 230 GHz (1.3 mm wavelength)

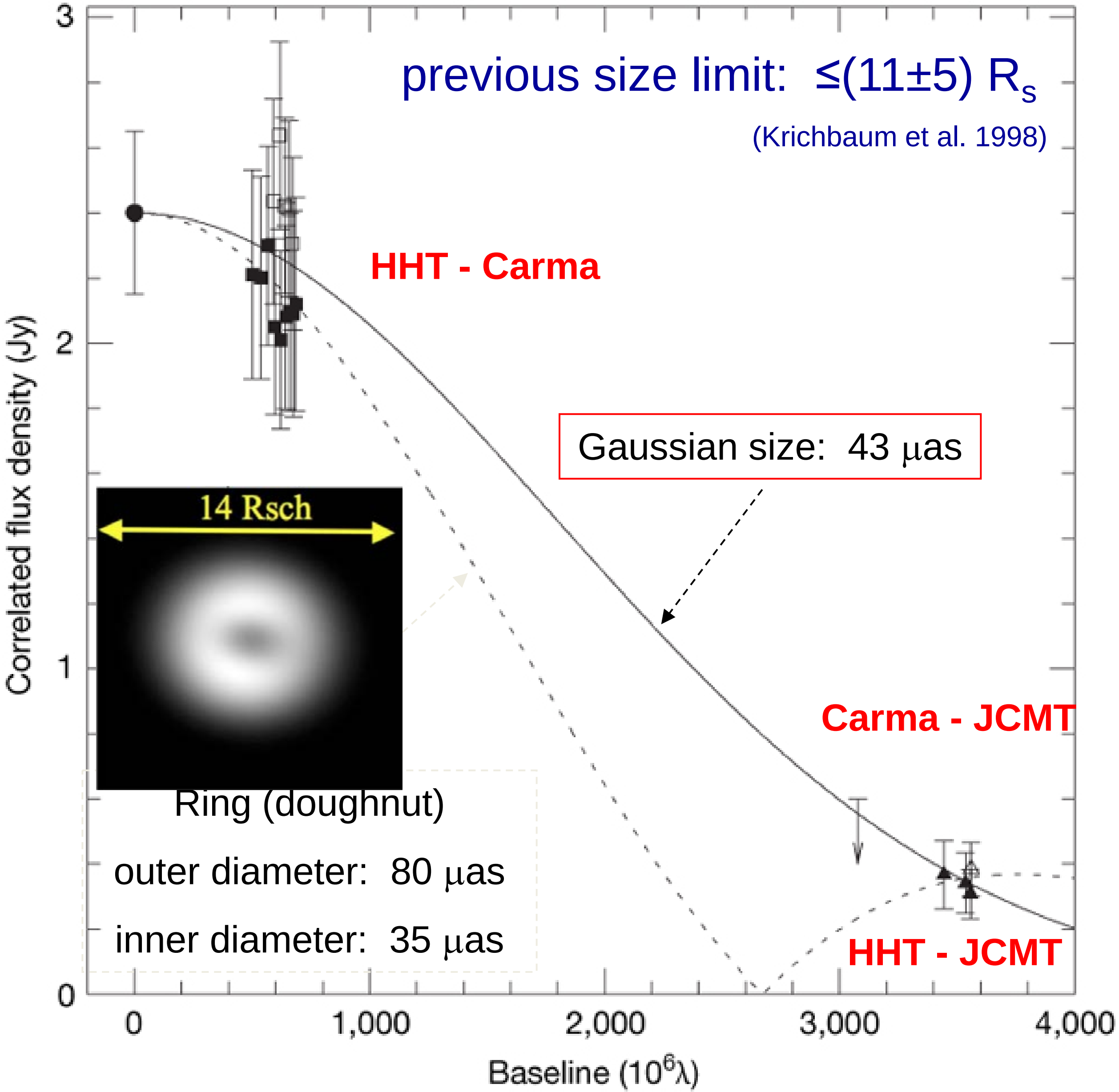

Doeleman *et al.* *Nature* **455**, 78-80 (2008)

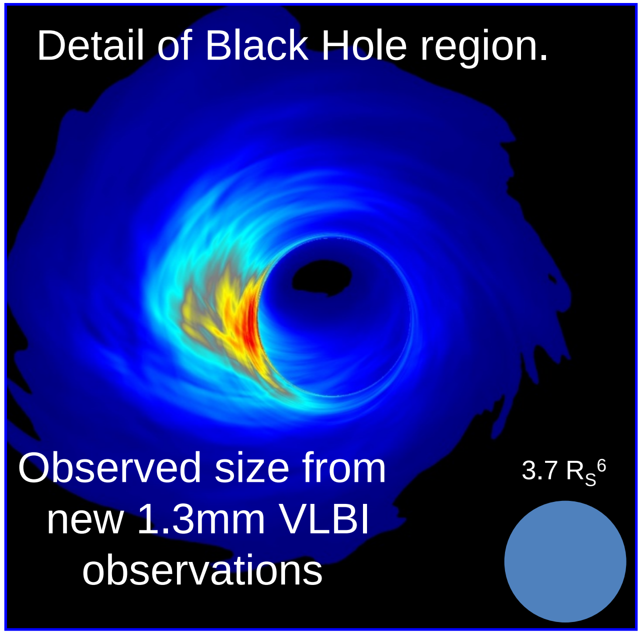

observed size:

43 (+14/-8) µas

deconvolved :

37 µas (3.7 R_S)

1.3mm VLBI Visibility of the Variable Source SgrA*

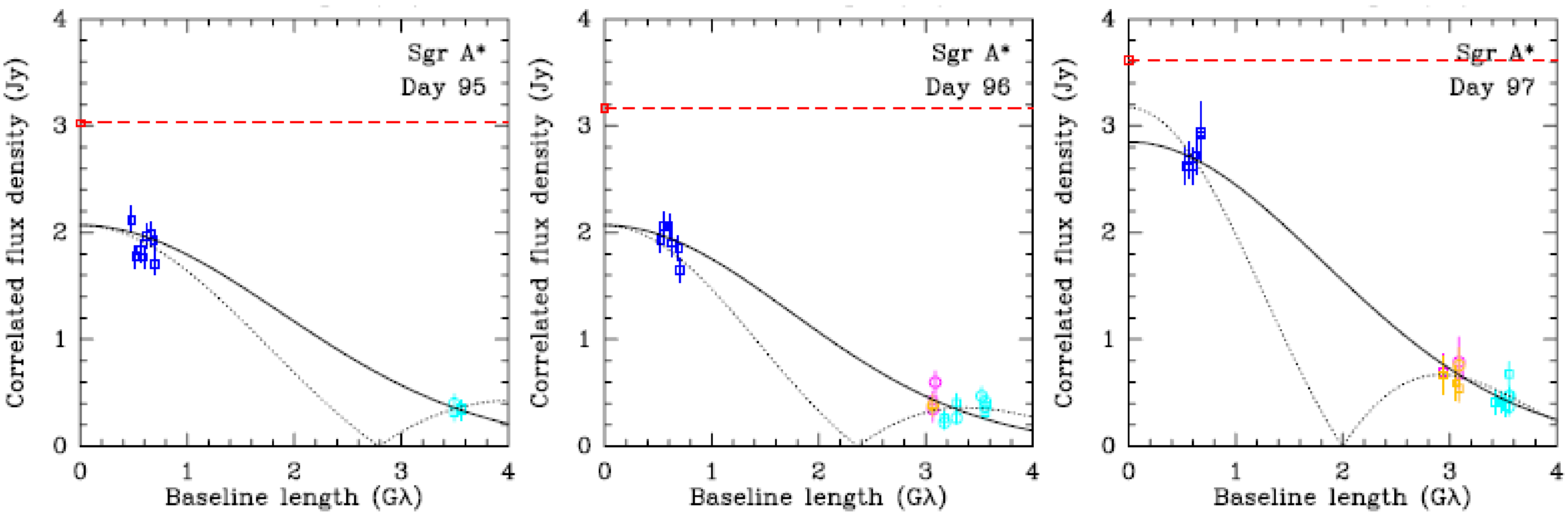

THE ASTROPHYSICAL JOURNAL LETTERS, 727:L36 (6pp), 2011 February 1
doi:10.1088/2041-8205/727/2/L36

1.3 mm WAVELENGTH VLBI OF SAGITTARIUS A*: DETECTION OF TIME-VARIABLE EMISSION ON EVENT HORIZON SCALES

VINCENT L. FISH[1], SHEPERD S. DOELEMAN[1], CHRISTOPHER BEAUDOIN[1], RAY BLUNDELL[2], DAVID E. BOLIN[1,3], GEOFFREY C. BOWER[4], RICHARD CHAMBERLIN[5], ROBERT FREUND[6], PER FRIBERG[7], MARK A. GURWELL[2], MAREKI HONMA[8], MAKOTO INOUE[9], THOMAS P. KRICHBAUM[10], JAMES LAMB[11], DANIEL P. MARRONE[12,14], JAMES M. MORAN[2], TOMOAKI OYAMA[8], RICHARD PLAMBECK[4], RURIK PRIMIANI[2], ALAN E. E. ROGERS[1], DANIEL L. SMYTHE[1], JASON SOOHOO[1], PETER STRITTMATTER[6], REMO P. J. TILANUS[7,13], MICHAEL TITUS[1], JONATHAN WEINTROUB[2], MELVYN WRIGHT[4], DAVID WOODY[11], KEN H. YOUNG[2], AND LUCY M. ZIURYS[6]

Fish et al. 2011

VLBI Image Reconstruction for SgrA*

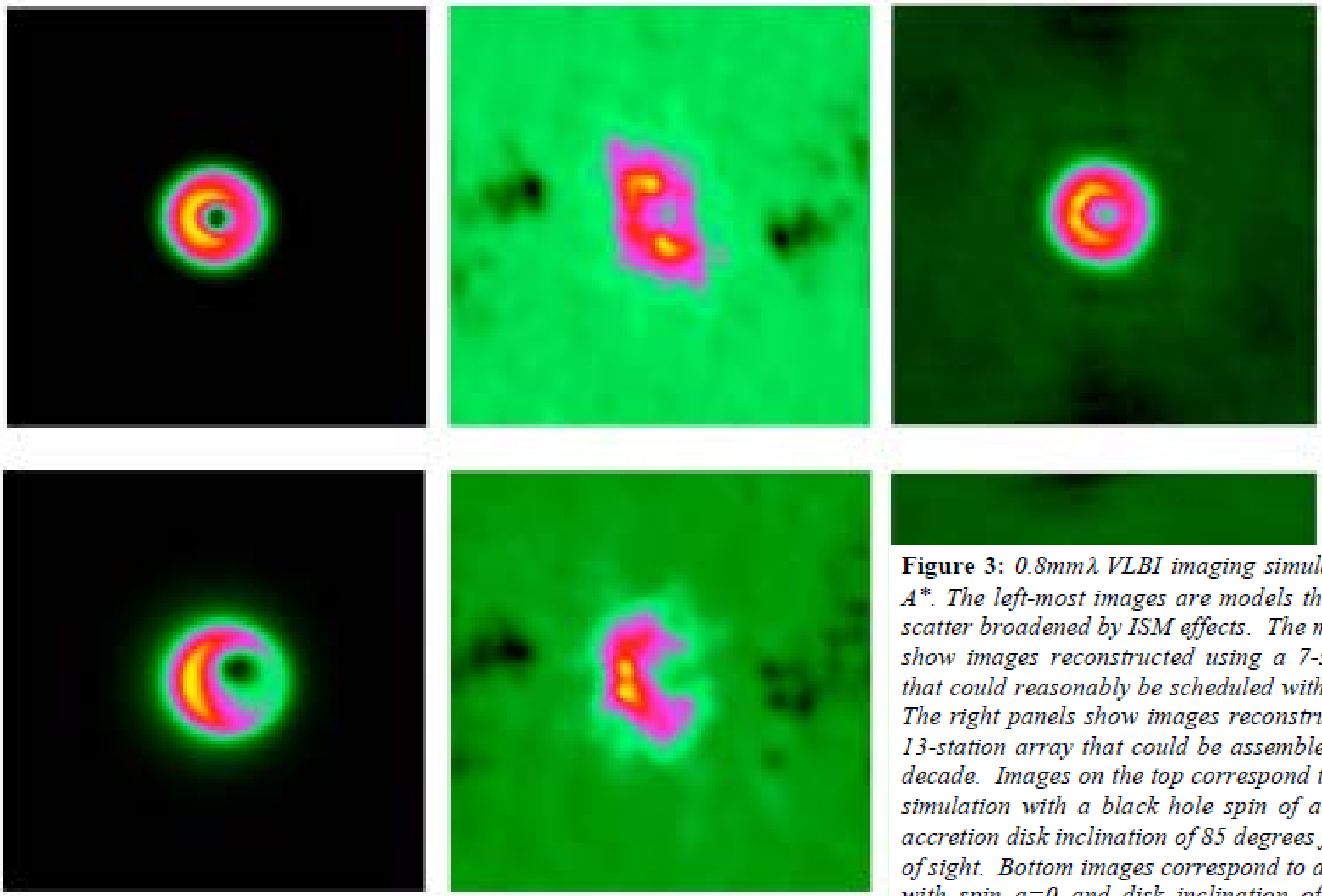

Figure 3: *0.8mmλ VLBI imaging simulations of Sgr A*. The left-most images are models that have been scatter broadened by ISM effects. The middle panels show images reconstructed using a 7-station array that could reasonably be scheduled within 3-5 years. The right panels show images reconstructed using a 13-station array that could be assembled within this decade. Images on the top correspond to a GRMHD simulation with a black hole spin of a=0.5 and an accretion disk inclination of 85 degrees from our line of sight. Bottom images correspond to a RIAF model with spin a=0 and disk inclination of 60 degrees. Models courtesy Charles Gammie and Avery Broderick.*

Doeleman et al. 2010 Decadel Survey

Imaging simulation of Sgr A* with the EHT.

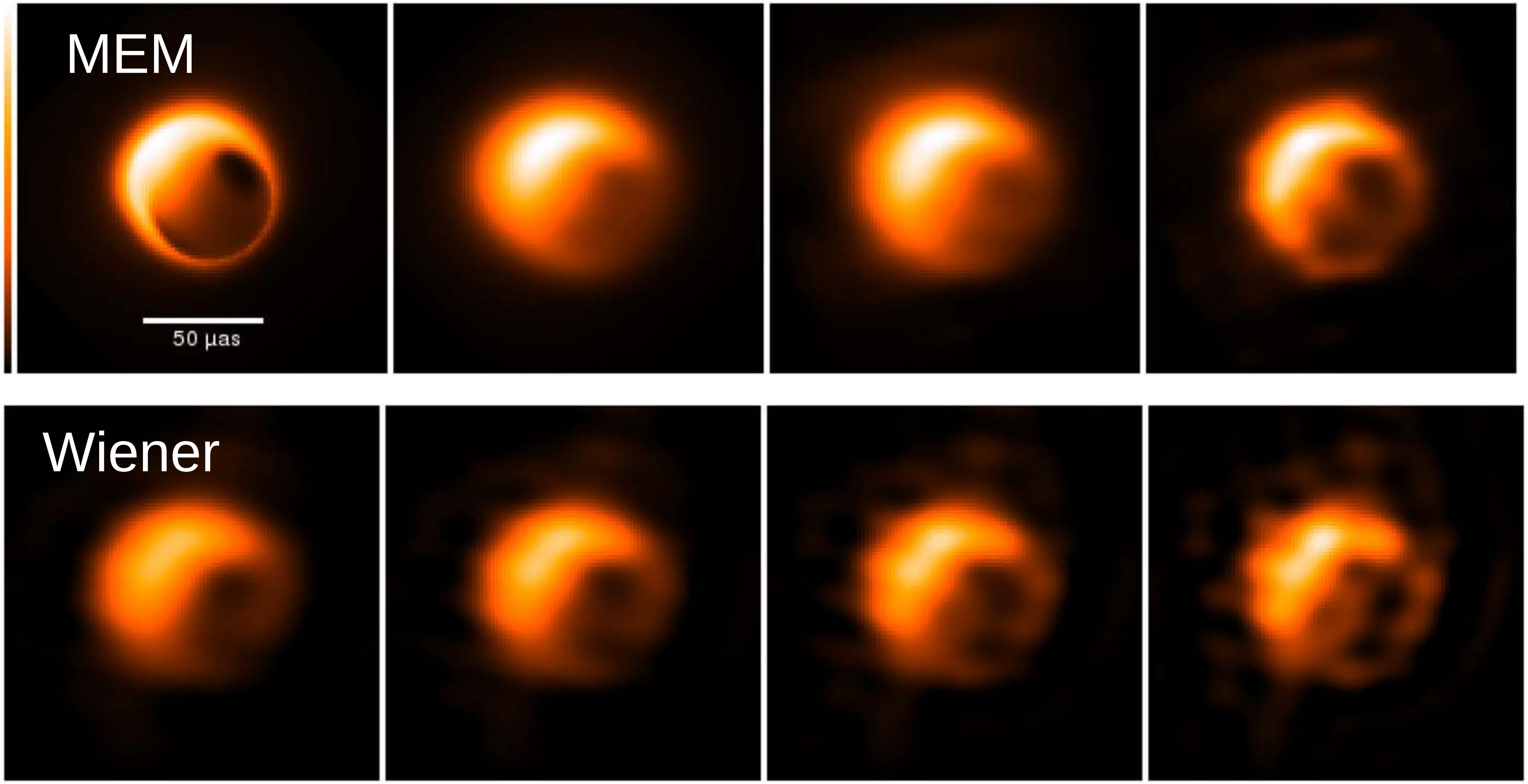

Fish et al. 2014 imaging in presence of scattering

Effect of a Polarized Spot Orbiting SgrA*

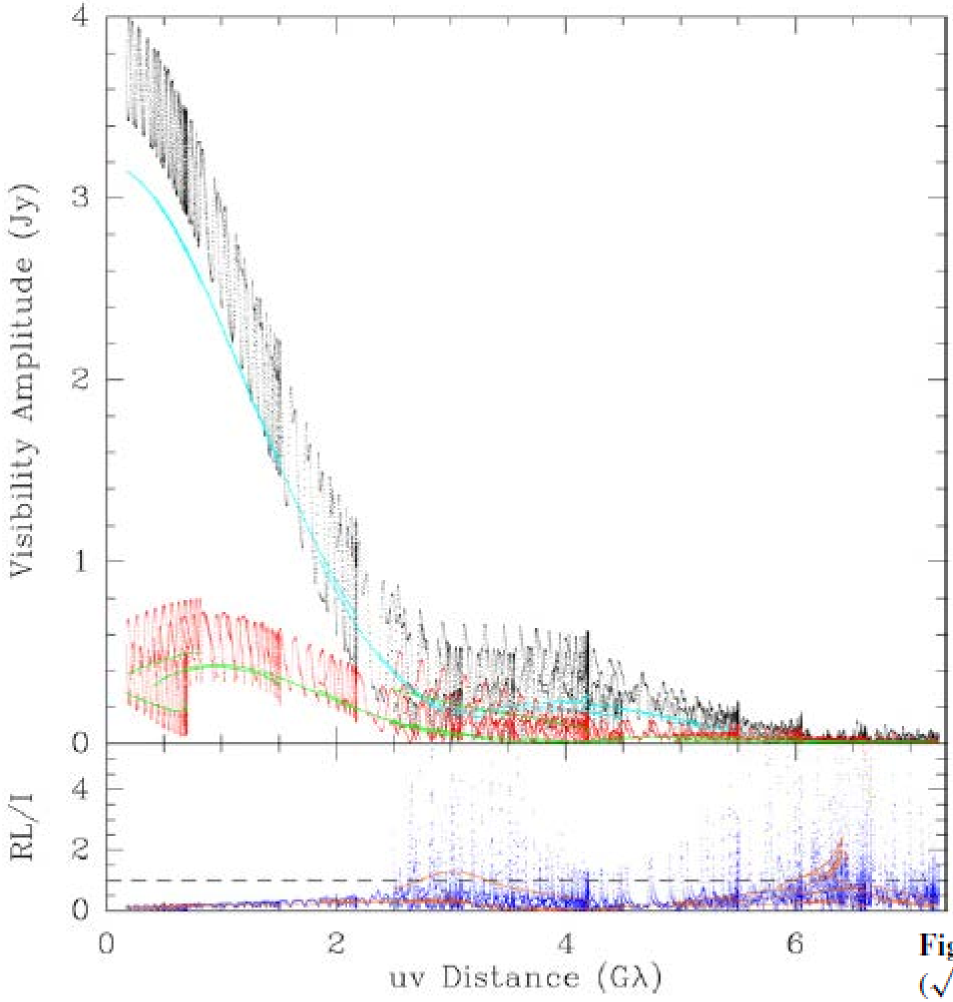

Fish et al. 2009

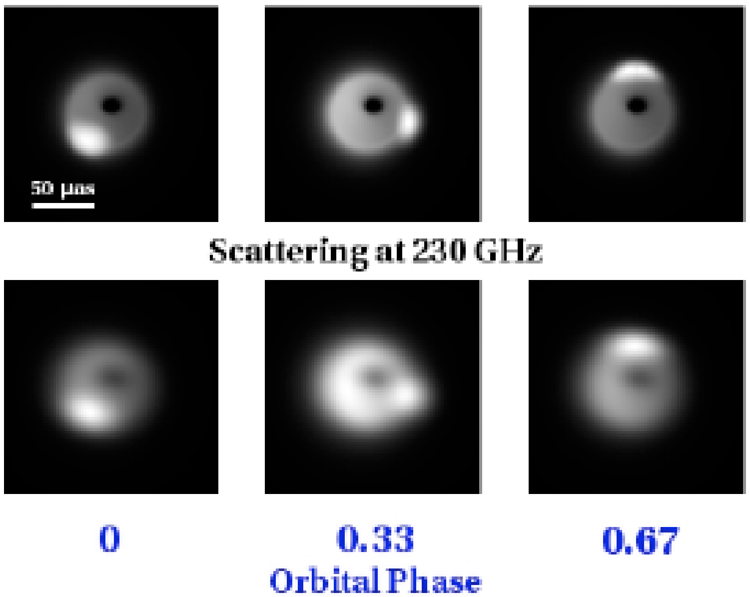

Doeleman et al. 2010 Decadel Survey

Figure 2. Top: visibility amplitude as a function of projected baseline length ($\sqrt{u^2+v^2}$) for Model A at 230 GHz (noiseless). Stokes I is shown in black, and RL is shown in red. A real orbiting hot spot would persist for only a small fraction of a day, producing a plot corresponding to a subset of the above points. Contributions from the disk alone in the absence of a hot spot are shown in cyan (Stokes I) and green (RL). Bottom: ratio of RL/I visibility amplitudes for the disk and hot spot (blue) and disk alone (orange). On small scales, RL/I can greatly exceed unity.

Effect of a Hot Spot Orbiting SgrA*

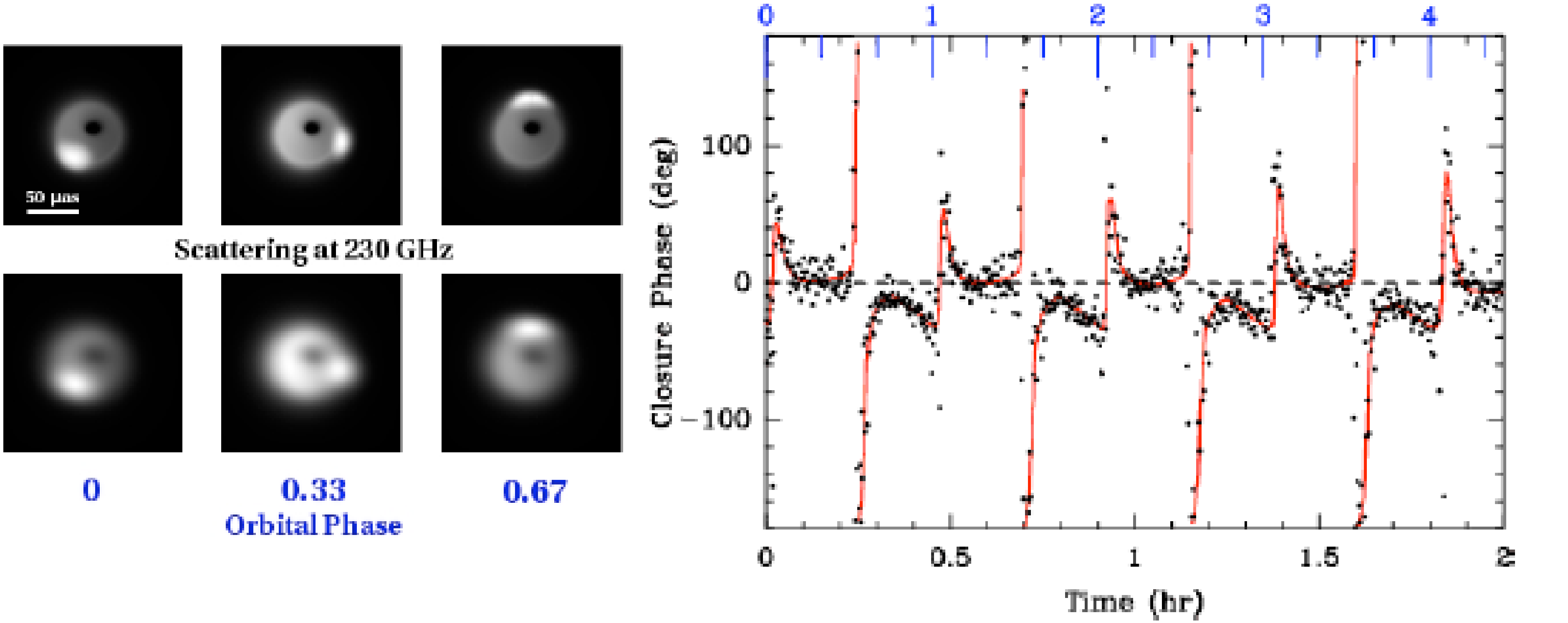

Figure 4: *Signature of a hot-spot orbiting the SgrA* black hole. The left panel shows a quiescent Radiatively Inefficient Accretion Flow (RIAF) model for a non-spinning 4x10^6 solar mass black hole, and a hot spot orbiting at the Innermost Stable Circular Orbit (ISCO), with a disk inclination of 60 degrees from line of sight. The raw model is shown for 3 orbital phases in the top three figures, and the bottom three show the effects of scattering by the ISM. VLBI closure phase (the sum of interferometer phase over a triangle of baselines) is non-zero when asymmetric structure is present. The right panel shows 1.3mm wavelength VLBI closure phases every 10-seconds on the ARO/SMT-Hawaii-CARMA triangle with the model phases shown as a red curve (Doeleman et al. 2009).*

Doeleman et al. 2010 Decadel Survey

Effect of a Polarized Spot Orbiting SgrA*

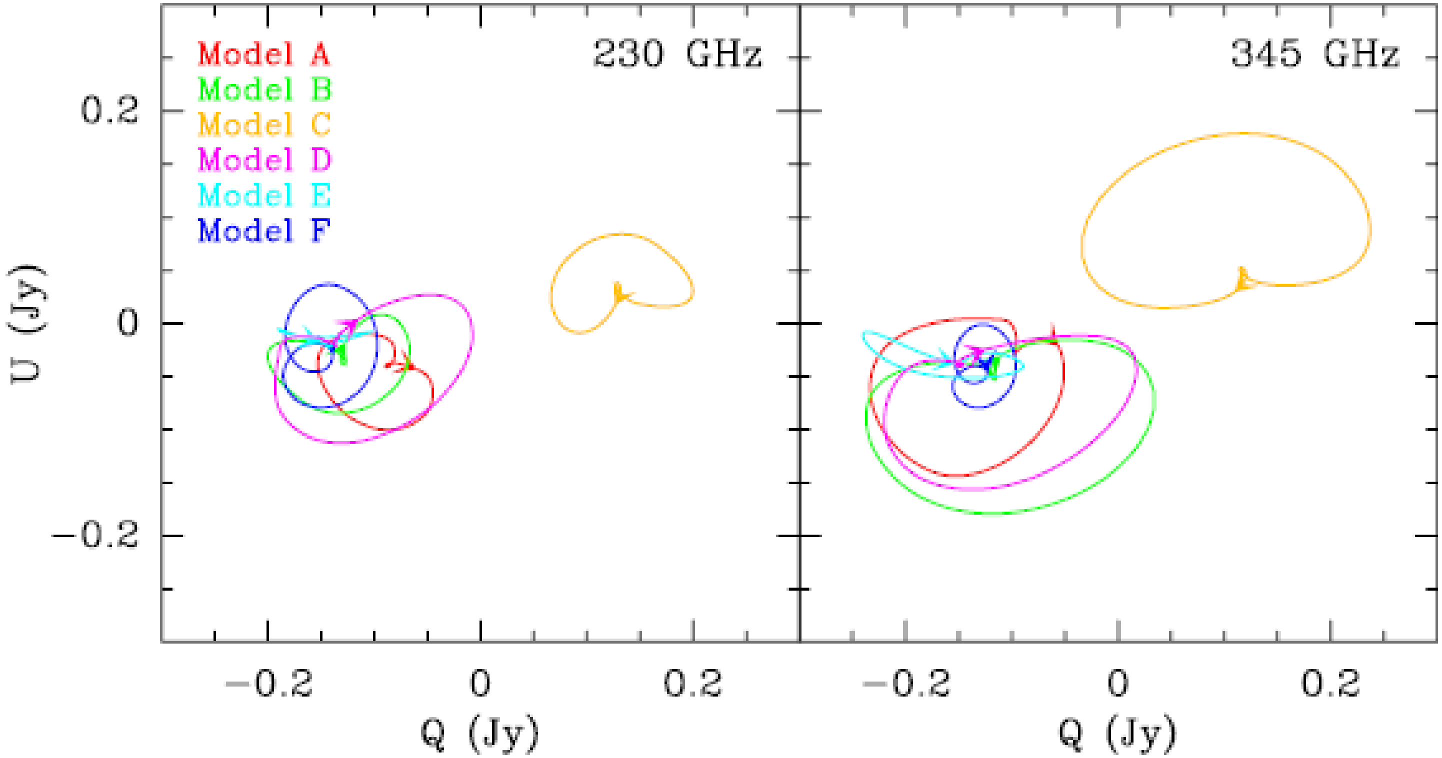

Figure 1. Integrated polarization traces of the models in the Stokes (Q, U) plane at 230 and 345 GHz over a full hot spot orbit, as would be seen by the SMA (for instance).

Fish et al. 2009

Jet vs. Core Luminosity in SgrA*

200x200 Rg | 20x20 Rg

$\left(\left(\frac{T_p}{T_e}\right)_{\rm disk}, \Theta_{\rm e,jet}\right)$

(5,20)

(15,20)

(25,20)

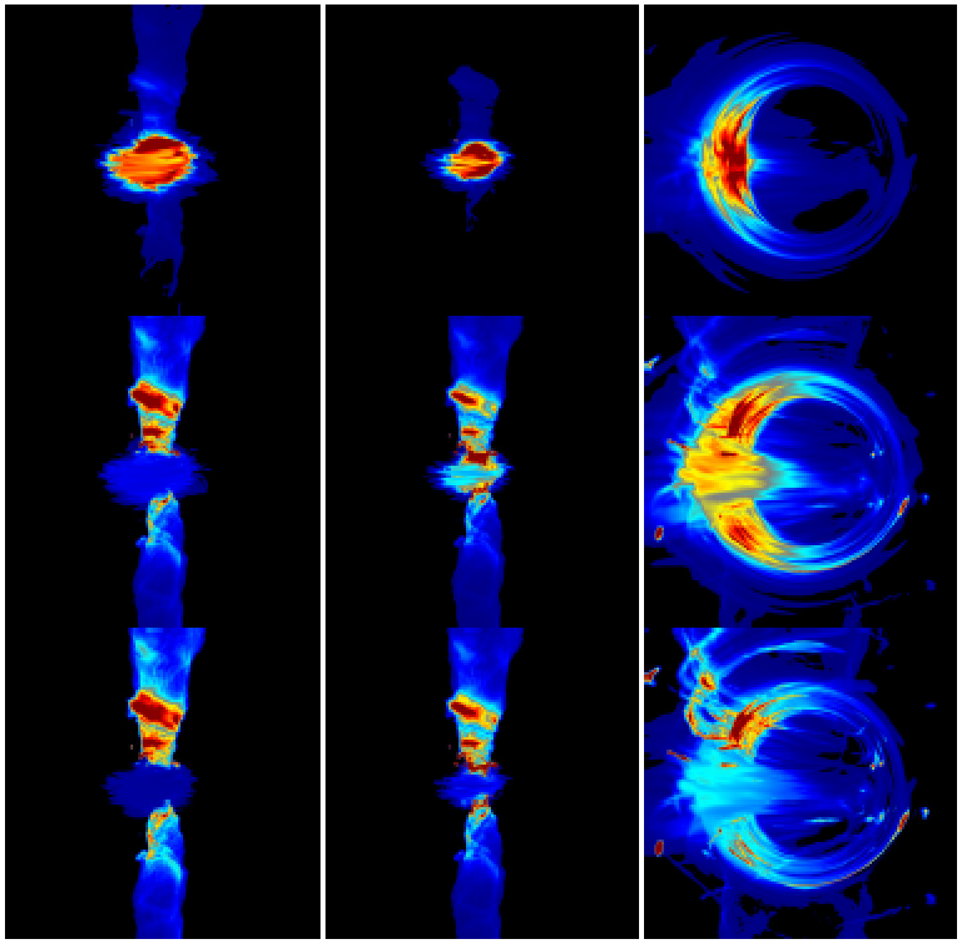

13 mm | 7 mm | 1.3 mm

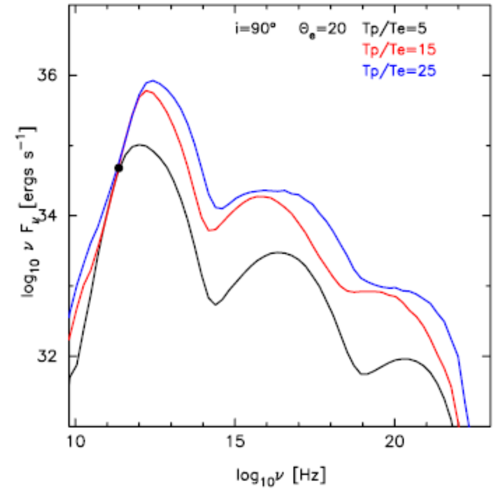

Jet:
const. E-Temp.

$$\frac{k_b T_e}{m_e c^2} = \Theta_{\rm e,j} = \text{const.}$$

Disk: proton
e-Temp. ratio

$$\frac{k_b T_e}{m_e c^2} = \left(\frac{k_b T_p}{\mu m_p}\right)\left(\frac{m_p}{m_e}\right)\frac{1}{(T_p/T_e)_{\rm disk}}$$

Moscibrodzka et al., A&A 570, A7, 2014

Nature of some SgrA* radio flares

7 mm VLBA

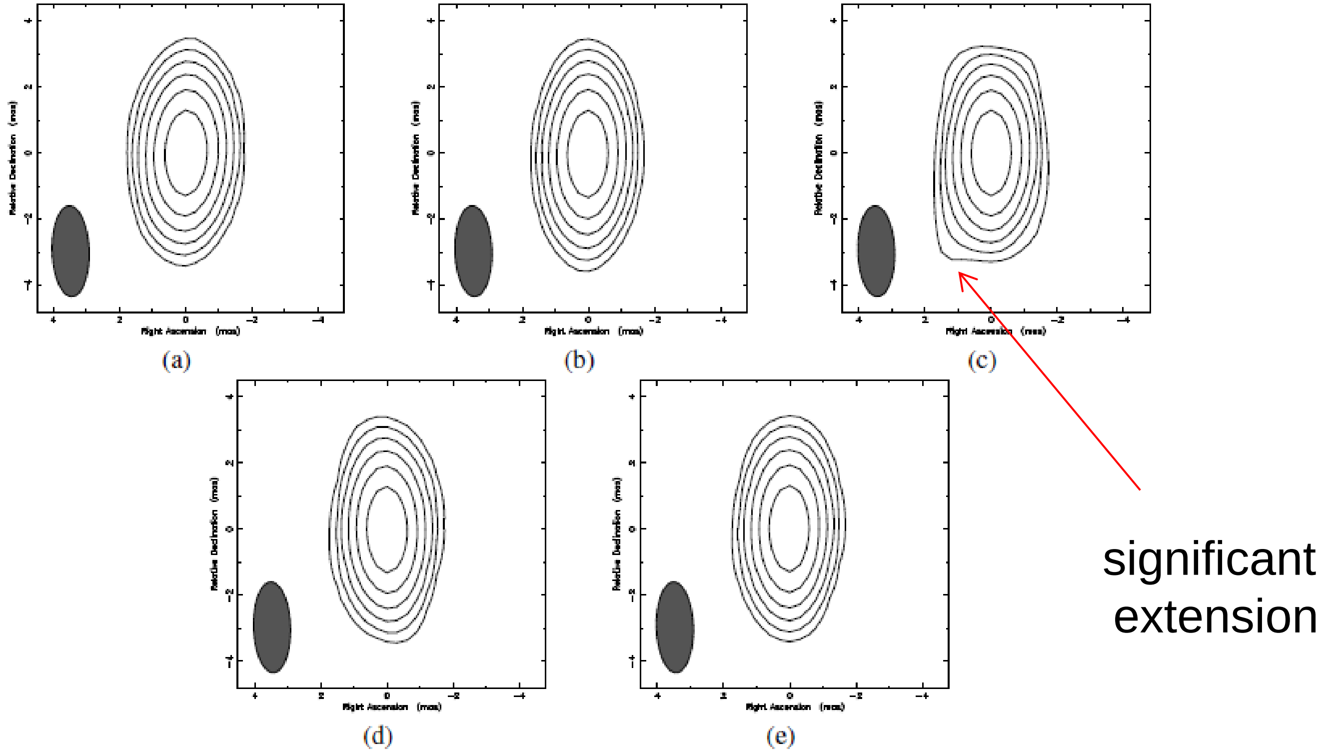

Fig. 5: 2 hour LCP maps of Sgr A* observed on May 17 2012. (a) May 17 6-8h. (b) May 17 7-9h. (c) May 17 8-10h. (d) May 17 9-11h. (e) May 17 10-12h. Summarized map parameters can be found in table 2.

Rauch et al. 2016

Nature of some SgrA* radio flares

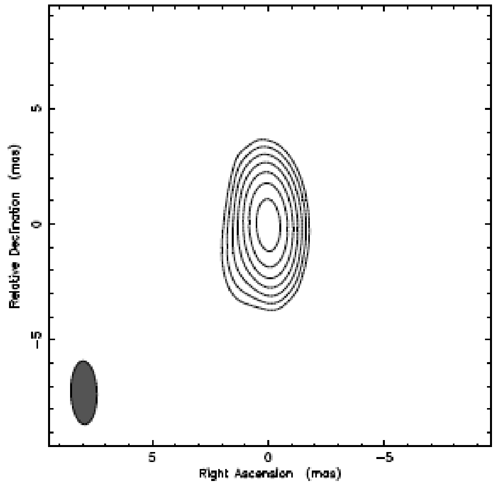

Fig. 7: RCP map of Sgr A* on May 17 2012 (8-10h UT). The map was convolved with a beam of 2.74×1.12 at 1.76°. Contour levels are 1, 2, 4, 8, 16, 32 and 64% of the peak flux density of 1.5 Jy/beam.

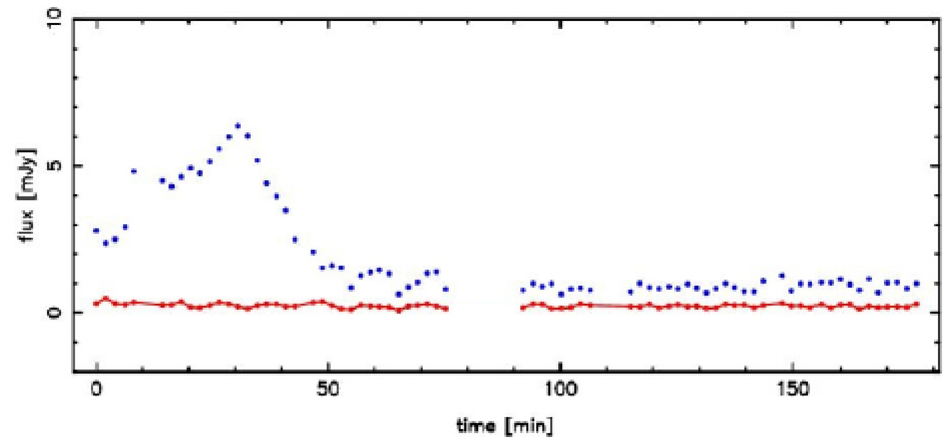

Fig. 3: NIR K_s-band (2.2 μm) light curve of Sgr A* observed in polarimetry mode on 17 May 2012. The light curve shown is produced by combining pairs of orthogonal polarization channels: 0° and 90° (taken from Shahzamanian et al. (2015)). Observations started at 4:55 AM UT.

Central component of 1.55 Jy secondary component of 0.02 Jy at 1.5 mas and 140 deg. E-N with a 4 hout delay relativ to the NIR flare

Bower et al. (2014) report major axis sizes of Sgr A* as an elliptical Gausssian of 35.4 × 12.6 R_S at an position angle of 95° east of north. Which is much lower than the discussed source morphology due to a secondary component of 0.02 Jy at 1.8±0.4 mas at 140° east of north.

Rauch et al. 2016

See also ‚Asyummetric structure in SgrA* …‘ Brinkerink et al. 2016, MNRAS 462, 1382 ‘speckle transfer function‘

Statistics of NIR light curves of SgrA*

Synchrotron radiation is responsible for flux density variations in the NIR – which can be studied there best – without confusion due to fluxes from the larger scale accretion stream.

Statistics of ongoing accretion

Measurements at 2 μm

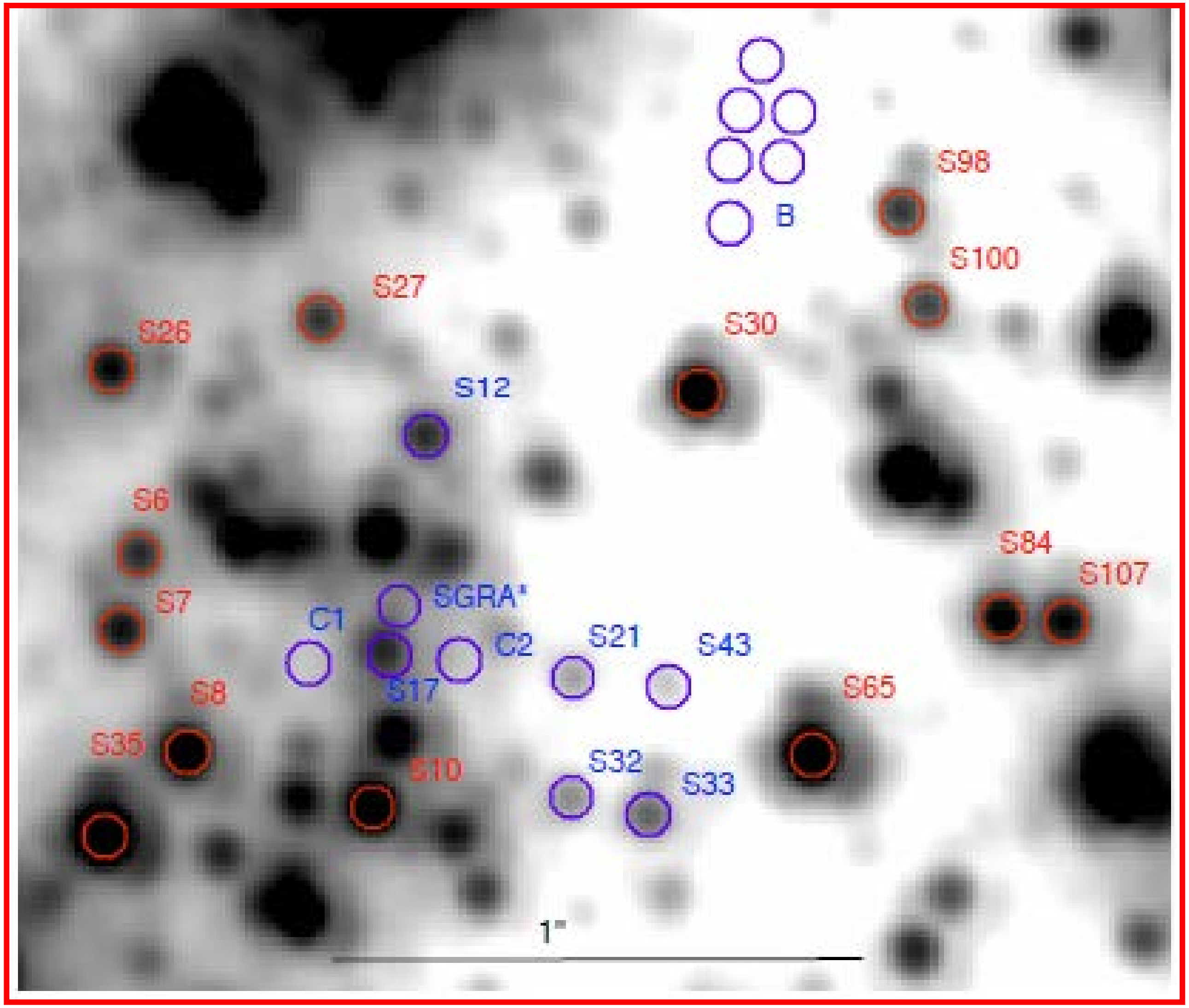

Apertures on
(1) SgrA*.
(2) reference stars,
(3) and off-positions

Ks-band mosaic from 2004 September 30. The red circles mark the constant stars (Rafelski et al. 2007) which have been used as calibrators, blue the position of photometric measurements of Sgr A*, comparison stars and comparison apertures for background estimation (Witzel et al. 2012).

Witzel et al. 2012

NIR light curve of SgrA* over 7 years

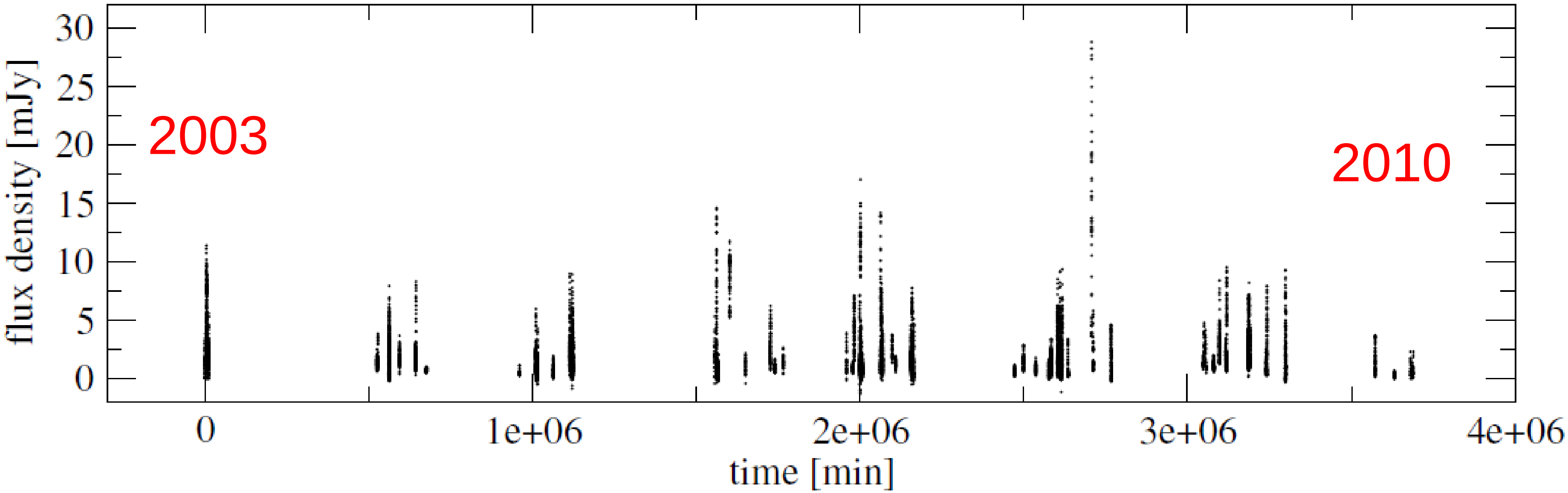

Light curve of Sgr A*. Here no time gaps have been removed, the data is shown in its true time coverage. A comparison of both plots shows: only about 0.4% of the 7 years have been covered by observations.

Witzel et al. 2012

Flux density histogram for SgrA*

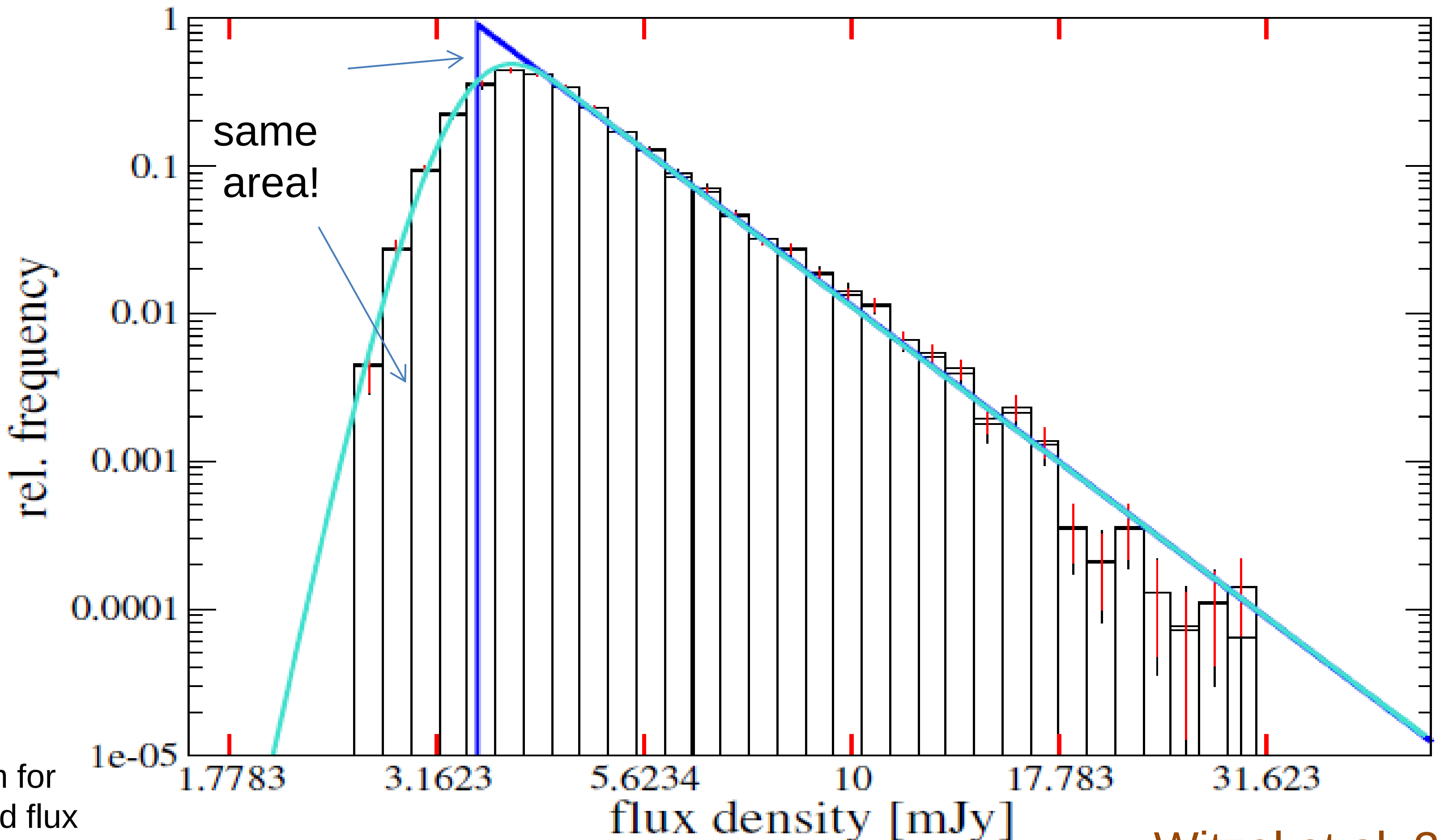

Diagram for polarized flux in work

Witzel et al. 2012

The brown line shows the extrapolation of the best power-law fit, the cyan line the power-law convolved with a Gaussian distribution with 0.32 mJy width.

The statistics allows to explain the event 400 years ago that results in the observed X-ray light echo

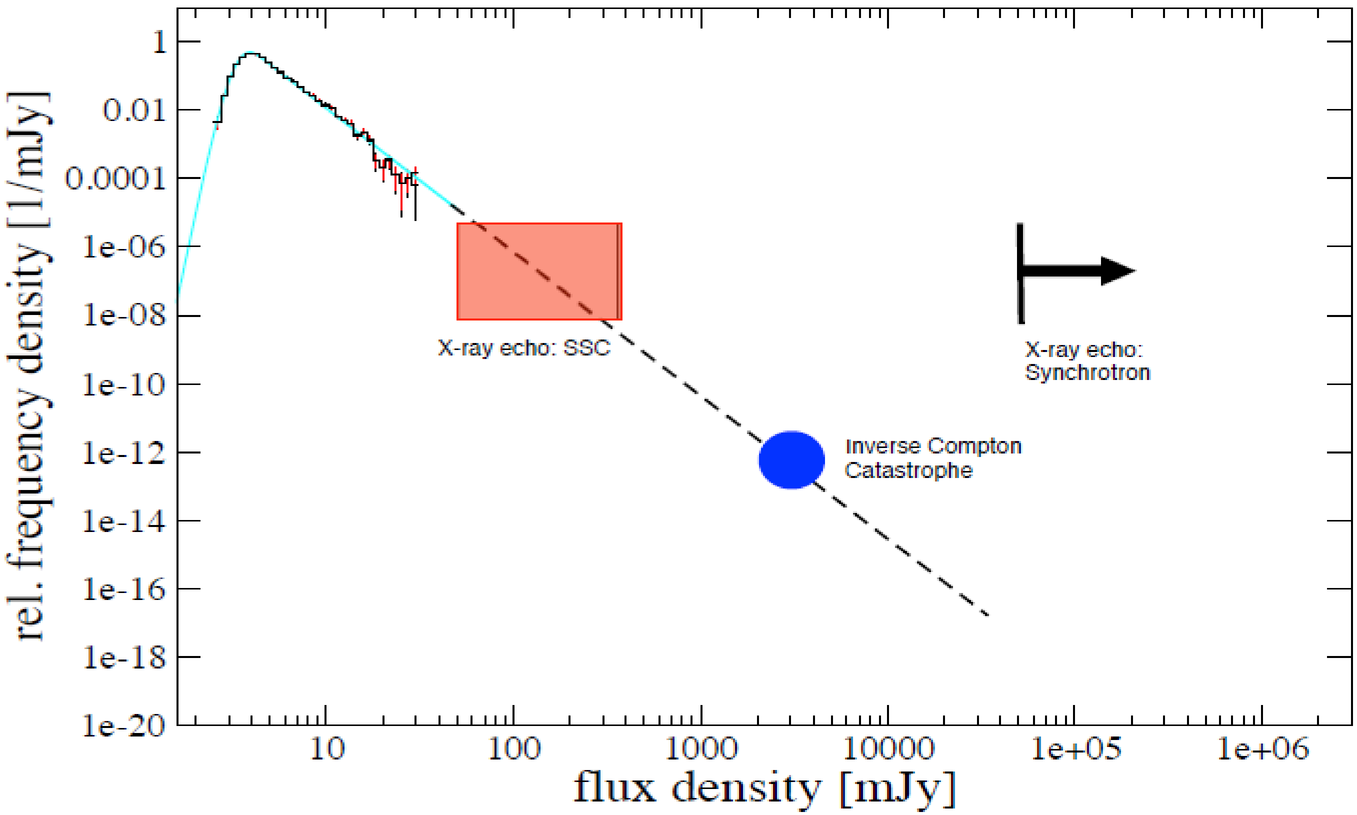

Fluorescent back-scatter from molecular clouds surrounding the GC:

Revnivtsev et al. 2004,
Sunyaev & Churazov 1998,
Terrier et al. 2010

and

Witzel et al. 2012

Illustration of a flux density histogram extrapolated from the statistics of the observed variability. The expected maximum flux density given by the inverse Compton catastrophe and a estimation of its uncertainty is shown
as the magenta circle, the SSC infrared flux density for a bright X-ray outburst as expected from the observed X-ray echo is depicted as the red rectangular.

NIR Polarized Light Curves of SgrA*

Probing the geometry of ongoing accretion through polarization measurements

Precision of NIR Polarization measurements

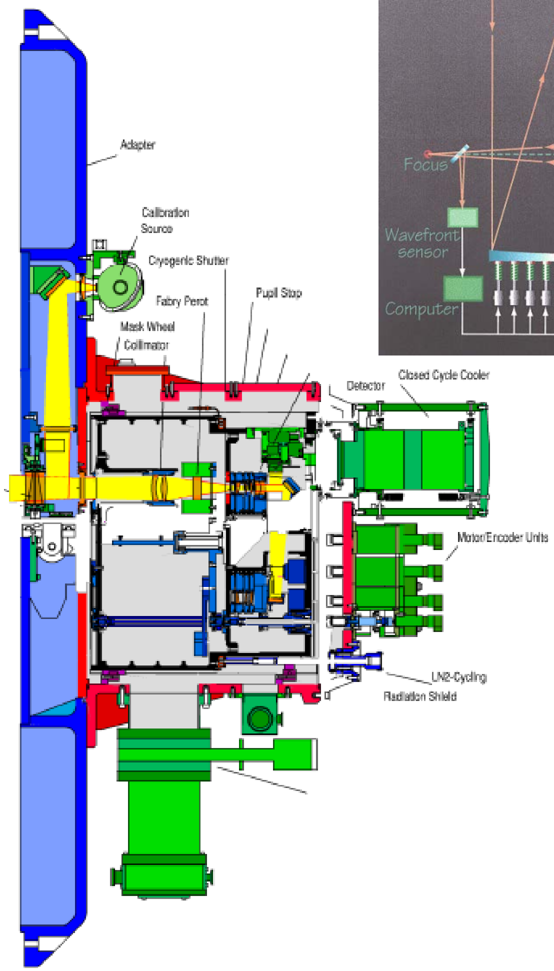

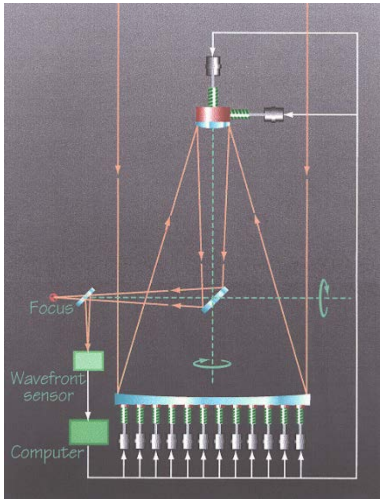

Instrument calibrated to ~1%
limited by systemetic effects: ~3-4%

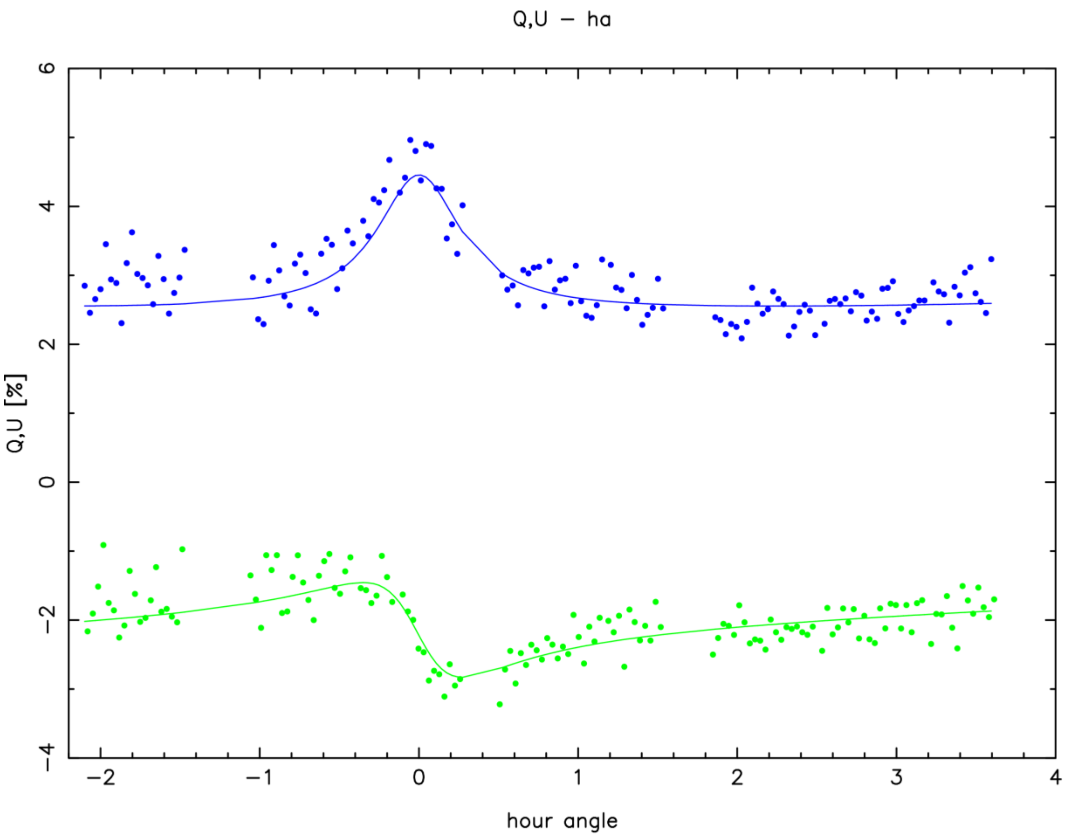

Witzel et al. 2011, A&A 525, 130

Polarized light from SgrA* in the NIR K-band

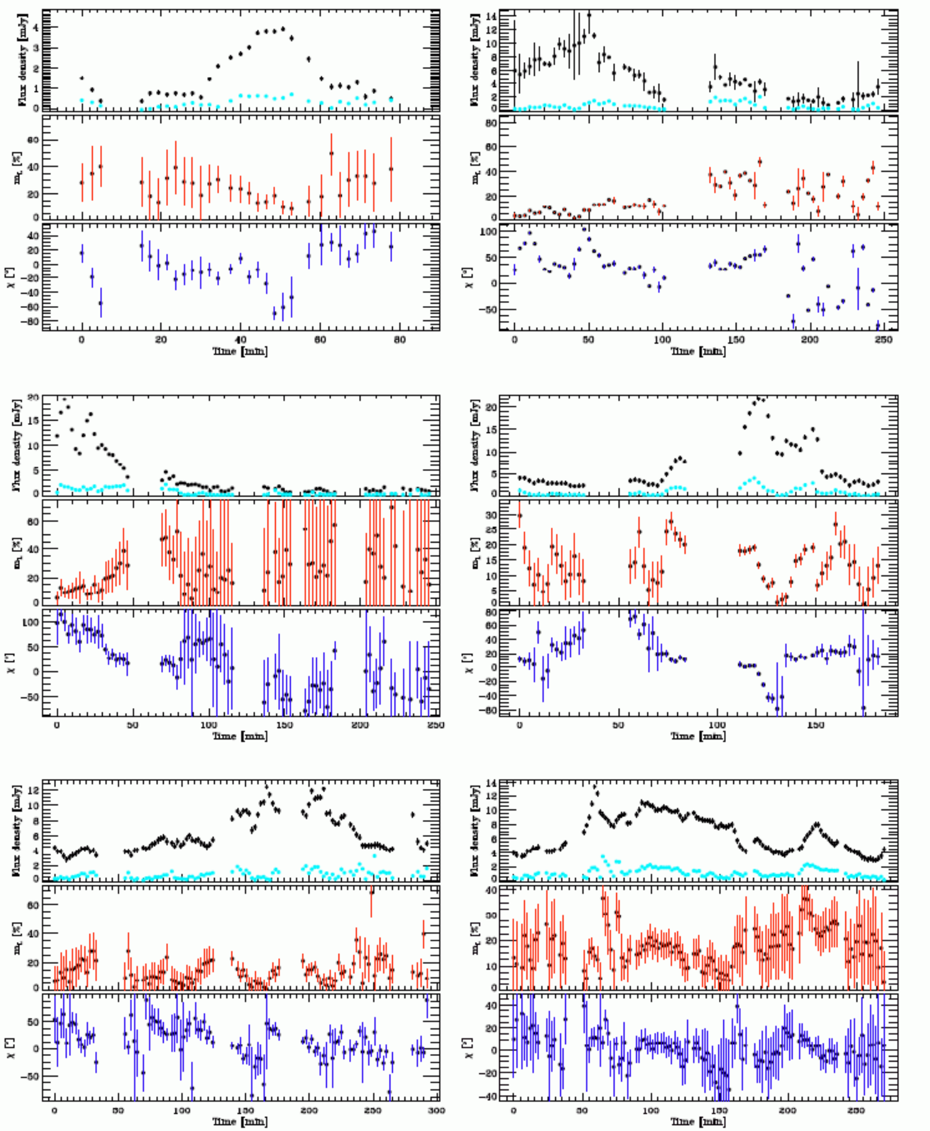

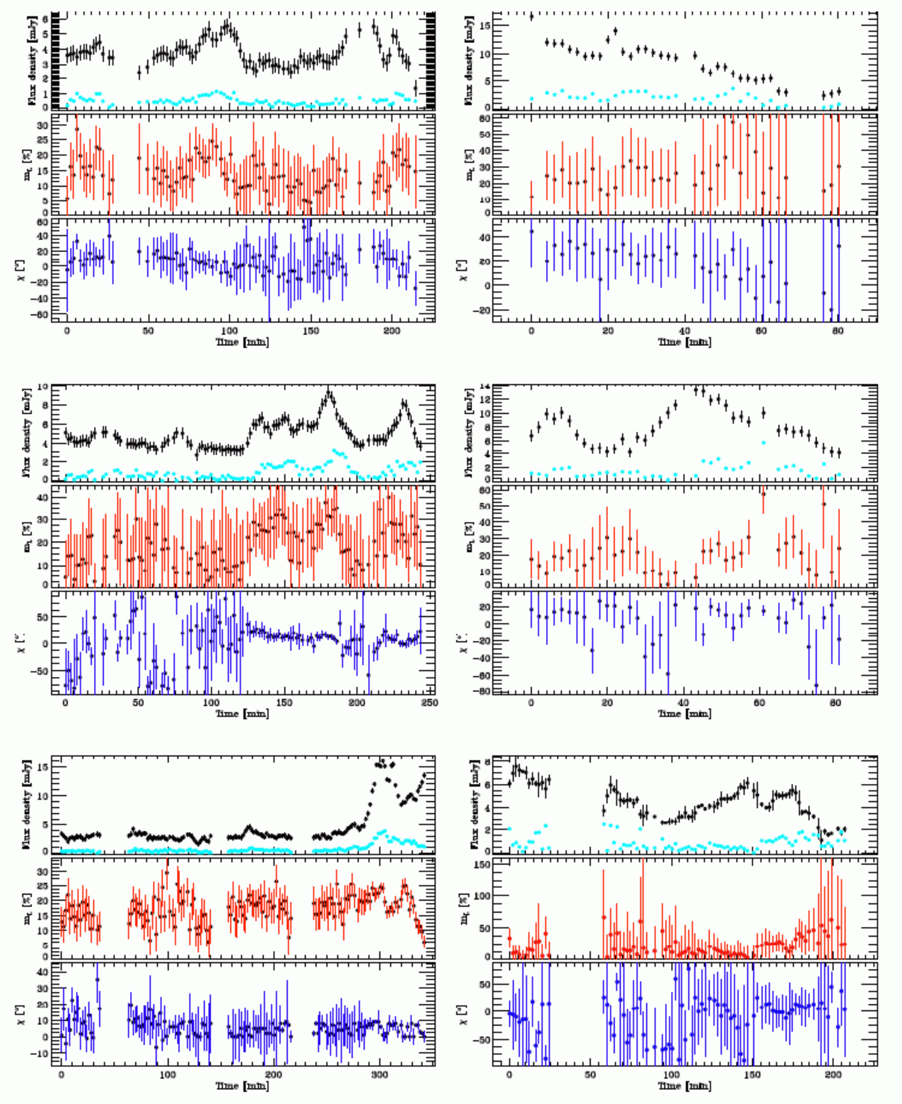

Polarization degree and angle

Degree

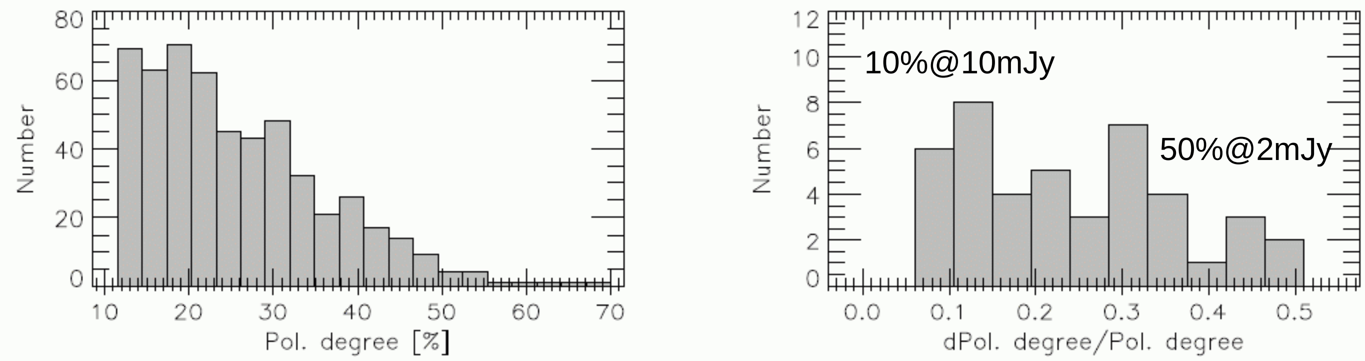

Fig. 8: Left: Distribution of K_s-band polarization degrees of Sgr A* for our data set considering the significant data points (based on Table 2). Right: Distribution of relative uncertainties of the polarization degrees.

Angle

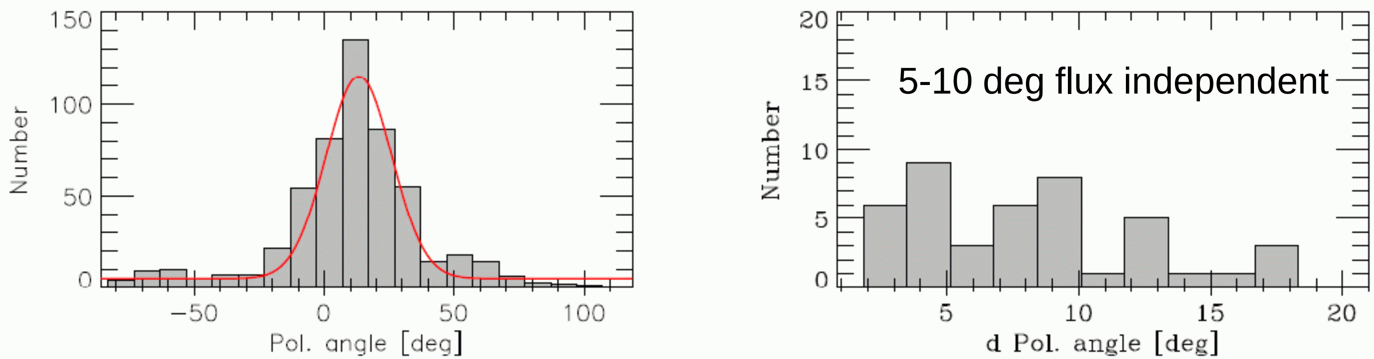

Fig. 9: Left: Distribution of significant K_s-band polarization angles of Sgr A*. The red line shows the fit with a Gaussian distribution. Right: Distribution of absolute errors of the polarization angles.

SgrA* - Stable Geometry and Accretion

SgrA* is a stable system

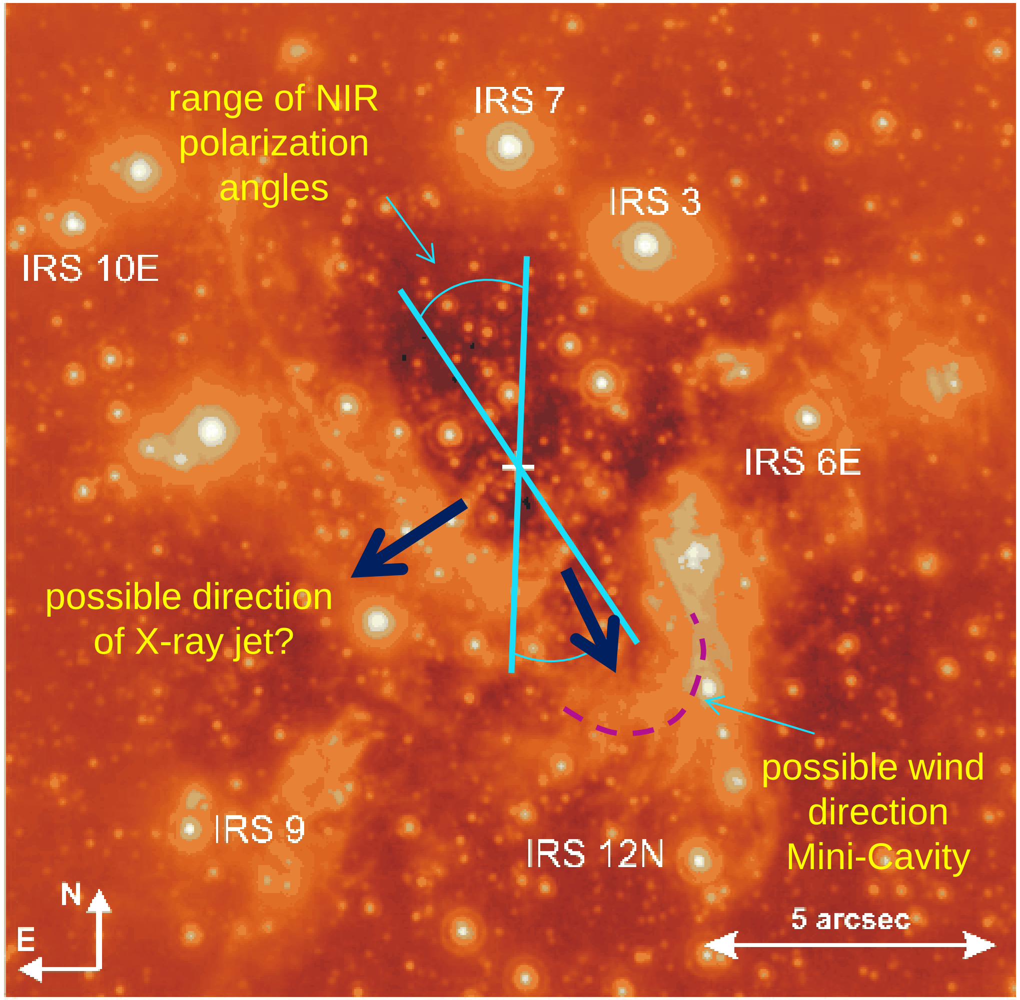

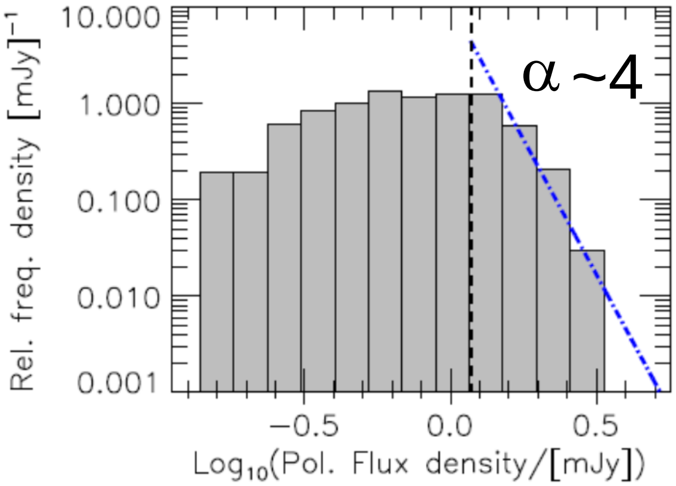

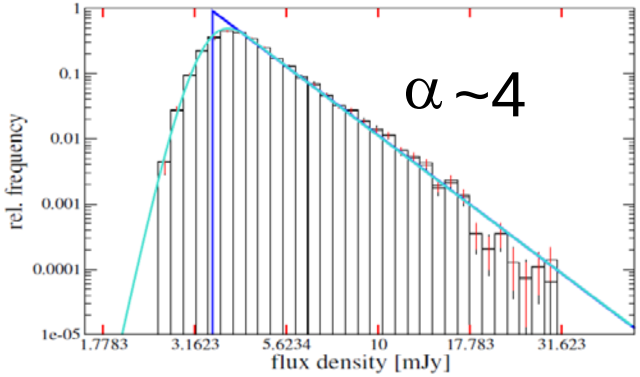

Synchrotron and synchrotron self-Compton modeling the NIR/X-ray flares of SgrA*

Basic physics of accretion;
Emission process and spectrum

Radiative Models of SGR A* from GRMHD Simulations

MOTION IN
OR CLOSE TO
THE MIDPLANE

relativistic effects
may become
observable here

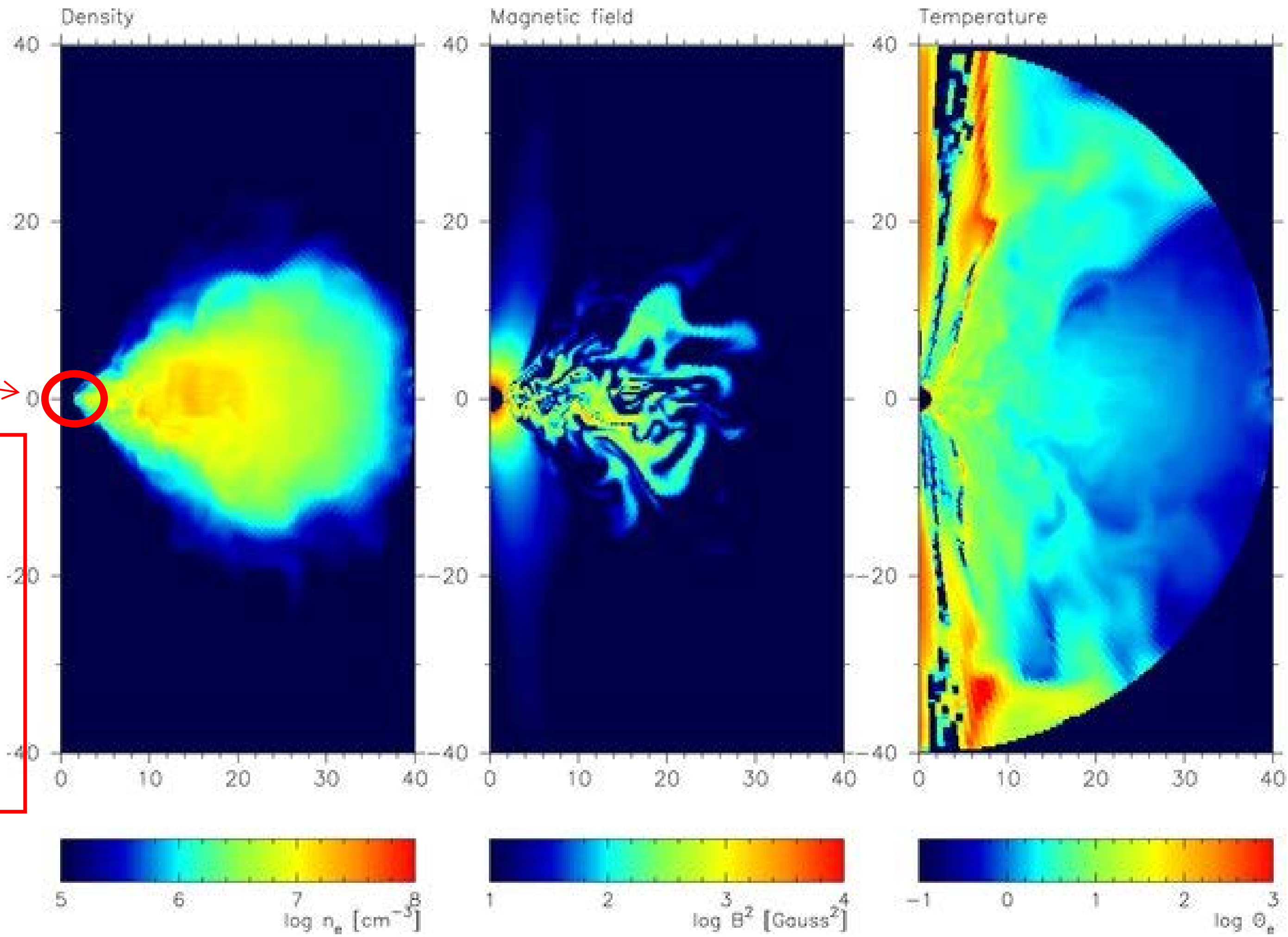

Accretion of matter onto SgrA* results in a variable spectrum

Mościbrodzka+ 2010, 2009
Dexter+ 2010

Flare Emission from SgrA*

Recent work on SgrA* variability

Radio/sub-mm:
Mauerhan+2005, Marrone+2006/8,
Yusef-Zadeh+2006/8 and may others

X-ray:
Baganoff+2001/3, Porquet+2003/2008,
Eckart+2006/8, and several others

NIR:
Genzel+2003, Ghez+2004, Eckart+2006/9,
Hornstein+2007,Do+2009, and many others

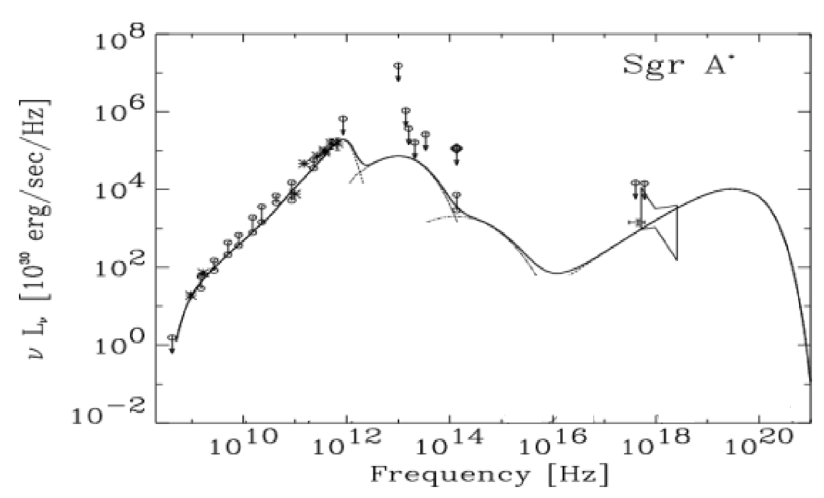

Multi frequency observing programs:
Genzel, Ghez, Yusef-Zadeh, Eckart and many others

Questions:

- What are the radiation mechanisms?
- How are the particles accelerated?
- (How) Are flux density variations at different wavelength connected to each other?

Possible flare scenarii

Possible flare models

NIR X-ray

SYN-SYN: Synchrotron-synchrotron

SYN-SSC: Synchrotron-Self-Compton

SSC-SSC: Self-Compton-self-Compton

Parametrization of the logarithmic expression

Two extreme cases:
High demands on electron acceleration or density

SYN-SYN: X-ray produced by synchrotron radiation;
<10% by SSC

$n_e \approx 10^6 cm^{-3}$ $\gamma_e \approx 10^{6-7}$

SSC-SSC: X-ray produced by synchrotron self-Compton;
<10% by SYN; required density higher than average

$n_e \geq 10^8 cm^{-3}$

Moderate demand on density and acceleration

SYN-SSC: radio/NIR by Syncrotron and X-ray by SSC

$n_e \approx 10^6 cm^{-3}$ $\gamma_e \approx 10^{3-4}$

Radiative Models of SGR A* from GRMHD Simulations

In the mid-plane the vertical particle distribution is well described by a Gaussian, with a dimensionless scale height of about 0.1-0.3 (1 σ).

DENSITIES CLOSE TO THE MIDPLANE WILL BE HIGHER THAN AVERAGE

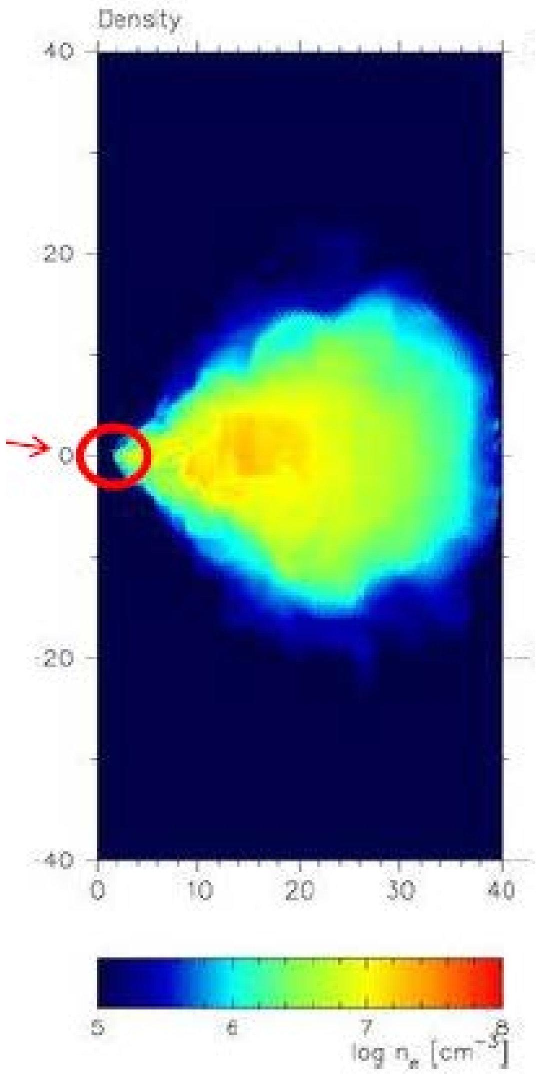

However, the thickness (and hence the mid-plane density) is mostly determined by the initial conditions and energy evolution methods used in the simulations rather than by the physics of the accretion flow.

Collisionless Shocks

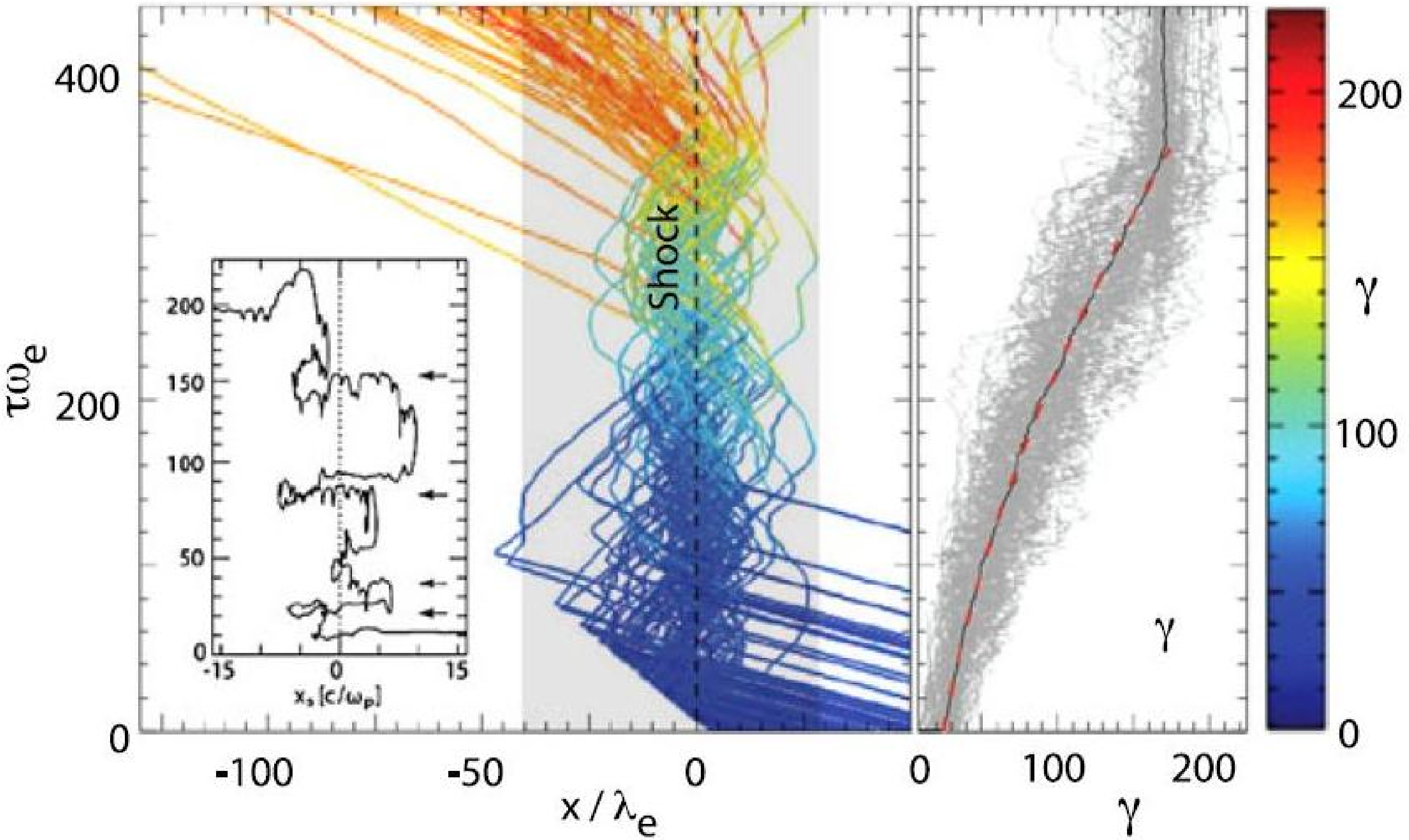

Left: Time-evolution of the orbits of the 80 most energetic ions in a non-magnetized relativistic shock simulation with $\Gamma = 20$. The particles are coming from the upstream flow, are back-scattered and accelerated in the magnetic turbulence in the shock transition, staying within the distance of an ion inertial length $\lambda i \approx 50\lambda e$.

Bykov & Treumann, 2011, Astr. Astro. Rev. 19, 42

Radiative Models of SGR A* from GRMHD Simulations

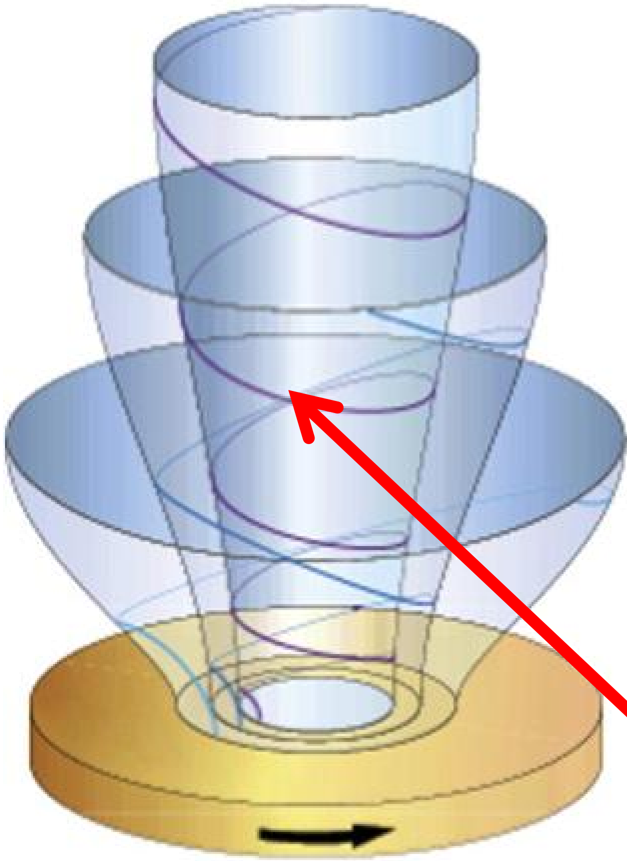

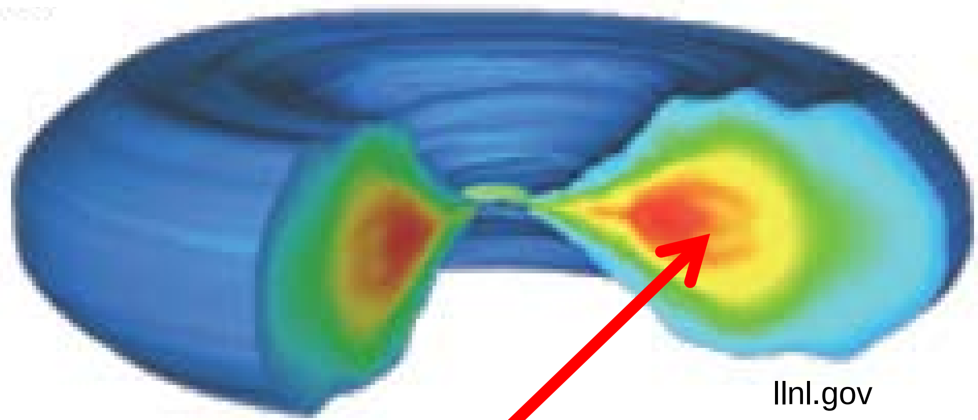

llnl.gov

Jonathan Ferreira, Remi Deguiran,
High Energy Density Physics
Volume 9, Issue 1, March 2013, Pages 67–74

Possible locations of electron accelerating collisionles shocks in the immediate vicinity of SgrA*.

Accretion of field dominated flare?

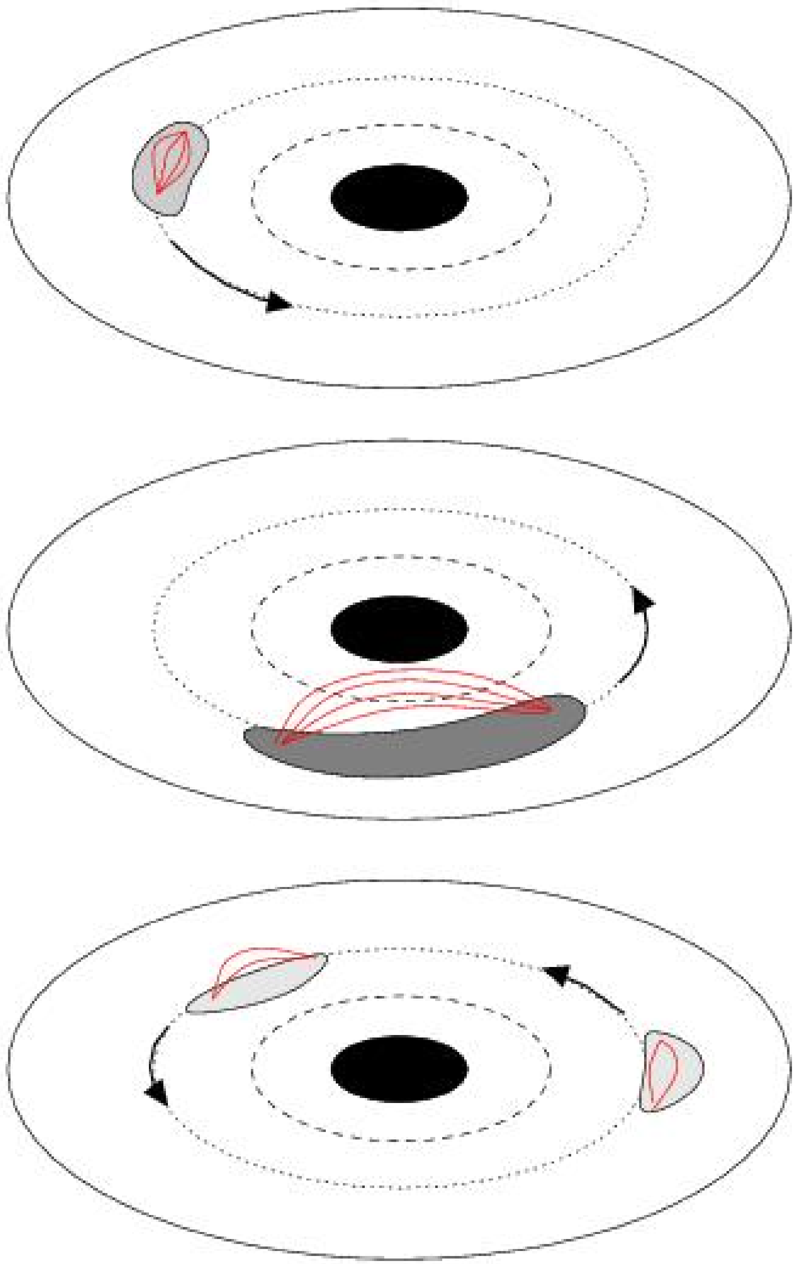

Yuan et al. 2009, Balbus & Hawley 1998, Balbus 2003

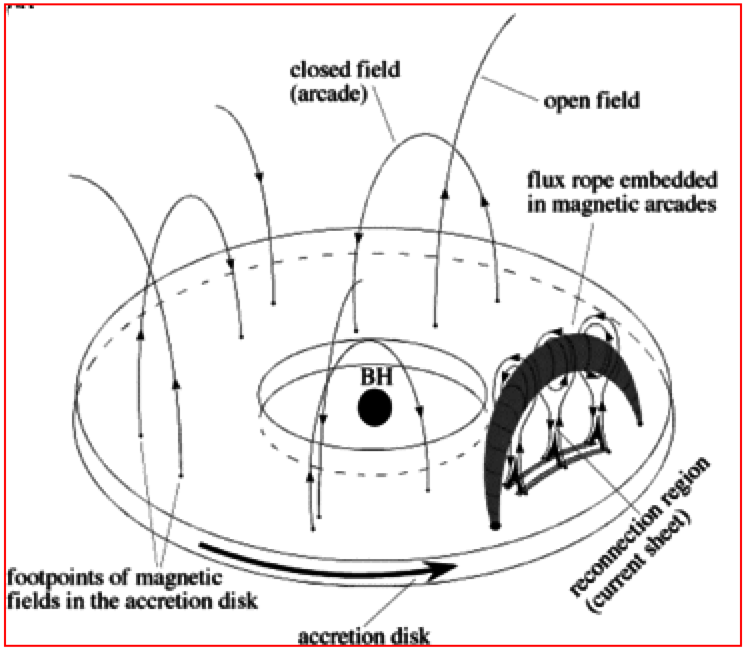

Yuan et al. 2009

Adiabatic Expansion of Source Components in the Temporary Accretion Disk of SgrA*

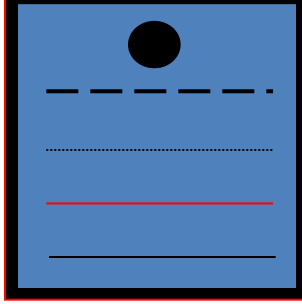

Black Hole
Last stable orbit
reference orbit
magnetic field lines
outer edge of disk

Eckart et al. 2008, ESO Messenger
Eckart et al. 2009, A&A 500, 935

Variability in the SYN-SSC case

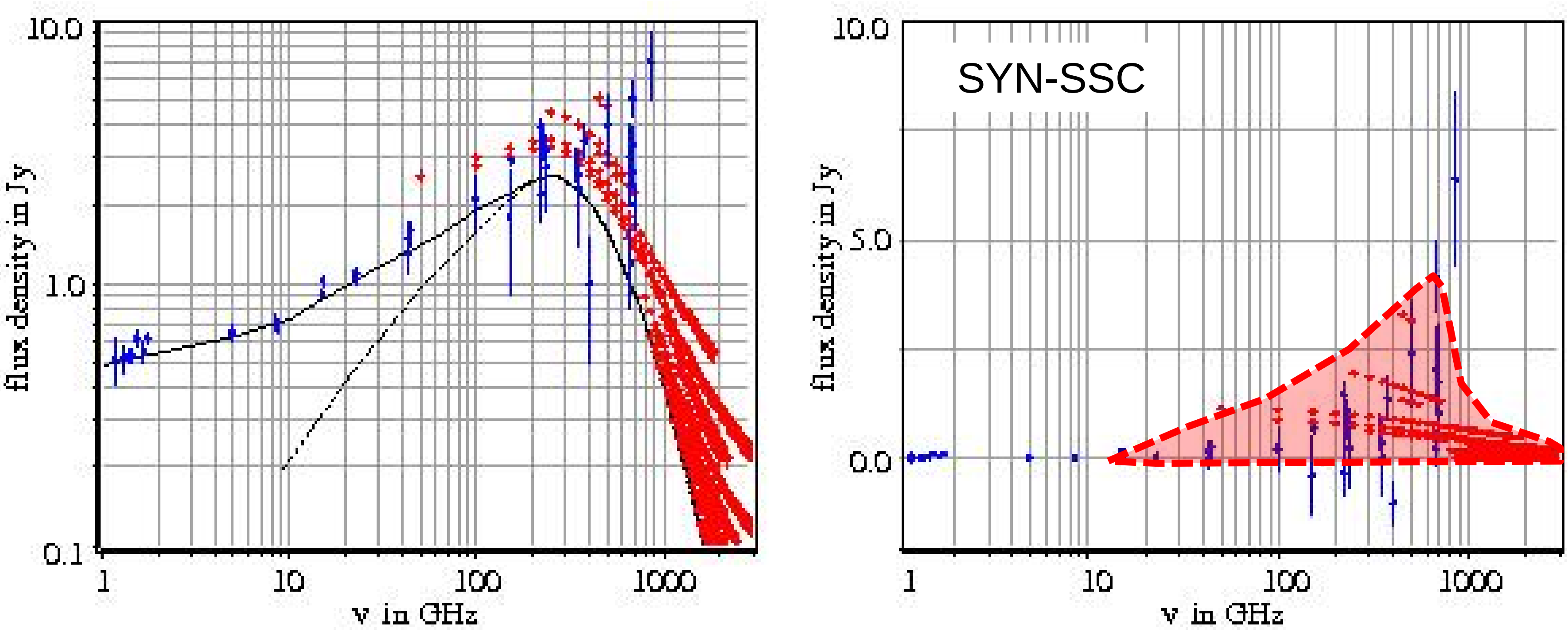

$$n_e \approx 10^6\, cm^{-3}$$

$$\gamma_e \approx 10^{3-4}$$

SYN-SSC: Density moderate
consistent with MHD model of mid-plane
Moderate demand on electron acceleration

Eckart et al. 2012

Monitoring the DSO (G2)

Externam influences on the of accretion
(possible enhancement ?)

Monitoring the Orbit of the DSO

Eckart, A., et al., 2014 ATel
Valencia-S., M., et al. 2015, ApJ 800, 125
Zajacek, Karas, Eckart, 2013, A&A 565, 17
Eckart et al. 2013, A&A 551, 18
Peissker et al. 2016 in prep

Zajacek, M.; Eckart, A.; Karas, V.; Kunneriath, D.; Shahzamanian, B.; Sabha, N.; Muzic, K.; Valencia-S., M. 2016, MNRAS 455,1257

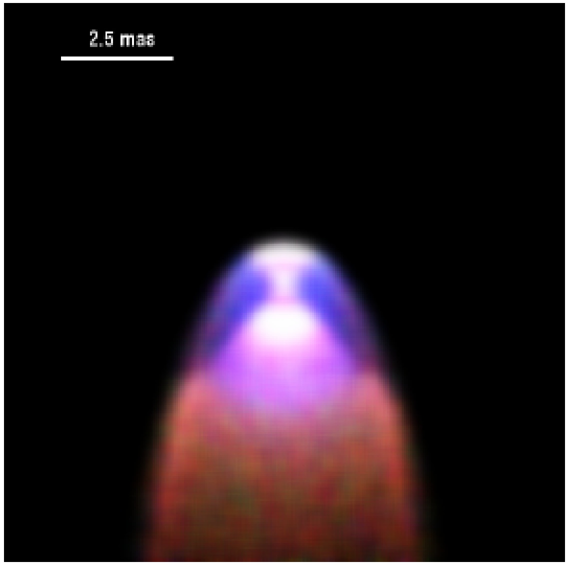

Dusty S-cluster Object(DSO/G2)

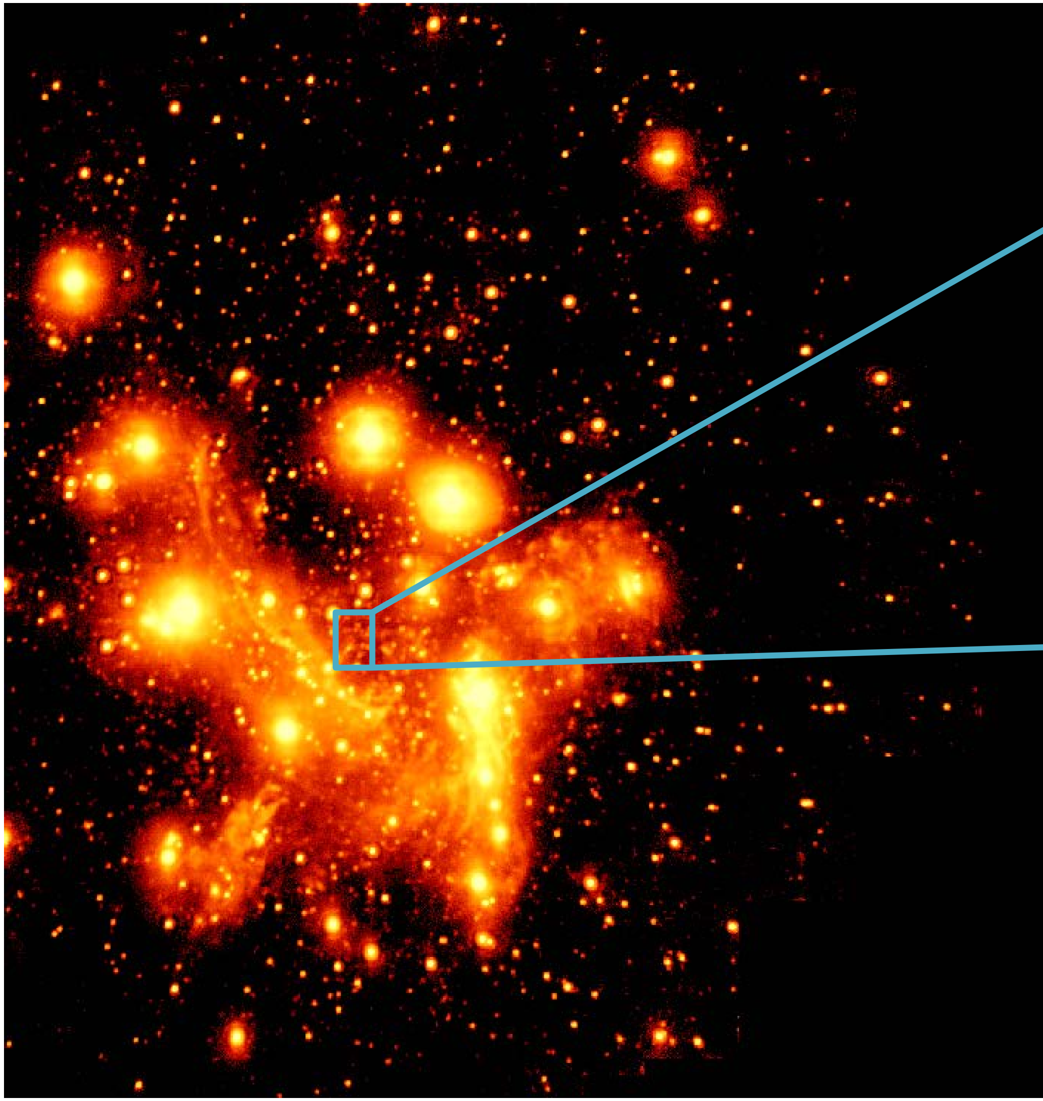

GC in L-Band. Courtesy: N. Sabha/Uni. of Cologne

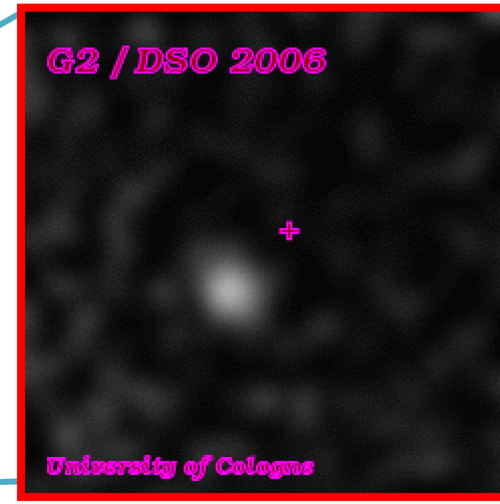

Gillessen et al. 2012,2013a,b; Eckart et al. 2013a,b; Phifer et al. 2013; Pfuhl et al. 2014; Burkert et al. 2012; Schartmann et al. 2012; Witzel et al. 2014; Valencia-S. et al. 2015; Zajacek, Karas, Eckart 2015… ...

DSO/G2 Approaching SgrA*

Gillessen et al. 2012/13
Burkert et al. 2012,
Schartmann et al. 2012

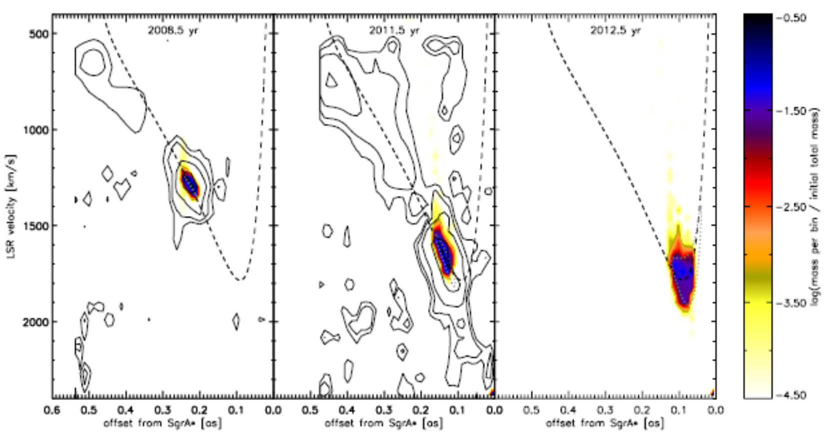

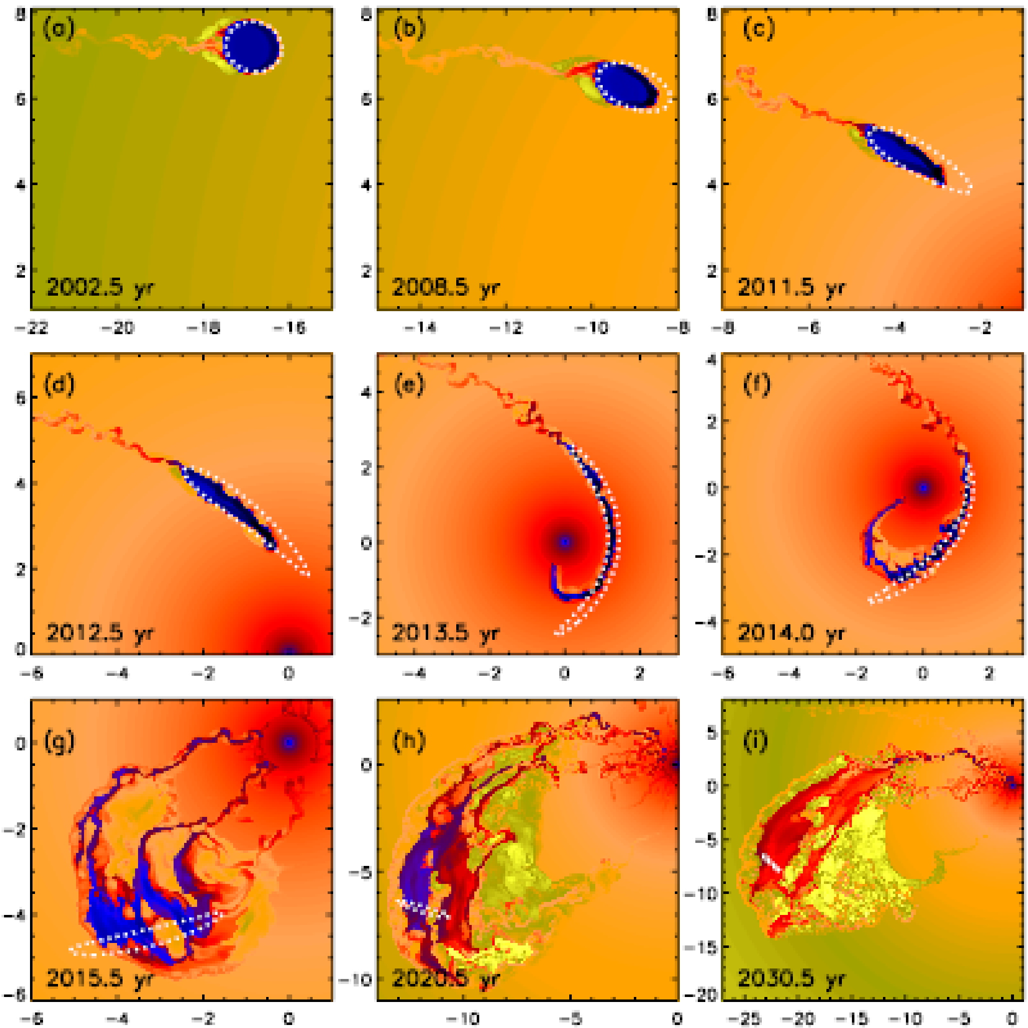

DSO/G2 has survived its closest approach to SgrA*

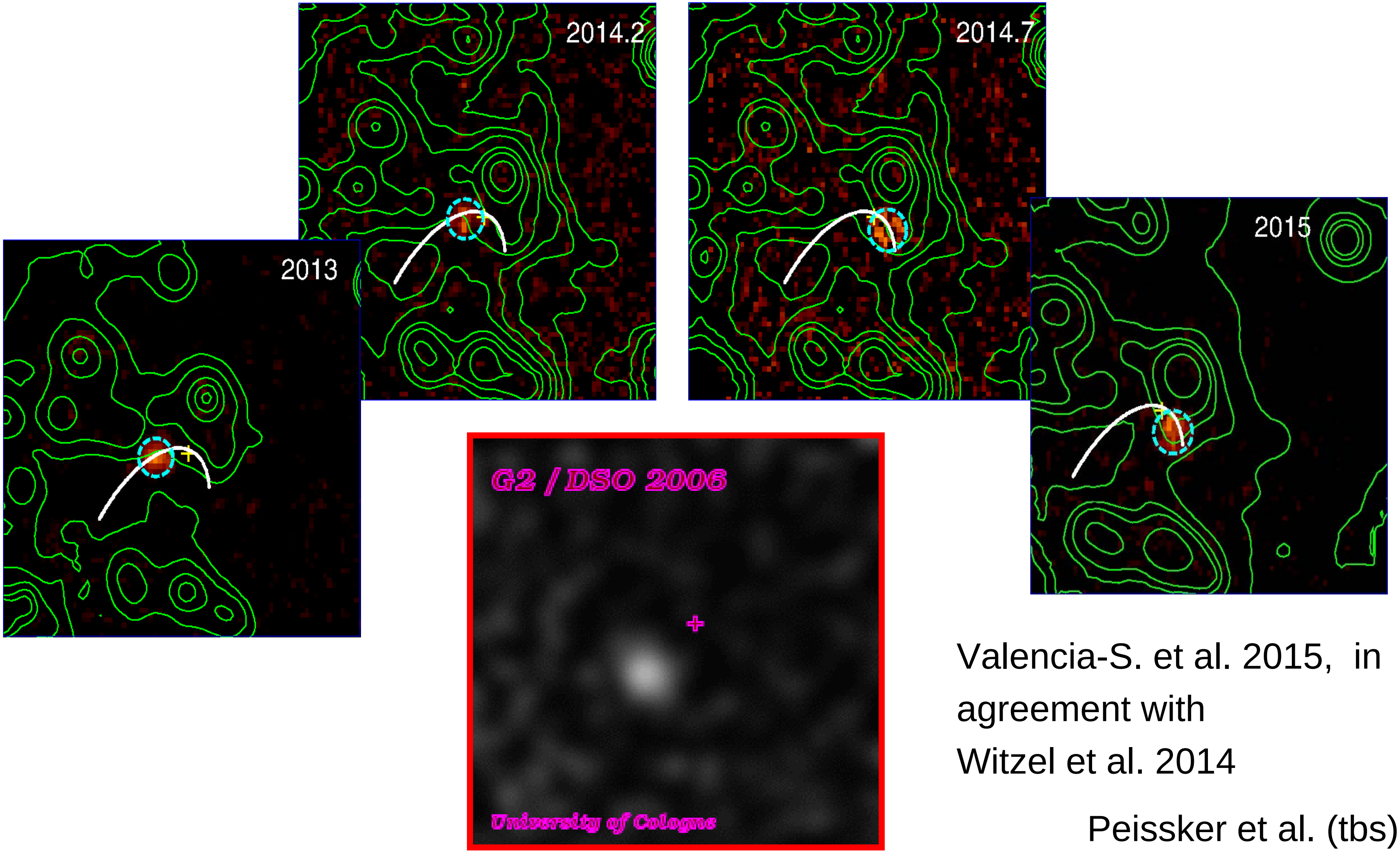

Valencia-S. et al. 2015, in agreement with Witzel et al. 2014

Peissker et al. (tbs)

Brγ line maps of the DSO

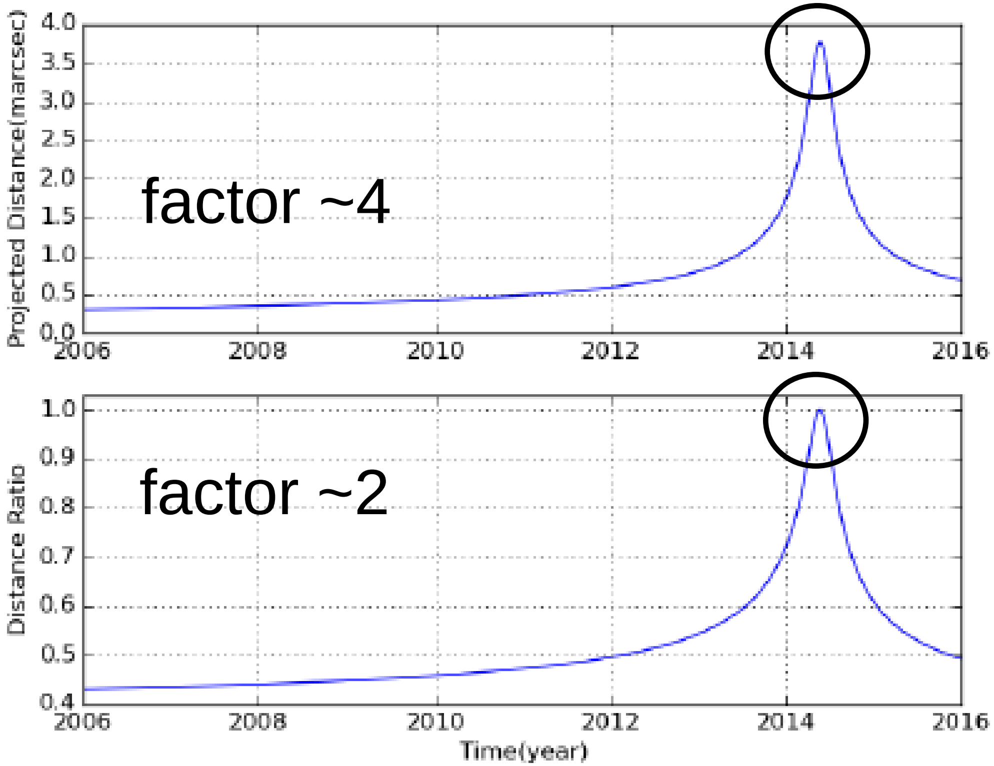

Orbital projection effects: Top: The evolution of the projected separation between two neighboring points of arbitrary 0.5 units in 2011. Bottom: Foreshortening factor of any structure along the orbital extent as a function of time.

During periapse the source is seen at its full size

Both Brγ and L-band continuum originate from a <20mas compact source

Valencia-S. et al. 2015 ApJ

DSO/G2 emits K-band continuum

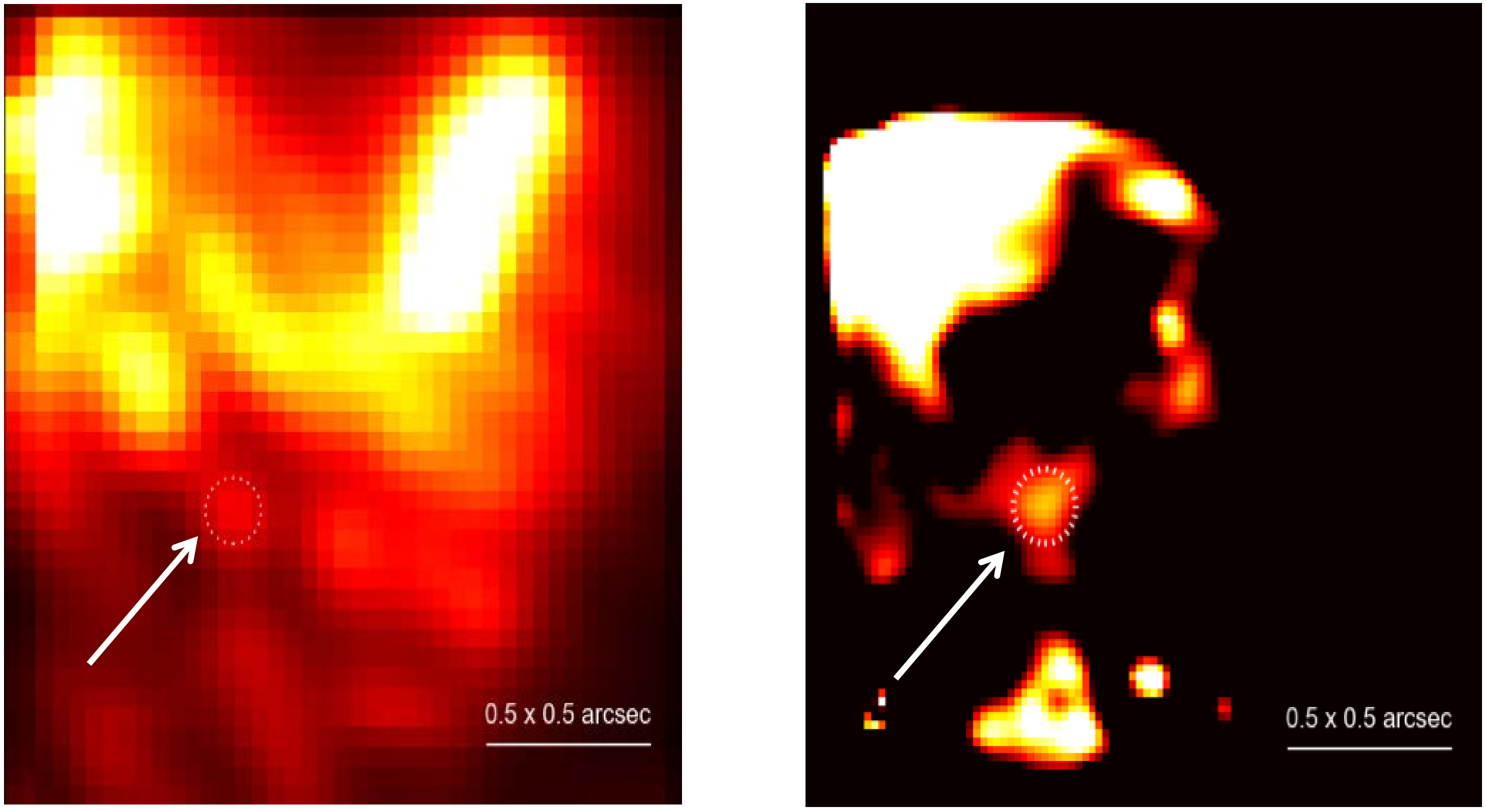

2006-2015 recentered at the DSO position and combined

Eckart et al. 2013

DSO/G2 orbit

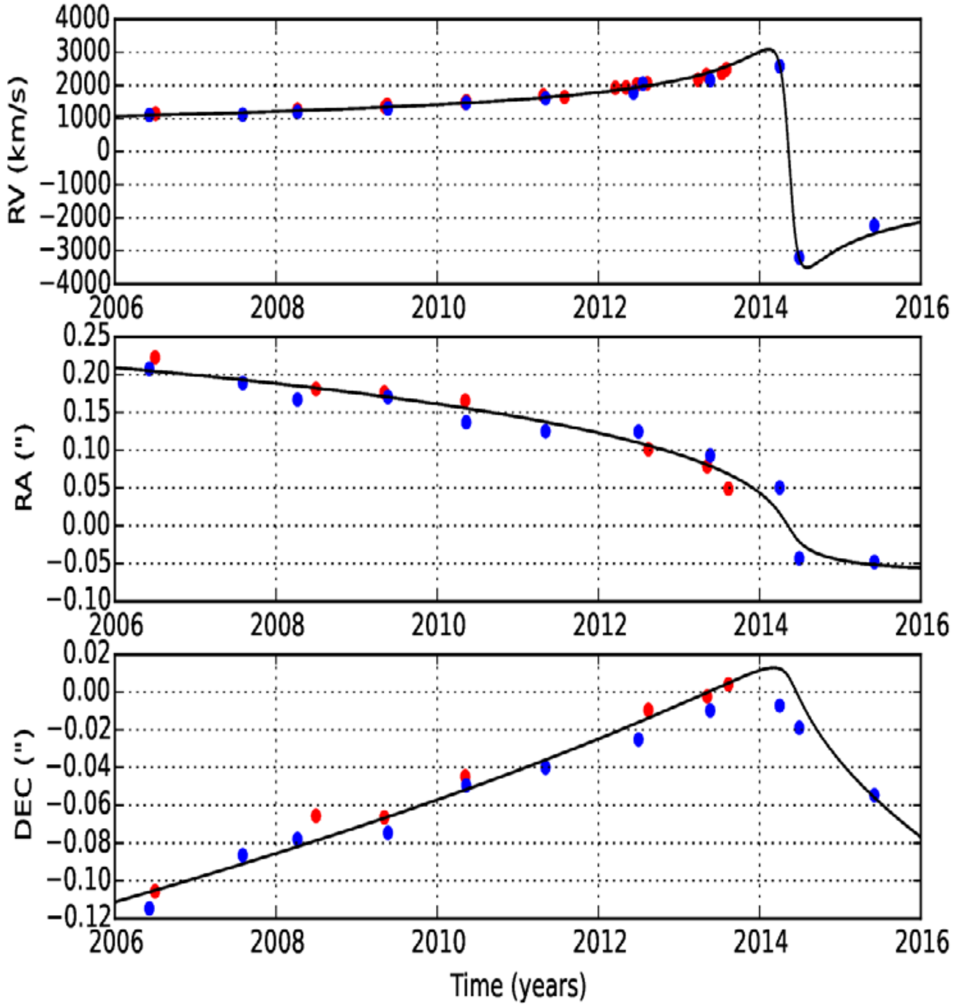

e=0.976

Pericenter distance: 163 AU

in agreement with Pfuhl et al. 2015; Phifer et al. 2013; Meyer et al. 2014b

Discovery of a new faint Dusty S-cluster member: OS1

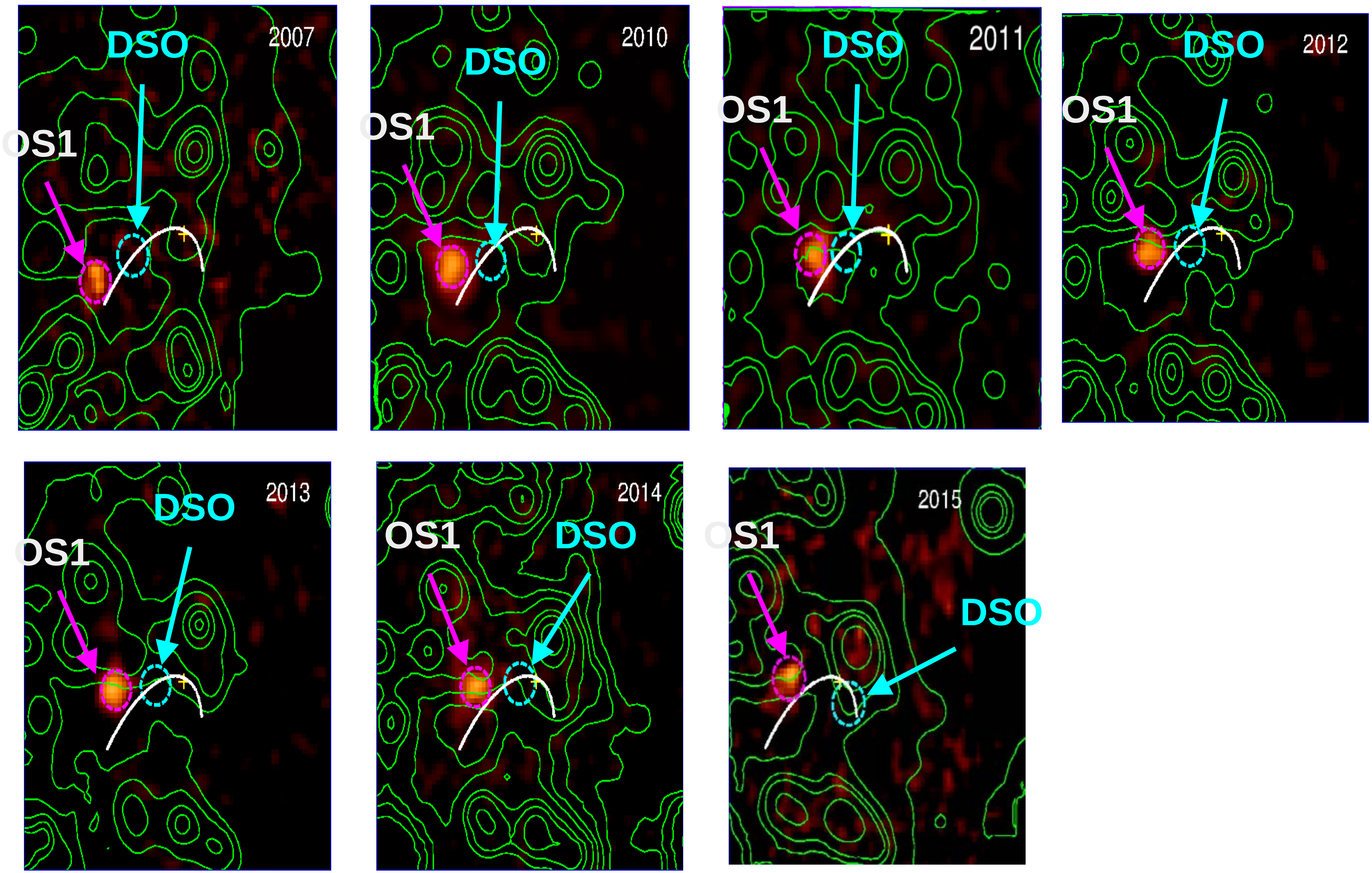

OS1 does not follow the DSO trajectory

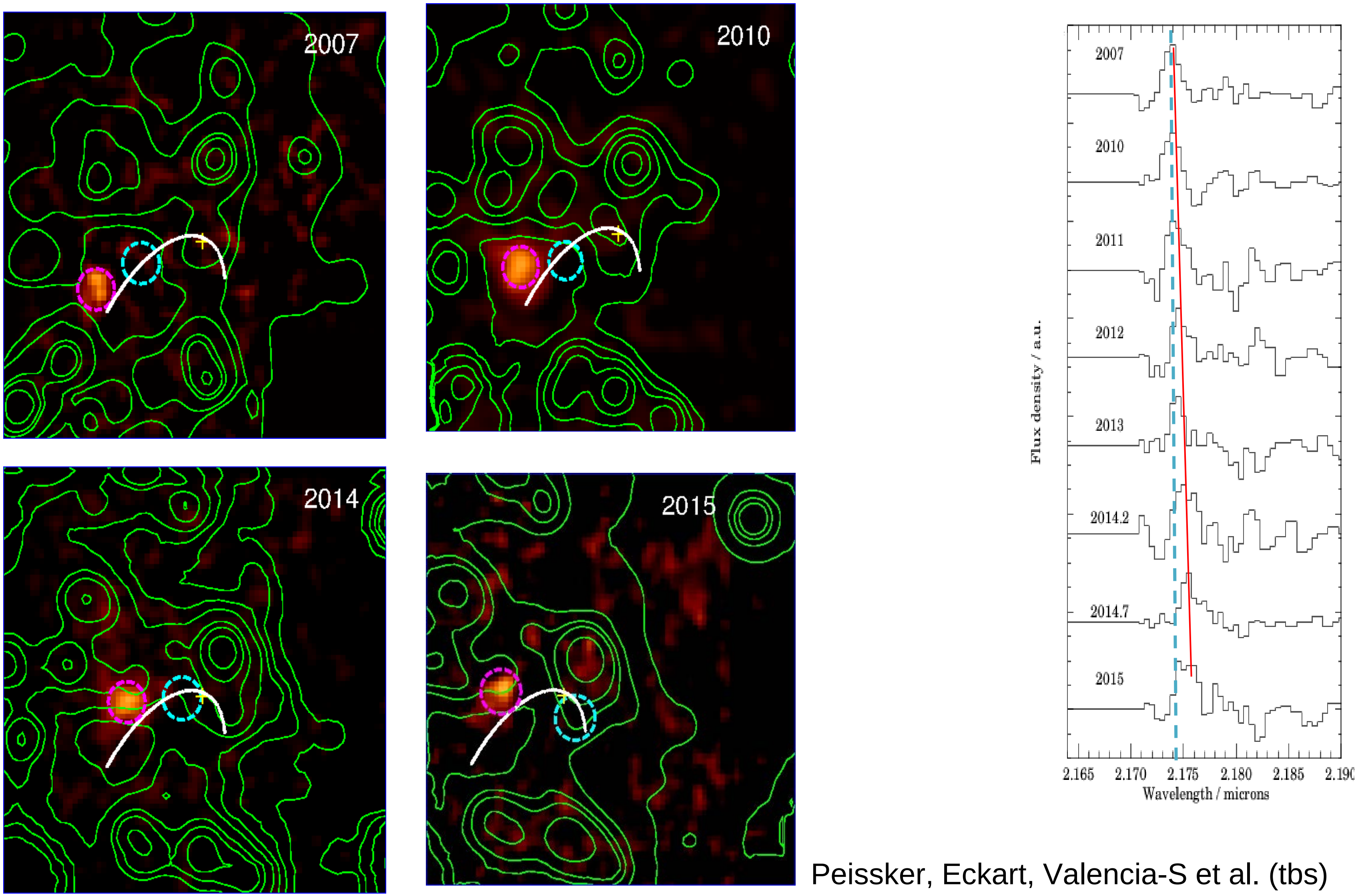

Peissker, Eckart, Valencia-S et al. (tbs)

OS1 does not follow the DSO trajectory

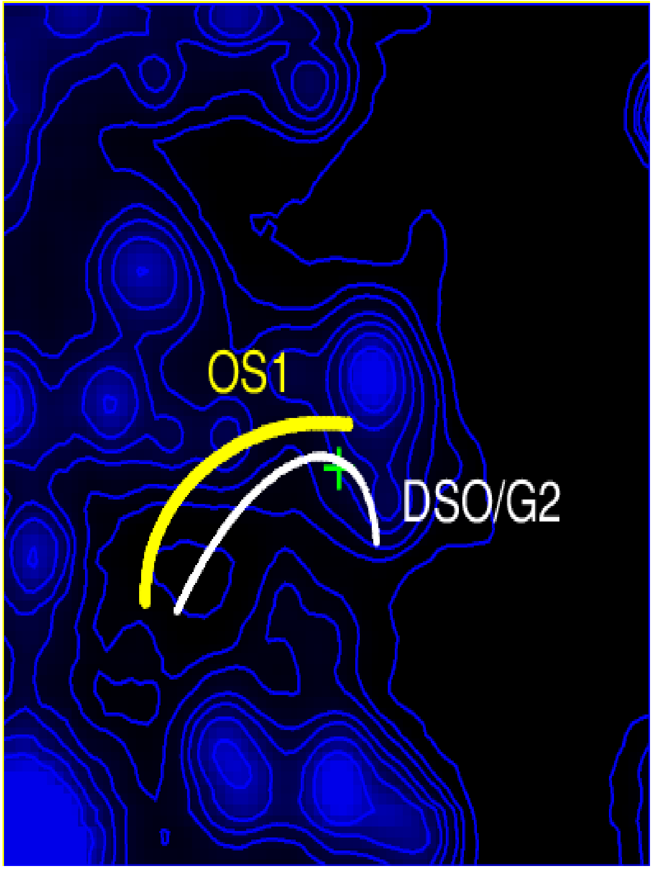

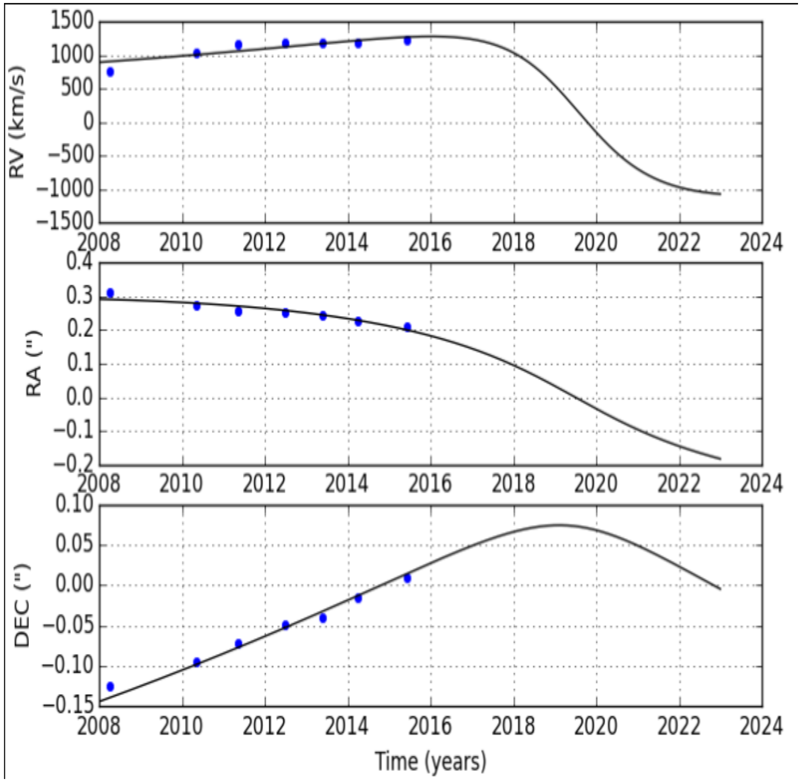

Periapse distance: 750 AU

Peissker, Eckart, Valencia-S et al. (tbs)

DSO/G2, OS1 (and other IR-excess sources) might belong to a population of faint, dusty, Brγ emitters

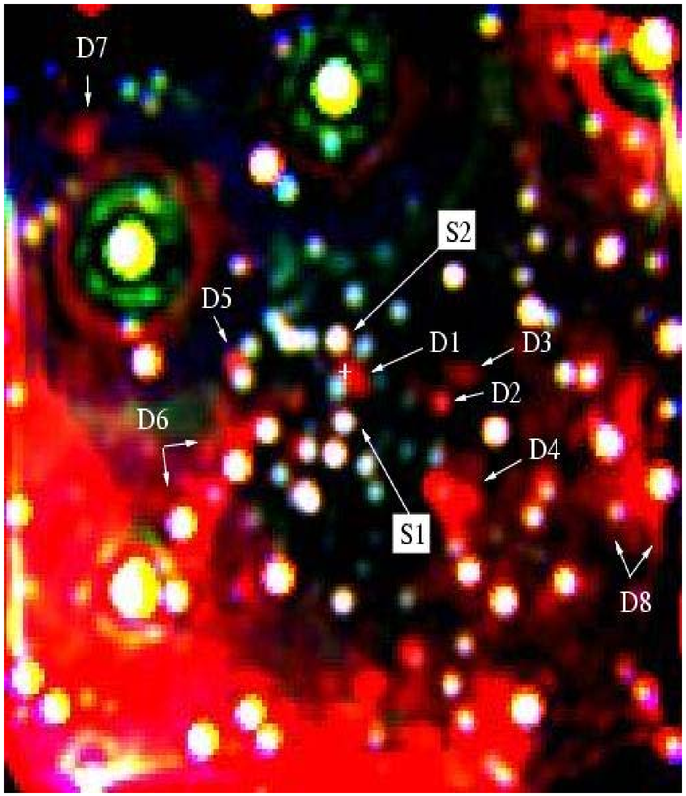

HKL composite. NACO/VLT.
Uni. of Cologne

=

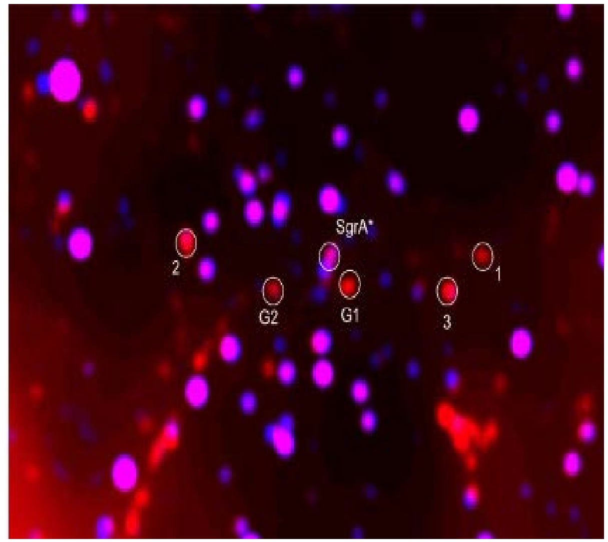

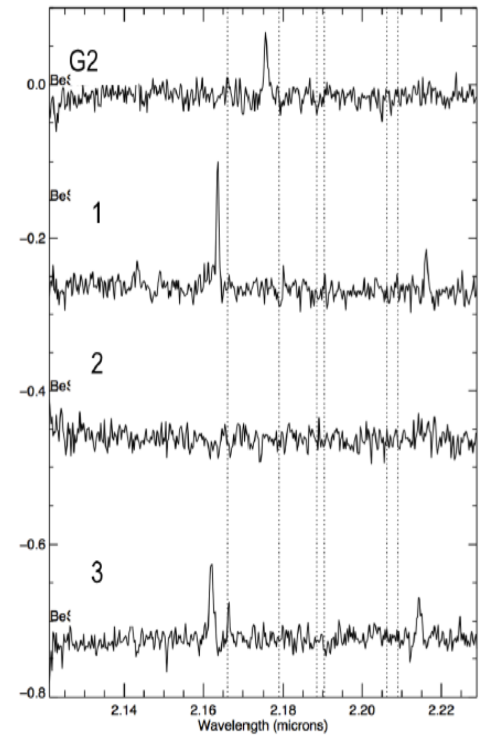

Meyer, L.; Ghez, A. M.; Witzel, G.; et al., 2013arXiv1312.1715M, IAU303 Symp.

Eckart et al. 2005

Extended L-band emission

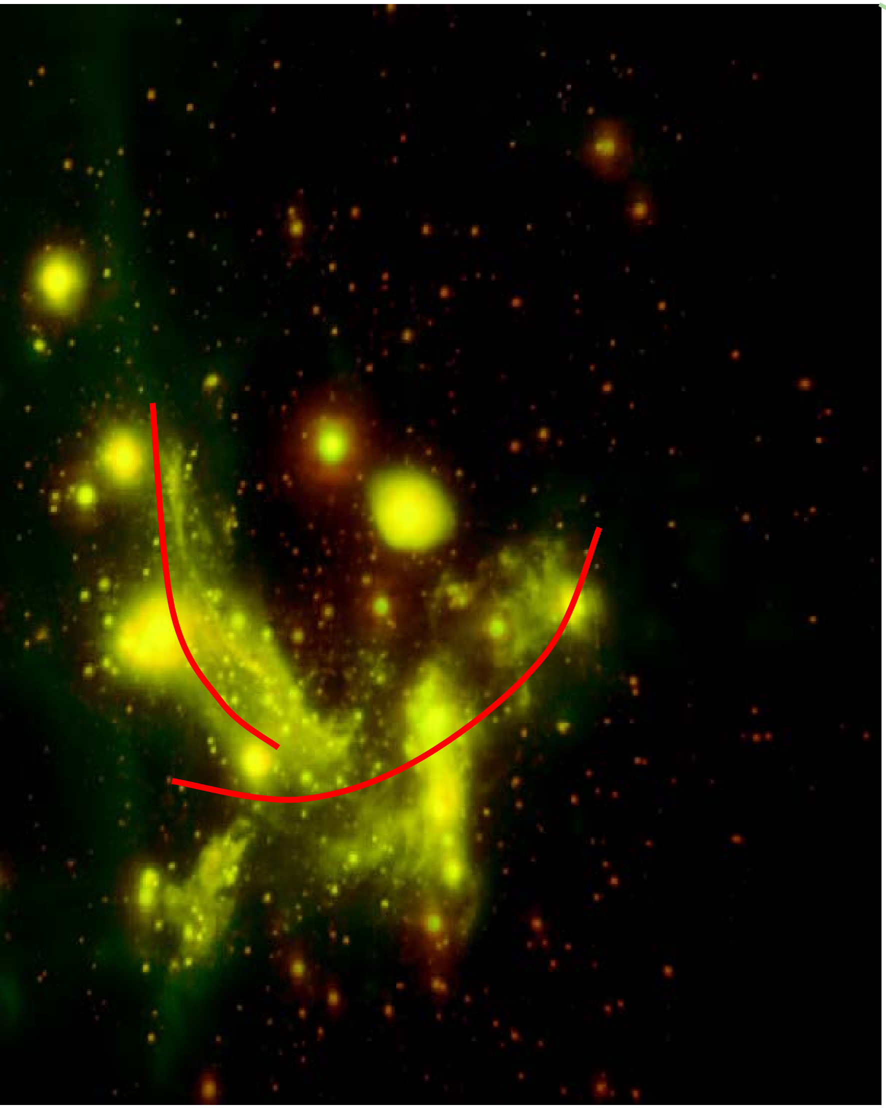

L-band(red)/PAH(green) composite. UCO

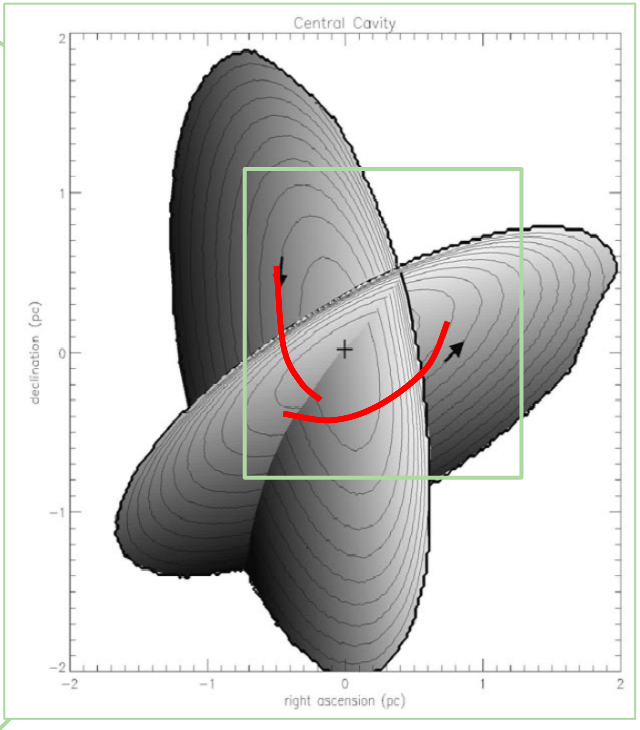

Vollmer & Duschl 2000

see Eckart et al 2013c,
2103arXiv1311.2753

Potential reasons for having a large line width

Plus interaction with ambient medium

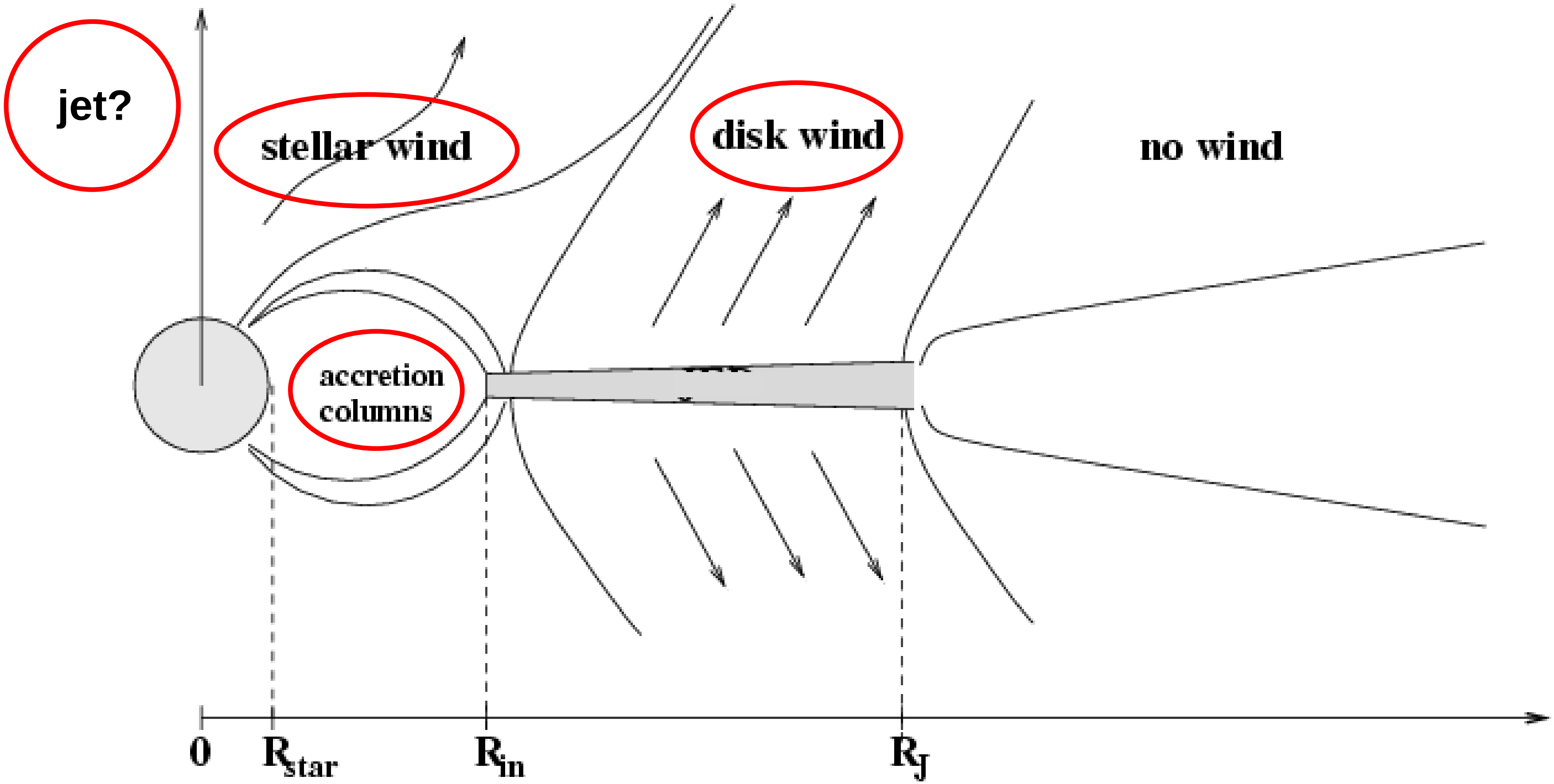

A&A 479, 481-491 (2008)
The radial structure of protostellar accretion disks
C. Combet and J. Ferreira

Pre-main sequence stars with large line widths

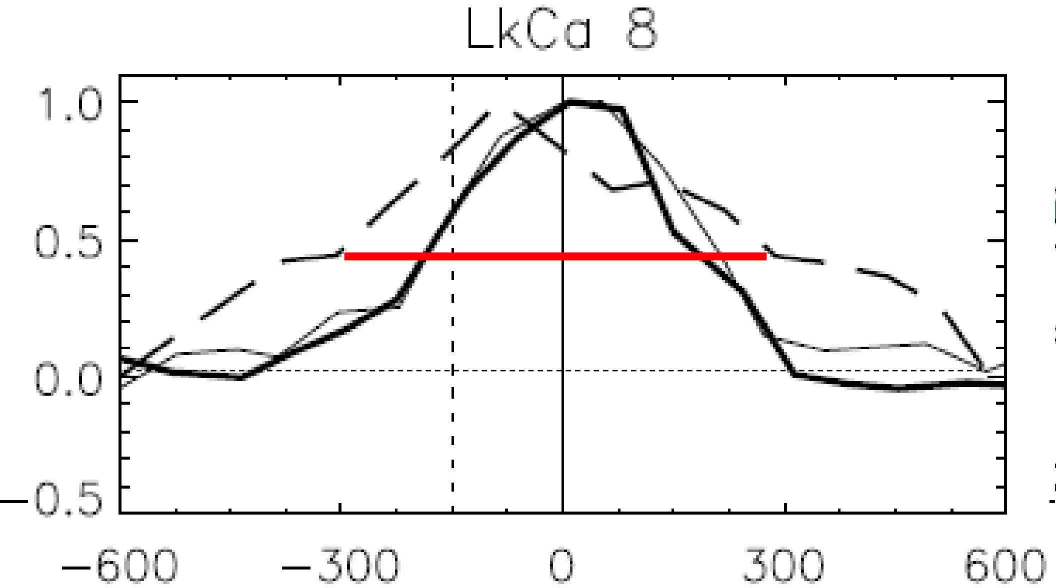

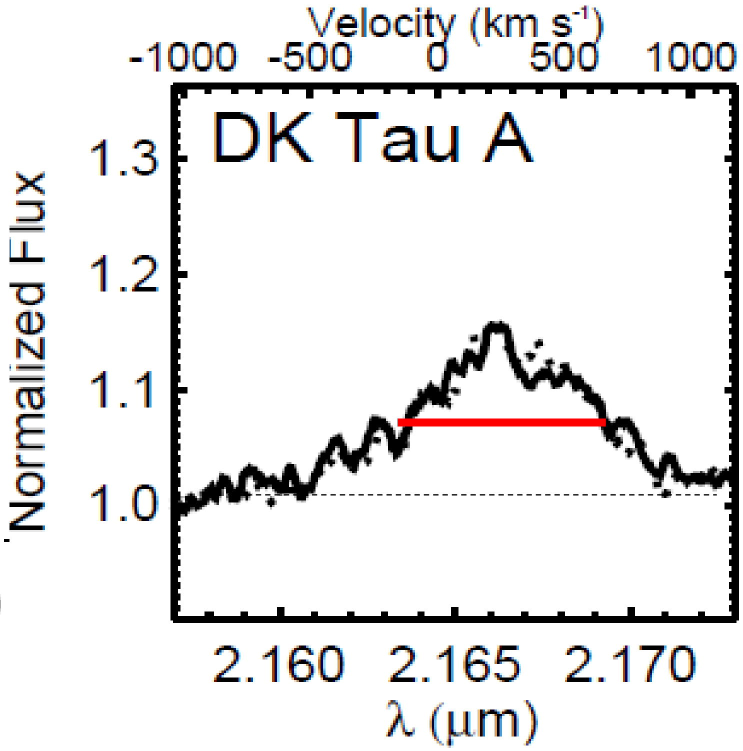

Edwards et al. 2013
M0V ; T Tauri ; around 2 solar masses
600-700 km/s in Brγ

Eisner et al. 2007
Herczeg & Hillenbrand 2014
K8.5 ; 0.68 solar masses
800 km/s in Brγ

DSO/G2 as a young stellar object

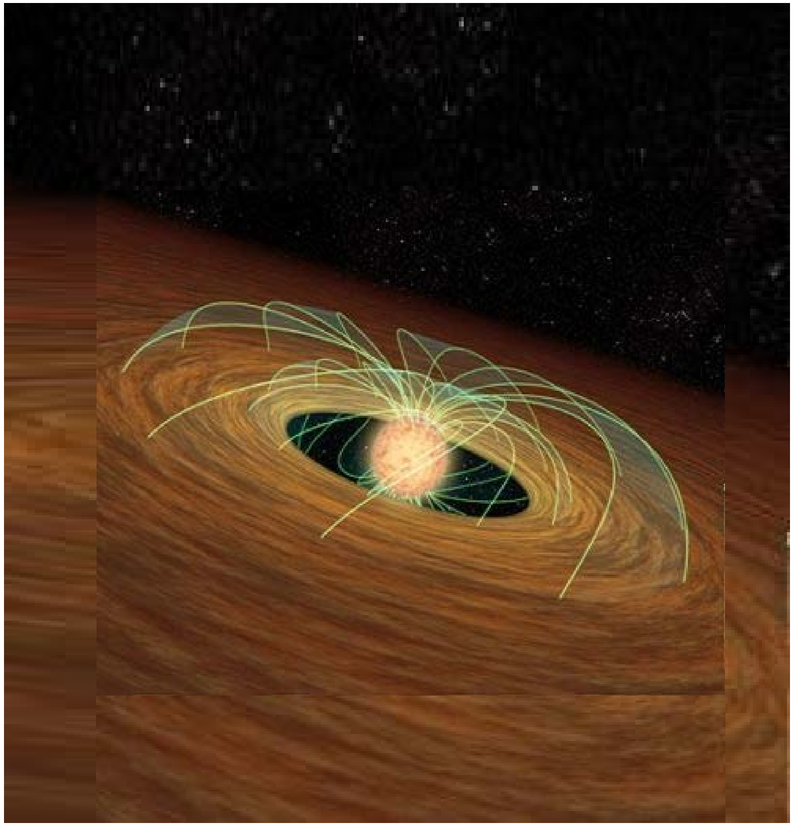

Davies et al. 2011; Rosen, Krumholz, Ramirez-Ruiz, 2012, Eckart et al. 2014

Brγ production mechanisms:
Ionized winds, accretion funnel flows, the jet base, bow shock layer

Brγ broadening:
Inclination of the system
magnetospheric accretion model (200-700 km/s)

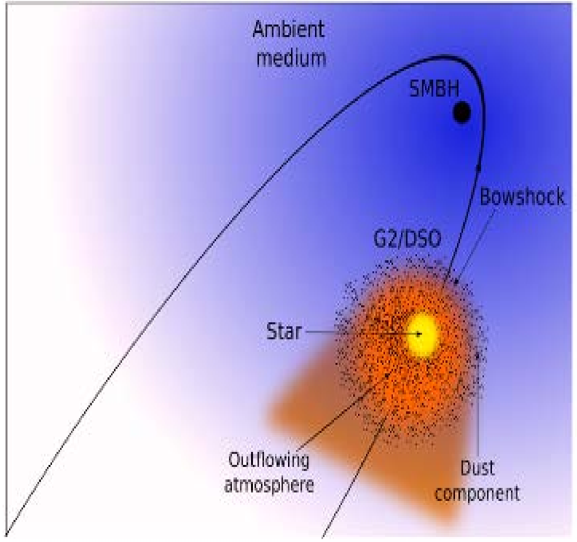

Zajacek, Karas, Eckart 2014

Possible model for DSO

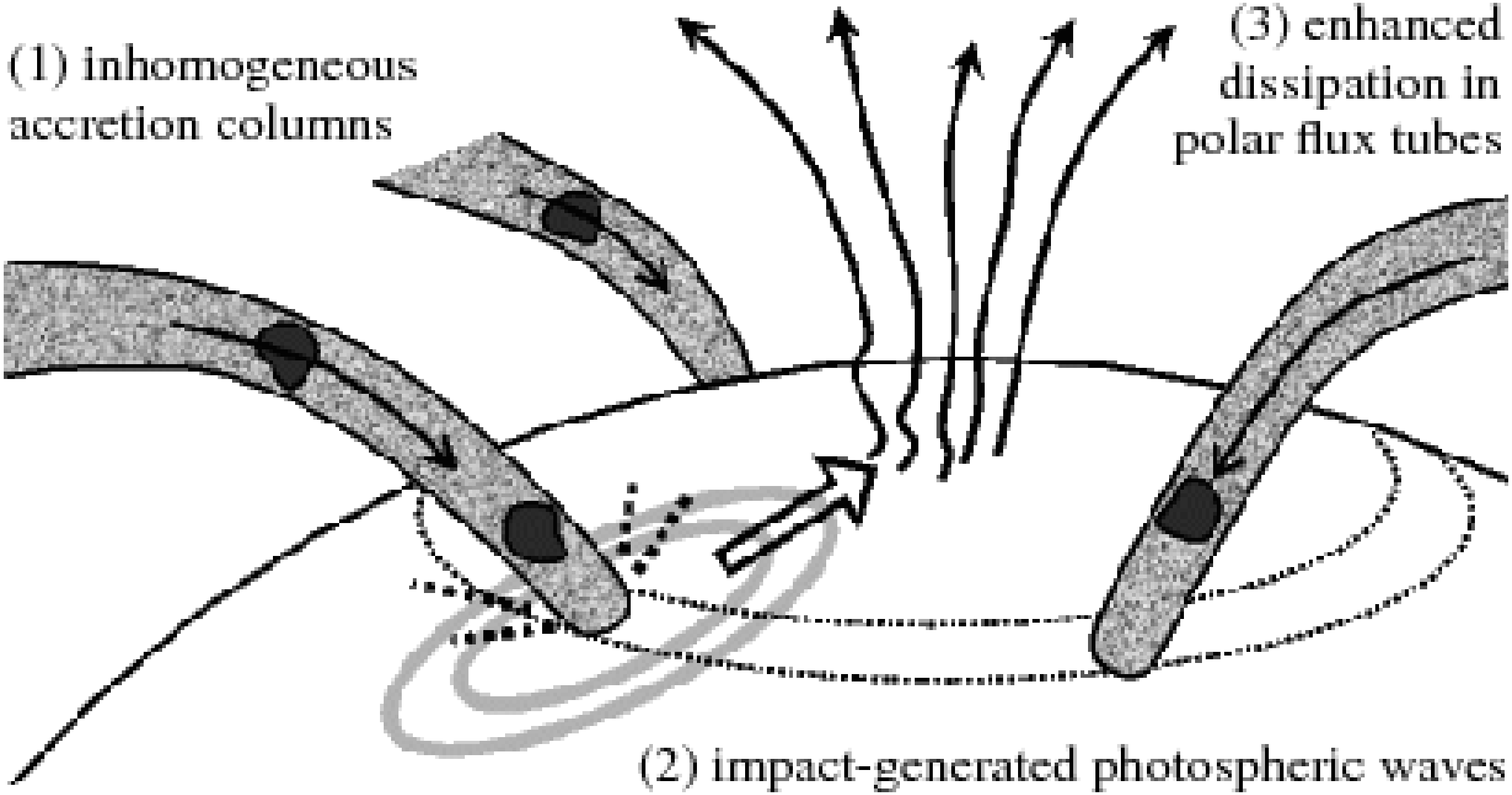

Cranmer, Steven R. arXiv:0808.2250 [astro-ph]

Pre-main sequence stars with large line widths

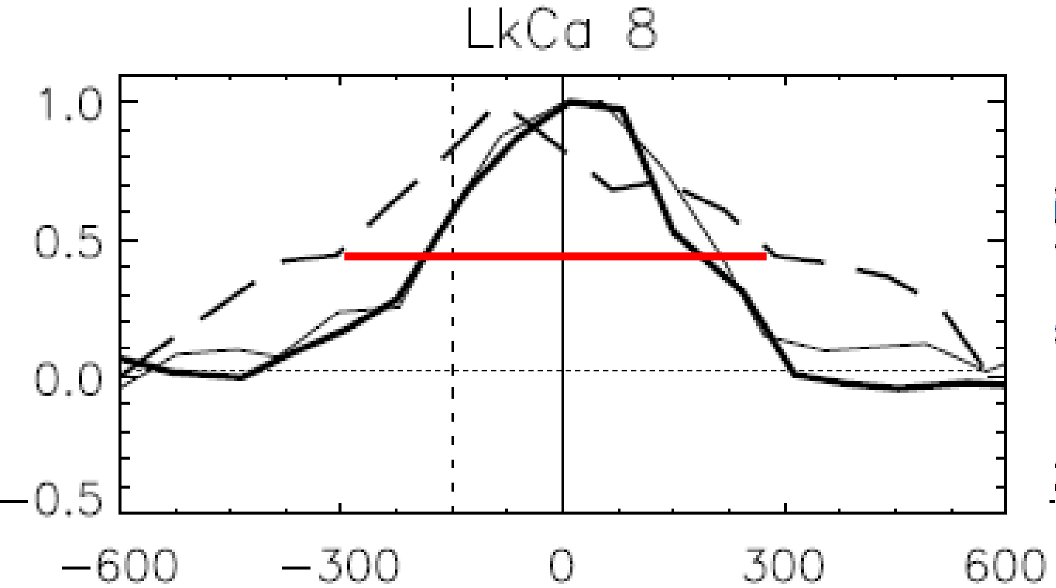

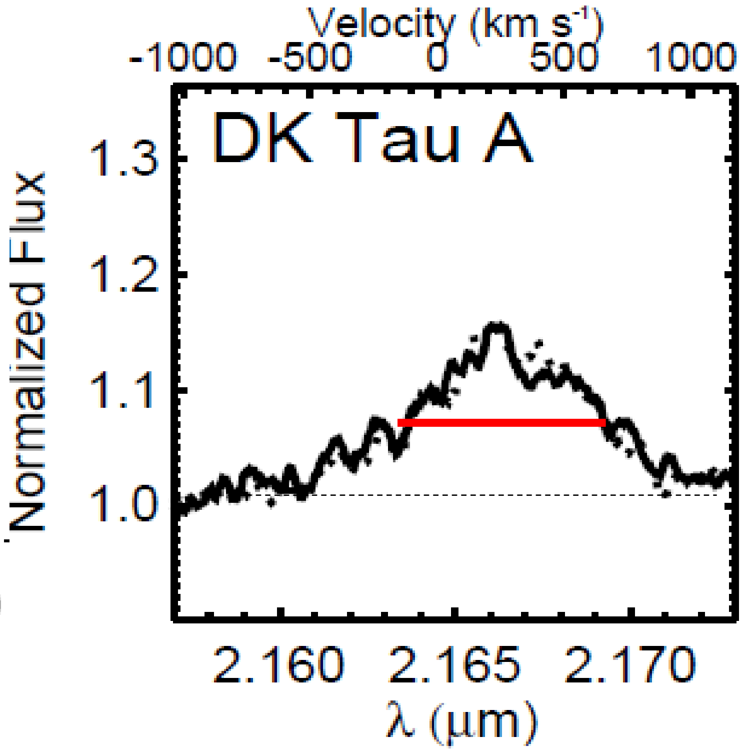

Edwards et al. 2013
M0V ; T Tauri ; around 2 solar masses
600-700 km/s in Brγ

Eisner et al. 2007
Herczeg & Hillenbrand 2014
K8.5 ; 0.68 solar masses
800 km/s in Brγ

The DSO is polarized in the NIR

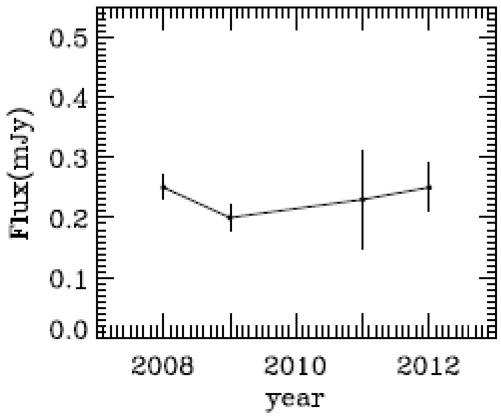

Fig. 2. NIR K_s-band light curve of the DSO observed in polarimetry mode in different years of 2008, 2009, 2011, and 2012.

Shahzamanian et al. 2016

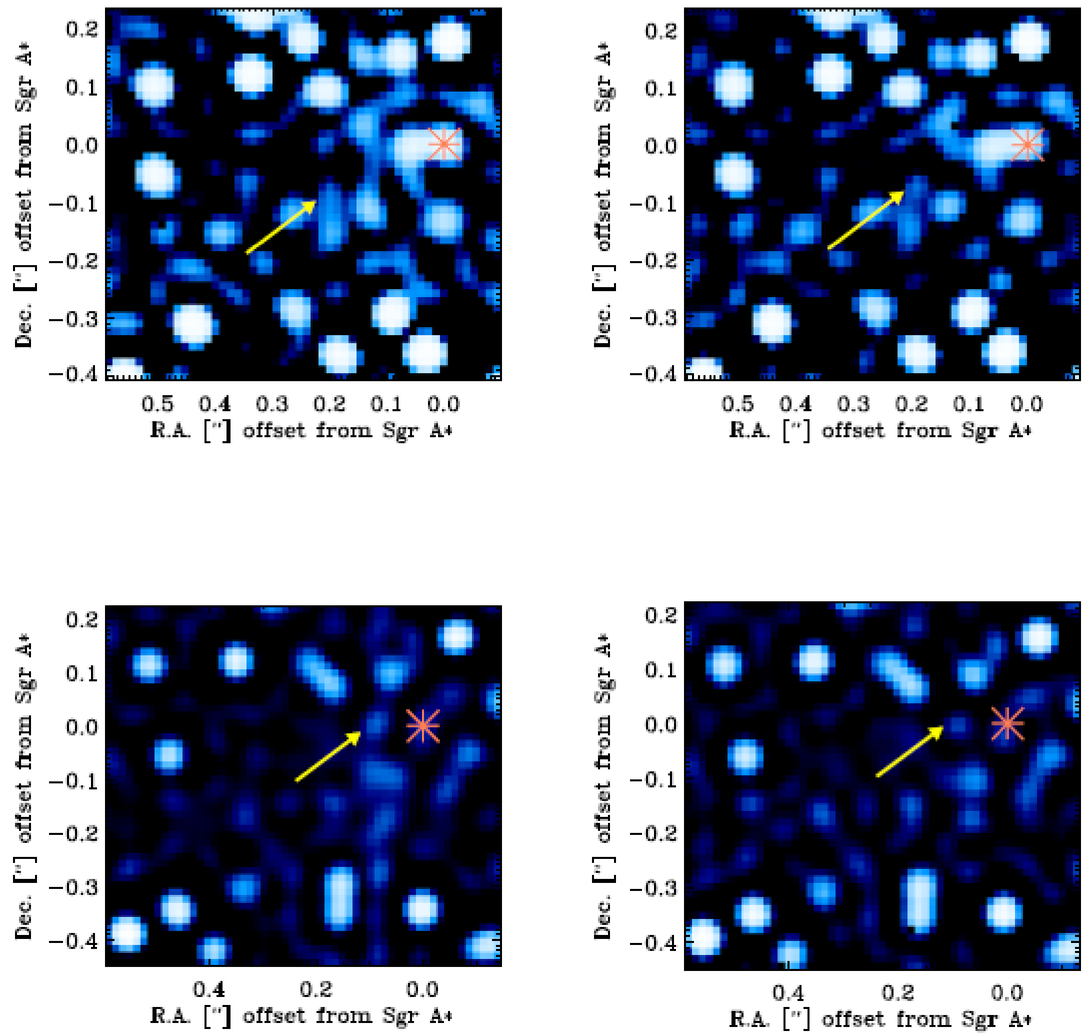

Fig. 1. The final K_s-band deconvolved median images of the central arcsecond at the GC in polarimetry mode (left: 0°, right: 90°) in the years 2008 (top) and 2012 (bottom). The arrow points to the position of the DSO and the asterix indicates Sgr A* position. In all the images North is up and East is left.

The DSO is polarized in the NIR

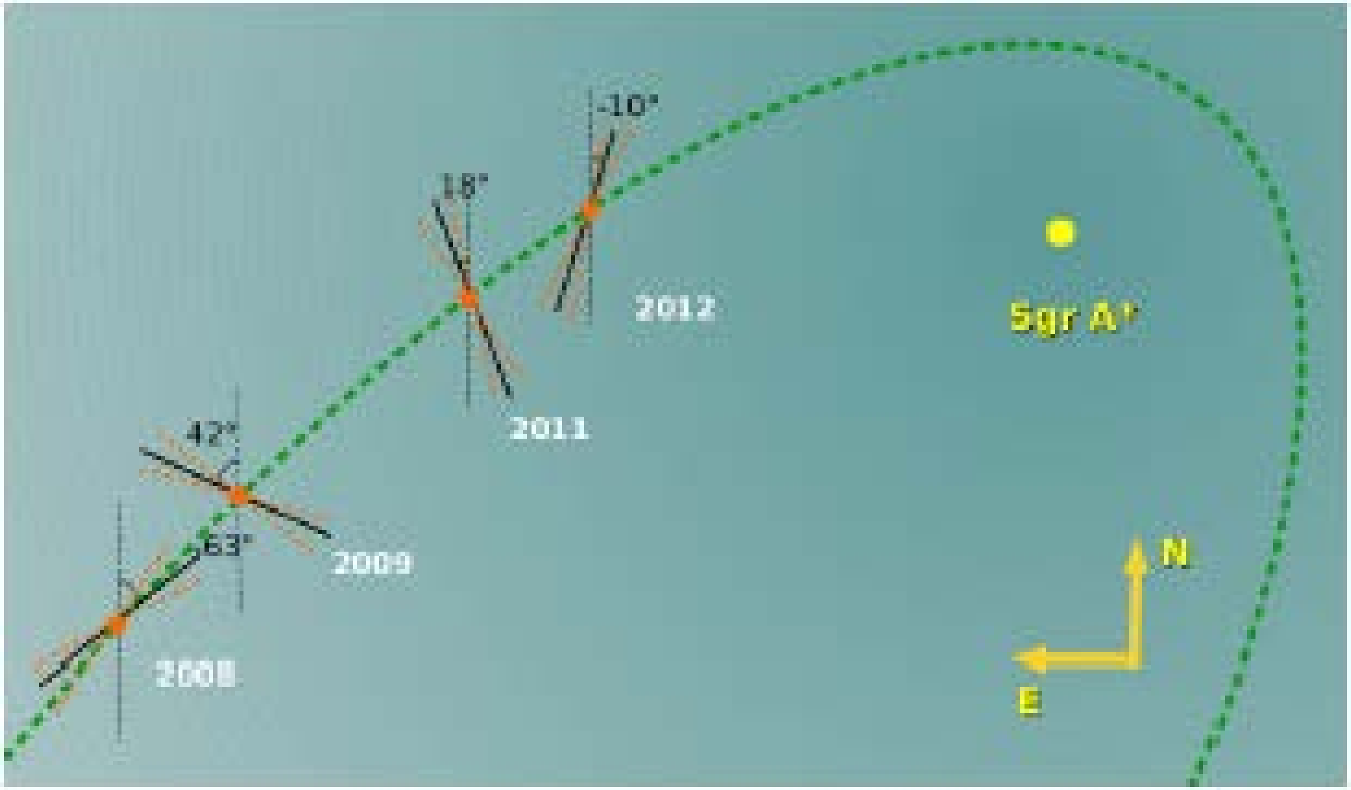

Fig. 3. Sketch of the DSO polarization angle variation when it moves on its eccentric orbit around Sgr A* position for four different years. : this part will change: The orange shaded areas show the range of possible values of polarization angle based on our observation and simulation results.

Shahzamanian et al. 2016

The DSO is polarized in the NIR

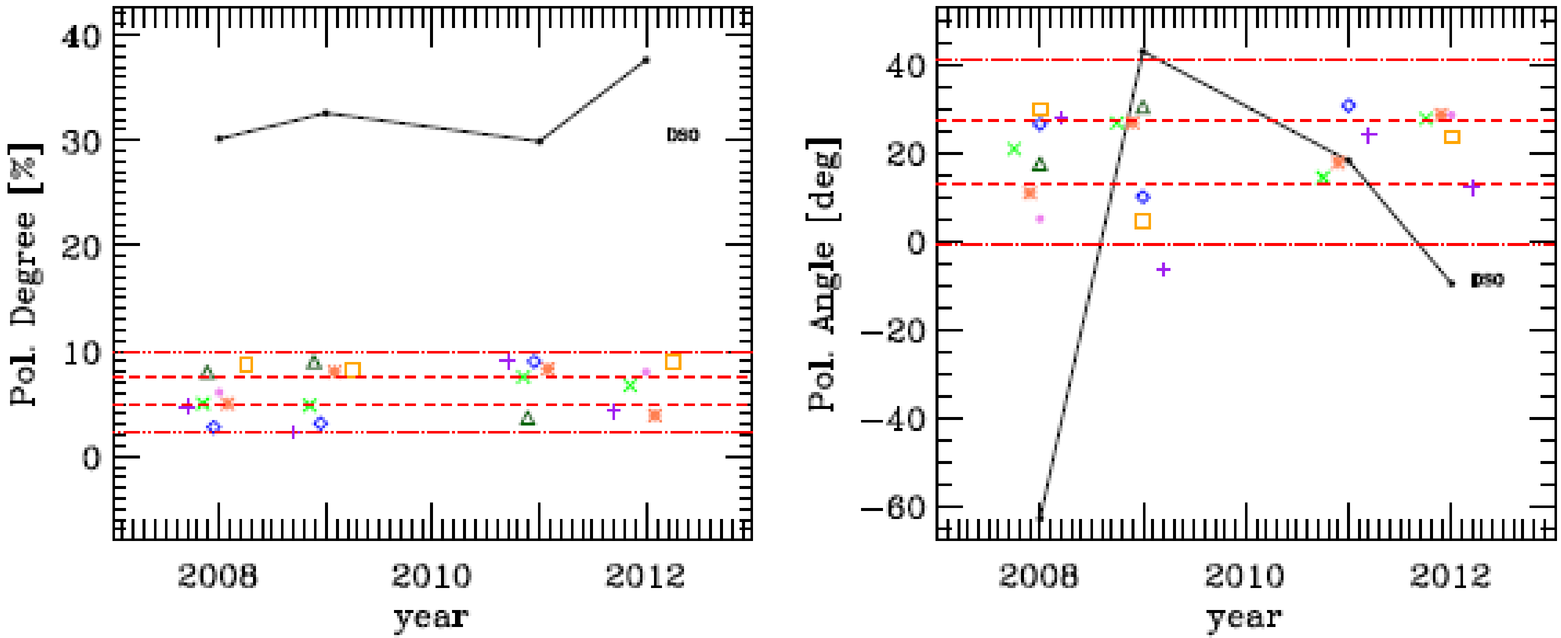

Fig. 4. Left: Comparison of the polarization degree of the DSO (black dots) with the ones of GC S-stars located close to the DSO position (S7, S57, S19, S20, S40, S23, S63). Right: Comparison of the polarization angle of the DSO (black dots) with the ones of the S-stars similar to the left panel. In both panels: Some of the considered stars are not isolated in some years in which it is difficult to calculate their polarization parameters, therefore we didnot show them as data points. The regions between two dashed red lines and dotted lines present the 1 and 3σ confidence intervals of the K_s-band polarization degree and angle distributions of the stars reported in Buchholz et al. (2013), respectively.

Shahzamanian et al. 2016

DSO model: shocked stellar wind

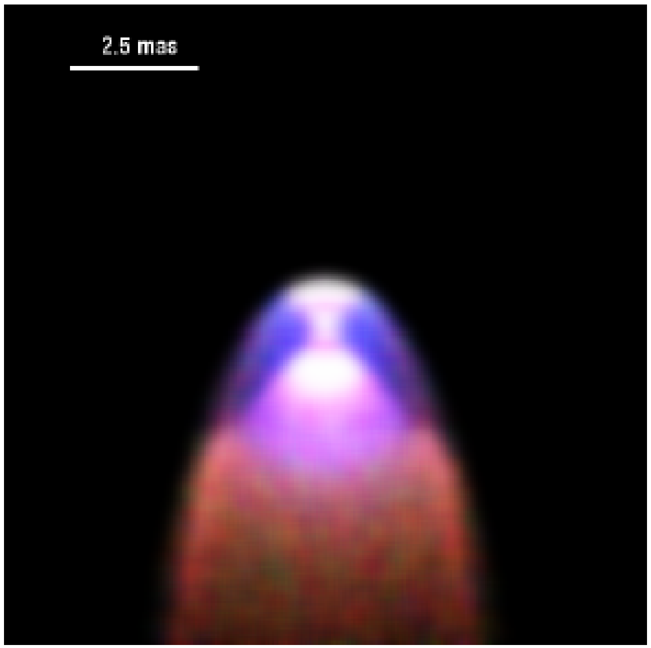

Fig. 9. The RGB image of the source model of the DSO. The explanation is in the text.

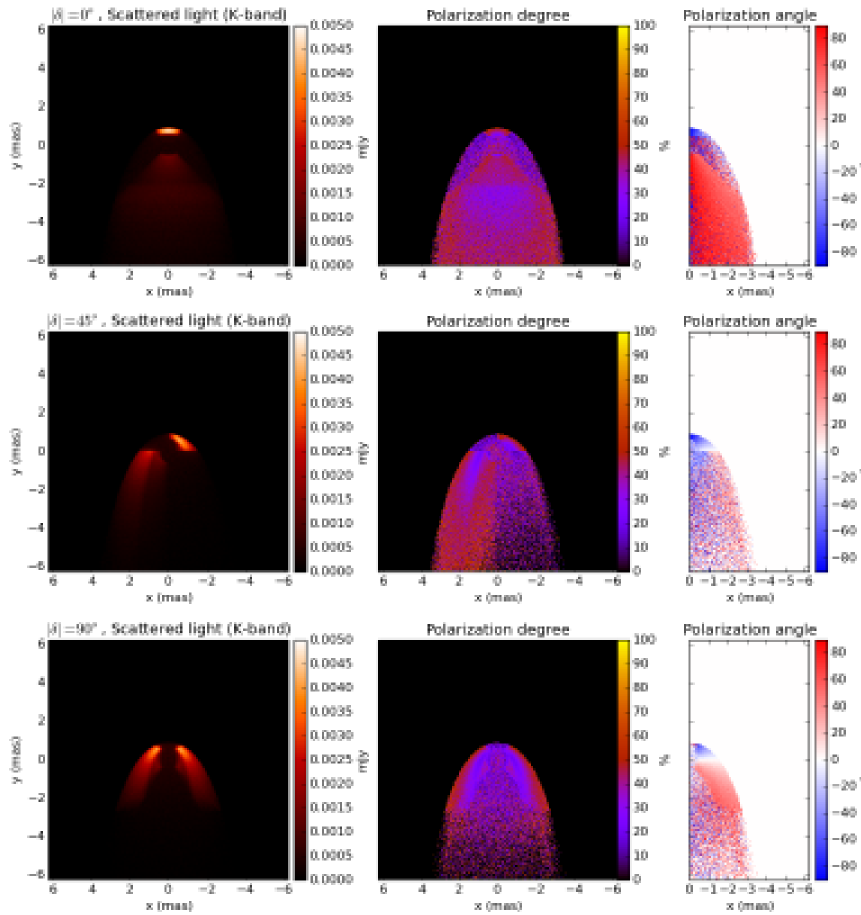

Fig. 8. The emission map of scattered light in K_s band, the distribution of the polarization degree and the angle in the left, middle, and the right panels, respectively for three different configurations of the star–outflow system: $\delta = 0°, 45°, 90°$ from the top to the bottom panels.

Shahzamanian et al. 2016

Zajacek et al. 2016

Origin

Origin of the DSO and potentially young stellar object in the immediat vicinity of a super massive black hole

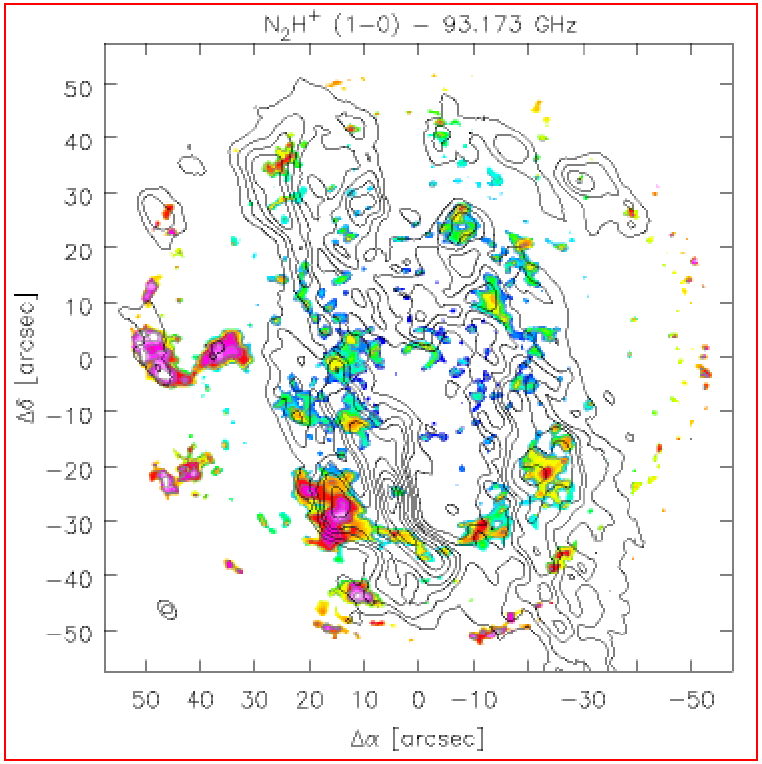

Contours: CN(2-1) Martin at el 2012

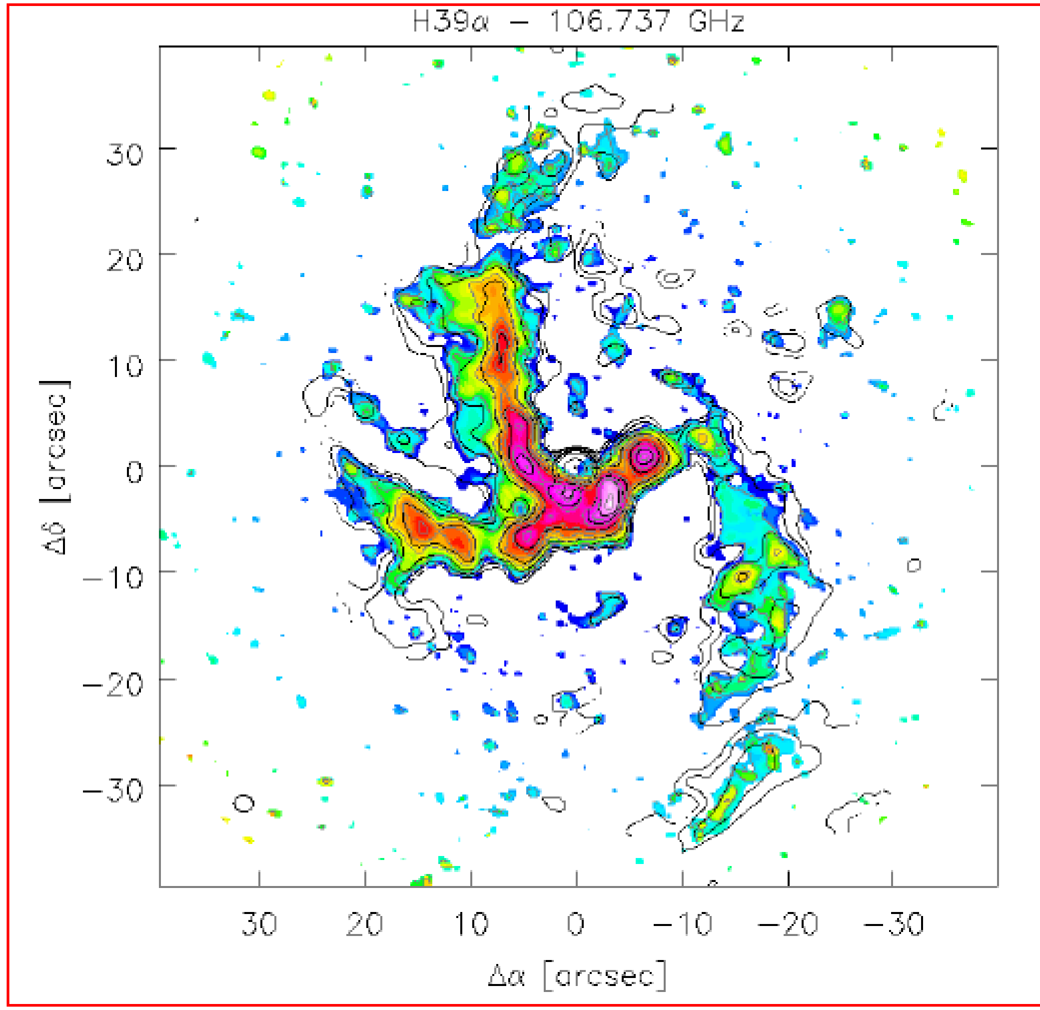

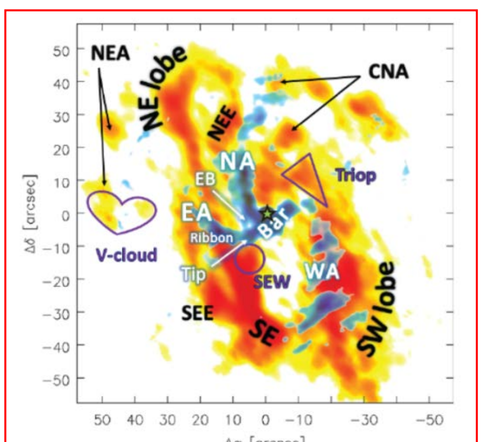

Summary of recent ALMA data on the Galactic center:

Moser, Lydia; Sánchez-Monge, Álvaro; Eckart, Andreas et al., 2016arXiv160300801M

Modeling Approach

100 Msun molecular clump,
0.2 pc radius,

Test with 10 & 50 Kelvin,
isothermal gas

Timescales:
clump free fall time ~ 10^5 yr
CND orbital period ~ 10^5 yr

Semi-major axis=1.8 pc →
orbital period ~10^5 yrs

two Orbits:
peri-center~0.1 pc → ecc.= 0.95
peri-center~0.9 pc → ecc.= 0.5

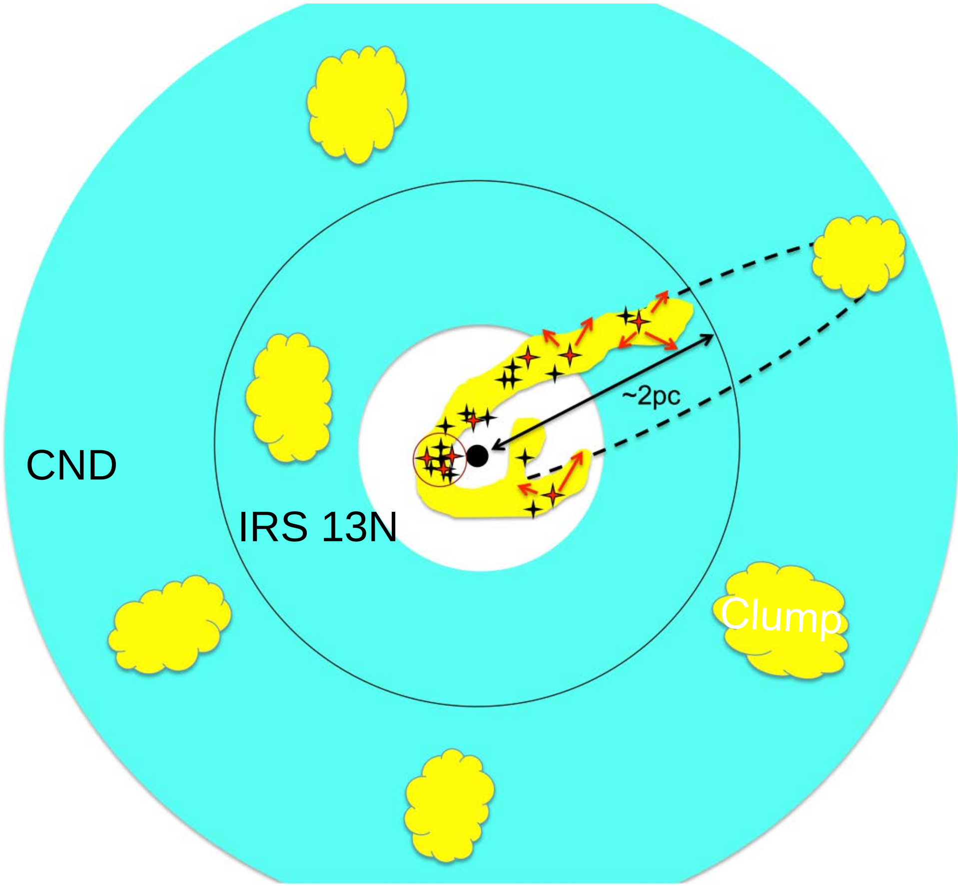

Behrang Jalali, I. Pelupessy, A. Eckart, S. Portegies Zwart, N. Sabha, A. Borkar, J. Moultaka, 2014 A&A.

Orbiting 50 Kelvin clump with e=0.94

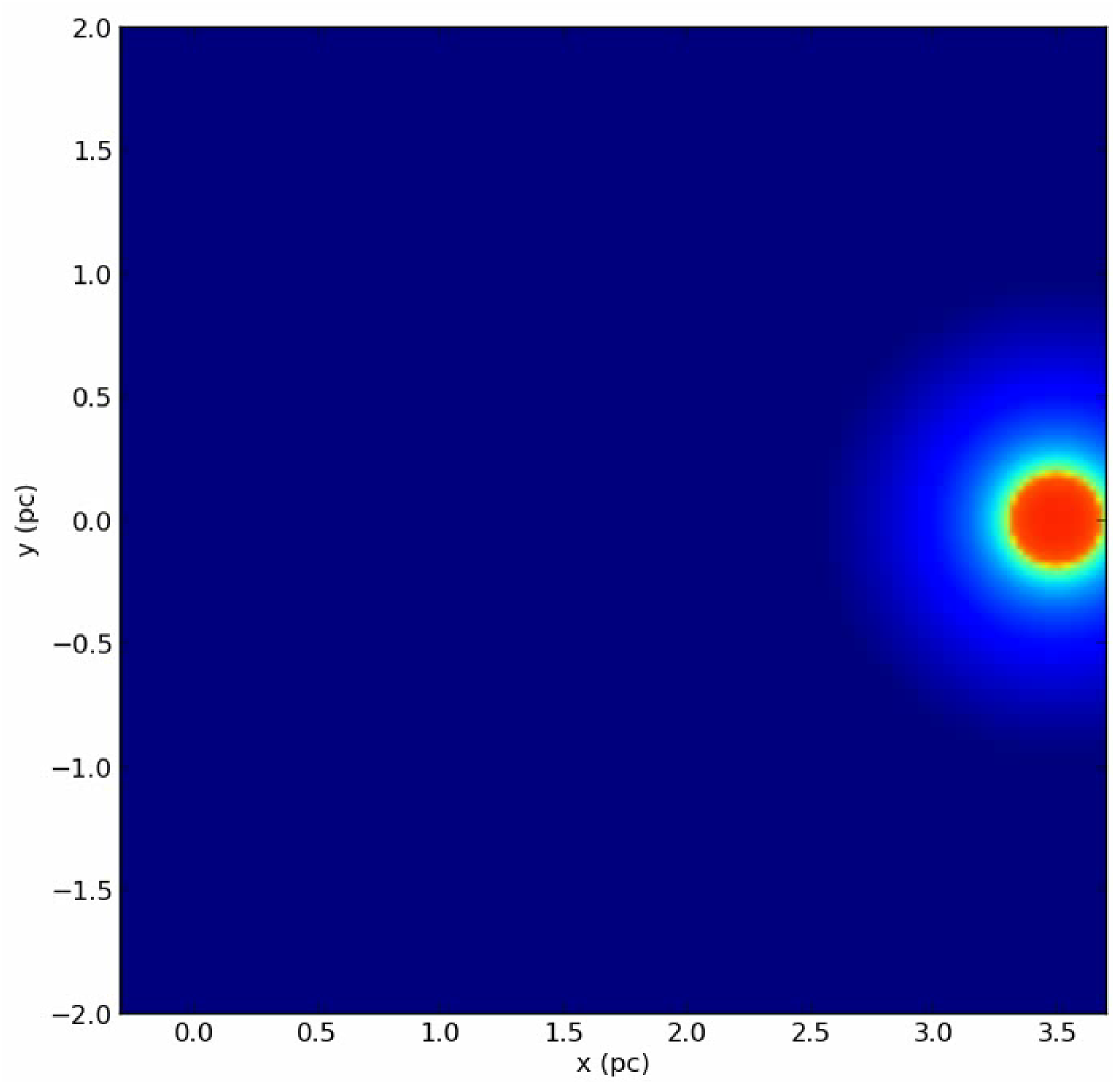

Behrang Jalali,

I. Pelupessy, A. Eckart,

S. Portegies Zwart,

N. Sabha, A. Borkar,

J. Moultaka

(arXiv:1311.4881)

published in A&A

General Summary

Experimental Indicators of Accretion Processes in AGN

Starformation and Black Hole Growth jet formation as well as NLR and BLR reverberation indicate compactness and accretion activity of the region around the Black Hole

SgrA* as a special nearby case

NIR polarization of SgrA* over the past ~10 years, as well as radio monitoring indicate that SgrA* is a stabily accreting system
Monitoring the Dusty S-cluster Object

Summary for the DSO

1. DSO/G2 line emission remains compact through the years. DSO/G2 emits K-band continuum emission (18 mag) and has survived the closest approach to SgrA*.
2. DSO/G2 PV diagrams can also capture emission from the fore/background and other line-emitting sources.
3. Discovery of OS1 → Existence of a population of faint, dusty objects.
4. The NIR continuum of the DSO is polarized

- DSO might be a YSO (T Tauri M=0.8-2.0$M_\odot$, ~0.1Myr)

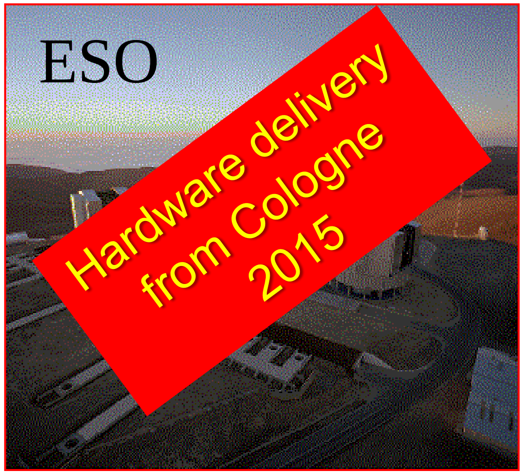

NL leads Euro-Team
Universitity of Cologne
studies for
METIS @ E-ELT

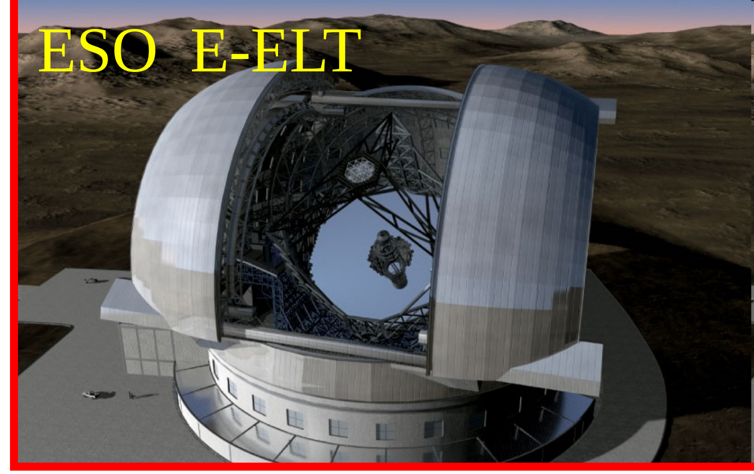

MPE, MPIA, Paris, SIM
Universitity of Cologne
participation
GRAVITY @ VLTI

The Galactic Center is a unique laboratory in which one can study signatures of strong gravity with GRAVITY

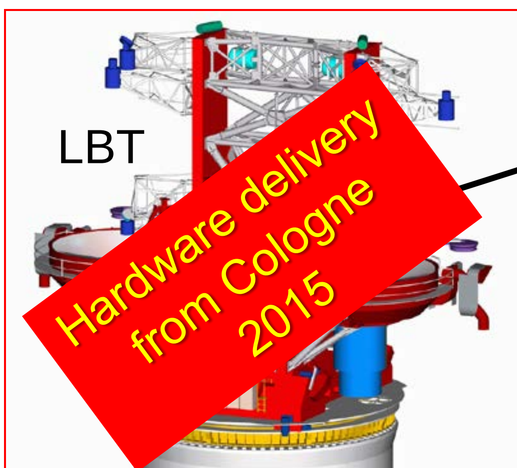

NIR Beam Combiner:
Universitity of Cologne
MPIA, Heidelberg
Osservatorio Astrofisico di Arcetri
MPIfR Bonn

Hardware delivery
from Cologne
2013

Cologne
contribution to
MIRI on JWST

Cologne built Fringe Tracking Spectrometer for GRAVITY

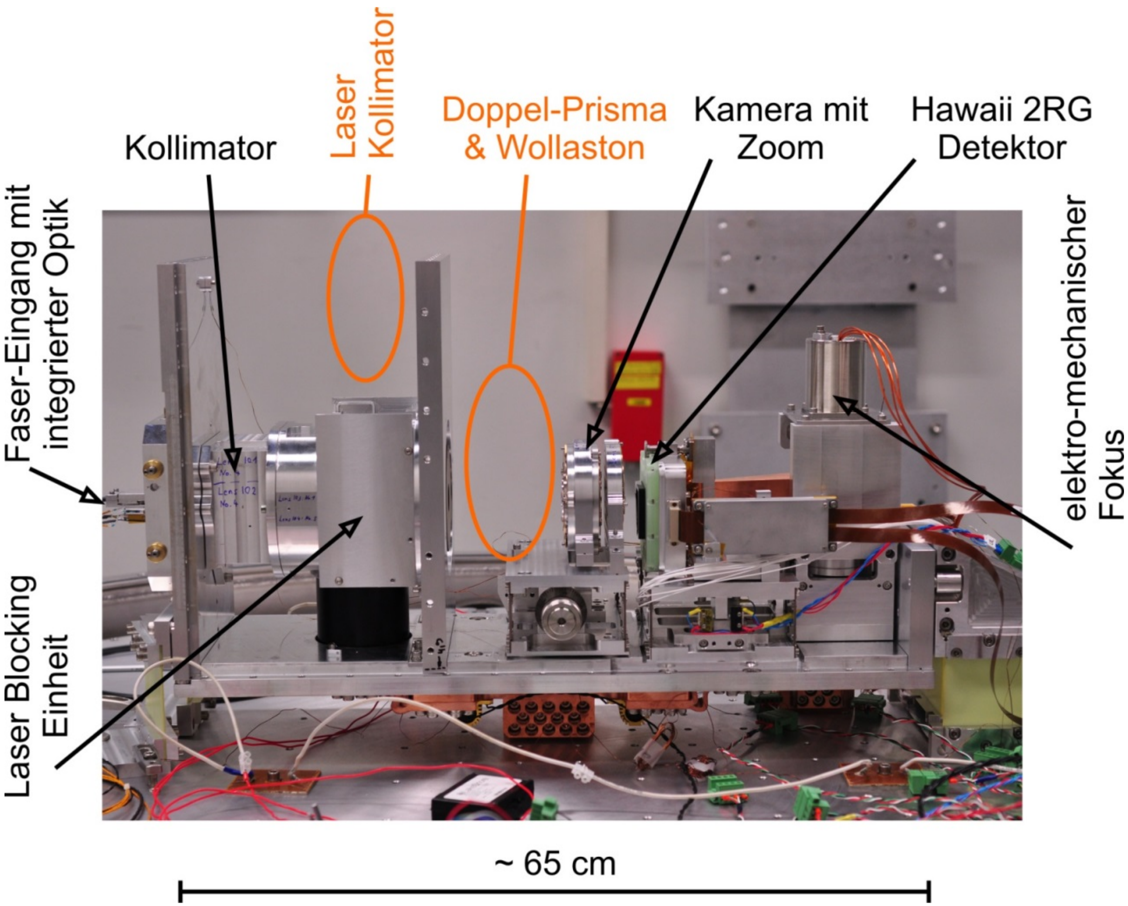

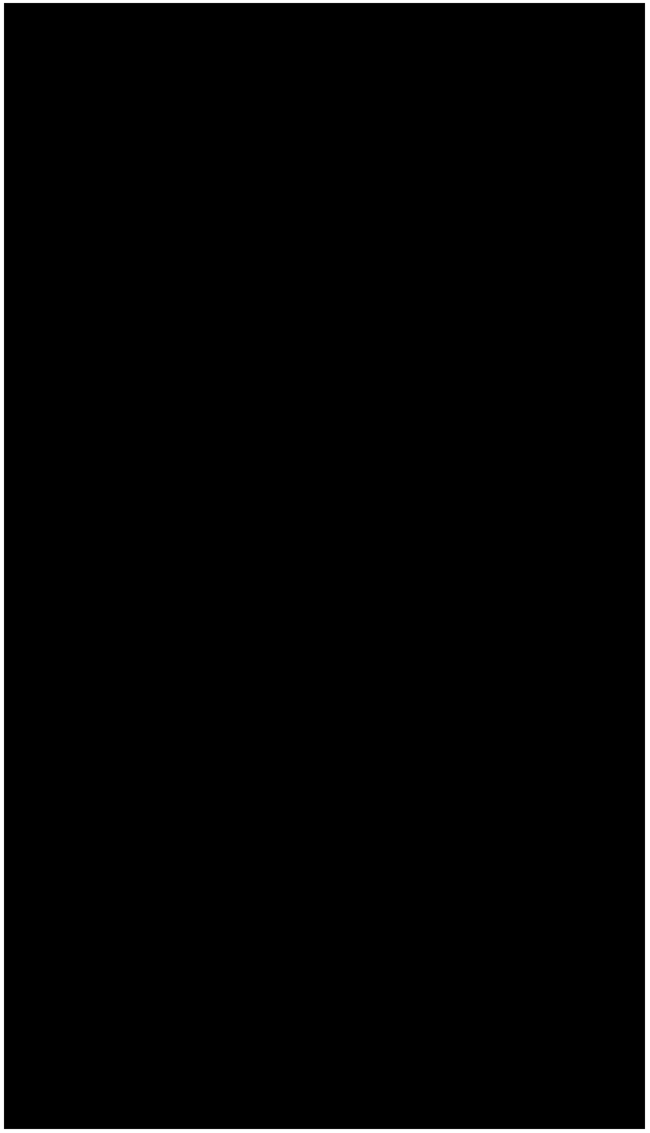

End